Investigation of Effect of Human Robot Interaction with Lower Limb Exoskeletons

Marukku Devage Sanka Dileepa Chandrasiri

(178035N)

Thesis submitted in partial fulfillment of the requirements for the degree Master of Science in Biomedical Engineering

Department of Mechanical Engineering

University of Moratuwa
Sri Lanka

November 2021

DECLARATION

I declare that this is my own work and this dissertation does not incorporate without acknowledgement any material previously submitted for a Degree or Diploma in any other University or institute of higher learning and to the best of my knowledge and belief it does not contain any material previously published or written by another person except where the acknowledgement is made in the text.

Also, I hereby grant to University of Moratuwa the non-exclusive right to reproduce and distribute my dissertation, in whole or in part in print, electronic or other medium. I retain the right to use this content in whole or part in future works (such as articles or books).

Signature: Date:

The above candidate has carried out research for the MSc thesis under my supervision.

Signature of the Supervisor(s): Date:

Prof. R.A.R.C Gopura
Professor,
Department of Mechanical Engineering,
University of Moratuwa, Sri Lanka.

Abstract

Continuous development of exoskeletons (wearable robots) is essential to enhance the user experiences and performances of the wearable device. Therefore, it is necessary to determine human ergonomics and the comfort levels of wearable robots. These aspects can be analyzed by determining human-robot interaction (HRI). HRI is classified in cognitive- HRI (cHRI) and physical-HRI (pHRI) in the literature. cHRI involves the identification of complex human expression and physiological aspects. These pieces of information can be observed using a human-robot cognitive interface. Electroencephalogram (EEG) and electromyography (EMG) are mainly used sensing methods in cHRI. EEG is used to identify electrical activities of brain, while EMG is used to identify electrical activities of muscles. Furthermore, pHRI involves evaluating physical quantities such as position, force, and pressure between humans and robots. In order to identify pHRI with wearable robotic interfaces, a novel surface muscle pressure (SMP) sensory system was developed. The SMP sensor was calibrated and evaluated using surface electromyography (sEMG) data for two separates experimental scenarios. Hence the system was proposed to determine the pHRI of wearable robotics.

In order to determine HRI, a dummy lower limb exoskeleton was designed and manufactured in compliance with human ergonomics and biomechanics. The exoskeleton consists of 8 degrees of freedom (DoF) motions with variable limbs and weight attachment locations. Furthermore, sEMG, motion analysis, and SMP sensory systems were used to carry out the experiments. Moreover, a human lower limb model simulation with ground force reaction prediction was developed to determine the inverse dynamics. The experiments were carried out without exoskeleton, with the exoskeleton, and with exoskeleton weight attachments with six healthy subjects for the walking motion. A qualitative, comfortable level analysis was carried out simultaneously for each experiment. Captured SMP, sEMG, inverse dynamics and qualitative results were processed and feature extracted to evaluate HRI for different weight distributions and attachment locations. The relationship between exoskeleton attachments and locations was observed. The experiment results have provided an improved understanding of HRI for developing practical and ergonomically comfortable lower limb exoskeleton devices.

***Keywords*-Lower-limb Exoskeletons, Human-Robot Interaction, Electromyography, Inverse Dynamics**

DEDICATION

To my parents,

Chandra Chandrasiri and Sudharma Chandrasiri

Thanks for your great support and

continuous care.

Without you none of my success would be possible.

ACKNOWLEDGMENTS

After immense ups and downs, I am writing this thanking note in remembrance of the great assistance provided by everyone who were there with myself for the successful completion of this research work. It has been a great run for me and it is time for myself to pay my sincere gratitude towards all these great people.

The long list of the people who have my unending homage, should be started with my thesis supervisor Prof. R. A. R. C. Gopura. For me choosing the path of higher studies was challenging and life changing. I am eternally grateful to him for accepting myself as his research student and for the continuous support given to reach great milestones which I would not have even imagined. Over the entire period of my research, his humane qualities left an example for me to look up to and I am honoured to be a student of him.

I wish to extend my gratitude to Eng.Pubudu Ranaweera for providing his valuable insights for the successful completion of this research work. Doing a research alone can be tiresome and restless at most of the time. However, it is the people around you who make that feeling disappear. I am very grateful to all the members of Bionics Laboratory, Department of Mechanical Engineering, University of Moratuwa, who had my back in each step of the way. Among them I would like to appreciate the support Dr. Kanishka Madusanka in shaping my Master's Degree work. Moreover, I would like to recall the motivational advices of Mr. Achitha Mihiran, Mr. Achintha Iroshan Mr. Dinesh Kumara and Mr. Dulanjana Perera.

I take this opportunity to express my gratitude towards the Senate Research Council of University of Moratuwa for the financial support granted to me under the grant no. SRC/ST/2019/56 to conduct my studies.

Moreover, enormous thanks to CSSM laboratory members for providing materials and support for development of sensory interfaces: Dr. Damith Chathuranga, Mr. Asitha Kulasekara , Mr. Rancimal Arumathanthri and Mr. Chanaka Prasad. guided me throughout the study.

support, love and motivation provided by my loving family. I would pay my sincere homage to them, with heavy heart for being the reason to keep moving forward when the things get hard.

Sanka Dileepa Chandrasiri
msankachandrasiri@gmail.com

TABLE OF CONTENTS

LIST OF FIGURES

LIST OF TABLES

LIST OF ABBREVIATIONS

cHRI	Cognitive Human Robot Interaction
DAQ	Data Acquisition
DC	Direct Current
DH	Denavit Hartenberg
DLS	Damped Least Squares
DoF	Degrees of Freedom
EEG	Electroencephalography
EMG	Electromyography
FSR	Force Sensitive Resisters
HRI	Human Robot Interaction
HK	Hip Knee
HKAF	Hip Knee Ankle Foot
KAF	Knee Ankle Foot
pHRI	Physical Human Robot Interaction
SMP	Surface Muscle Pressure
THKF	Trunk Hip Knee Foot
THK	Trunk Hip Knee

Appendix A

INTRODUCTION

Robots have been incorporated with human daily life activities since the last half-century. According to the Robotics Institute of America, a robot is a reprogrammable, multifunctional mechanical manipulator intended to move material, tools, or specific devices through various programmed motions to perform a variety of tasks [2]. The term robot is originally coined in Karel Capek's Rossum's Universal Robots (RUR) play in 1921, which has the meaning of 'forced laborer' in Czech [3]. The robots were initially intended for use in industrial environments to replace humans in monotonous tasks. However, rather than replacing human tasks, robots expand to perform and assist human tasks. Therefore, interaction with humans is expanding from a mere exchange of information to a close interaction involving physical and cognitive modalities [4], [5].

In this context, the concept of Wearable Robots has emerged. Wearable robots are person-oriented robots that supplement the function of limbs or replace it entirely alongside the wearer limbs. The exoskeleton can be identified as a wearable device that is anthropomorphic, which interacts with the wearable device's joints and links with the wearer's joints and limbs [6]. The exoskeleton and human limb interaction can be achieved through internal or external force systems. Augmenting limb motions of able humans and rehabilitation of people with disabilities are the main applications of exoskeletons [7]. In the early 1960s, research development of robotic exoskeletons started and US Department of Defense became interested in developement of a powered 'suit of armor.' Simultaniuosly, at Cornel Aeronautical Laboratories started to develop the concept of man–amplifiers

– manipulators to enhance the strength of a human operator. The existing technological limitations on developing the concept were established in 1962. These are related to servos, sensors, and mechanical structure and design [8].General Electric Co. further developed human–amplifiers through the Hardiman project from 1966 to 1971. The Hardiman concept was more of an automatic master-slave configuration [9]. Recently, exoskeletons are well advanced and concern a range of non-military applications, including strength enhancement and medical rehabilitation. Some products have recently been commercialized. There has also been significant progress in the development of robotic wearable devices [10]

The extension of application domains for exoskeletons is growing due to the elderly-dominated and specially-abled person scenarios of most developed countries. Safety and dependability are the primary solutions to the successful development of wearable robots into humans. Wearable robots for physical assistance to humans should reduce fatigue and stress, increase human capabilities in force, speed, and precision, and improve life quality [11]. Therefore, Researchers are studying the factors of human-robot interaction (HRI) to dependability of wearable devices.

A.1 Motivation

. In general, currently available lower limb exoskeletons could be uncomfortable to the user when wearing over a long period. Mass distributions of exoskeletons structure and attachment locations of robots on humans play a crucial part in the wearer's comfort levels. Even though several lower limb exoskeletons have been developed, influences of factors as mentioned earlier are rarely studied in the literature, indicating the gap in knowledge and possible limitations.

In order to overcome the undesirable effects of human-robot interface, design guidelines must be improved considering ergonomics and biomechanics of humans. To achieve this, the effect of mass distribution and attachment locations of exoskeleton should be systematically studied. In addition, the dimensions of human-robot interfaces should also be identified for a better anthropomorphic wearable design.

A.2 Contribution of the Thesis

. The research work presented in this thesis investigates the effect of human-robot interaction with lower limb exoskeletons. The significant contributions of the thesis are listed down below.

- Propose a novel method of surface muscle pressure (SMP) detection method.
- Develop an experiment setup for determining the HRI with lower limb exoskeletons.
- Propose an improved experiment protocol for determining the comfort levels of the wearer with lower limb exoskeletons.
- Derive a guideline for the better ergonomically comfortable lower limb wearable devices.

A.3 Thesis Overview

. The thesis consists of five chapters. The structure of the thesis is as follows. Chapter 2 includes the literature review. Chapter 3 explains the development of the surface muscle pressure monitoring system. Chapter 4 explains the experimental setup, results, and discussion. The final chapter concludes the thesis. Figure 1.1 shows the overview summary of the thesis.

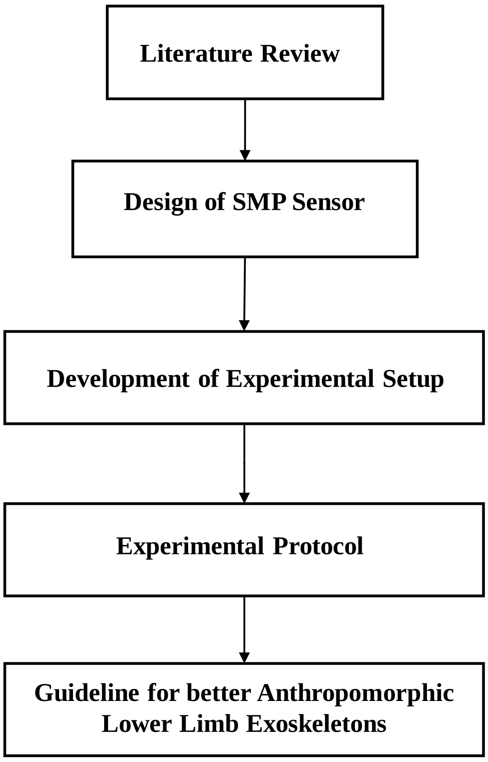

Figure A.1: Summary of research work.

Chapter 2:- Literature Review

This chapter covers the lower limb biomechanics, currently available lower limb exoskeletons, and other relevant areas to investigate HRI. These areas include kinematics of the human lower limb, investigation of physical human-robot interactions (pHRI), cognitive human-robot interactions (cHRI), and human comfort levels. Moreover, the significance of ergonomically comfortable wearable robots has been discussed.

Chapter 3:- Development of Surface Muscle Pressure Monitoring System

The steps involved in developing pressure sensors for detecting SMP were presented in this chapter. Two sensor models were developed separately to achieve desirable measurements: force sensitive resisters based and pneumatic based sensor interfaces. These sensors were experimentally evaluated for detecting pHRI.

Chapter 4:- Experiments and Results

This chapter describes the steps involved in experiments and results to determine the effect HRI with the lower limb exoskeletons. Since many lower limb exoskeleton categories were described in the literature, a dummy exoskeleton prototype was designed and manufactured for the HRI experients. Furthermore, a human model designed in Anybody software to evaluate the kinematics and dynamics of experimental subjects. In order to obtain the HRI results, an experiment setup and a protocol were proposed. Finally, the obtained experimental results were analyzed and discussed.

Chapter 5:- Conclusion

This chapter concludes the thesis with future directions.

Appendix B

LITERATURE REVIEW

The motivation section [see section 1.1] specify that it is required to investigate HRI to develop user comfortable lower limb exoskeletons ergonomically to prolong the wearer's usage. Therefore, a literature review was carried out to identify the relevant factors for identifying user comfort of lower limb exoskeletons. Furthermore, this chapter presents comprehensive details on the background of lower limb exoskeletons. Moreover, anatomical details, HRI, and comfort level evaluation methods of the lower limb exoskeleton wearer are discussed in this chapter.

B.1 Biomechanics and Kinematics of Lower Limb

. Biomechanics and kinematics of lower limb play an essential role in designing lower limb exoskeletons ergonomically. Therefore, the lower limb exoskeleton's joints and movements should be designed in conformity with the biomechanics and kinematics of the human lower limb.

Biomechanics of Lower Limb

Biomechanics of the lower limb is the study of the mechanical aspect of the human lower limb. In order to investigate biomechanics, the human lower limb can be divided into four major components: hip complex, knee complex, ankle, and foot. The hip complex contains two significant bones: pelvis and femur,

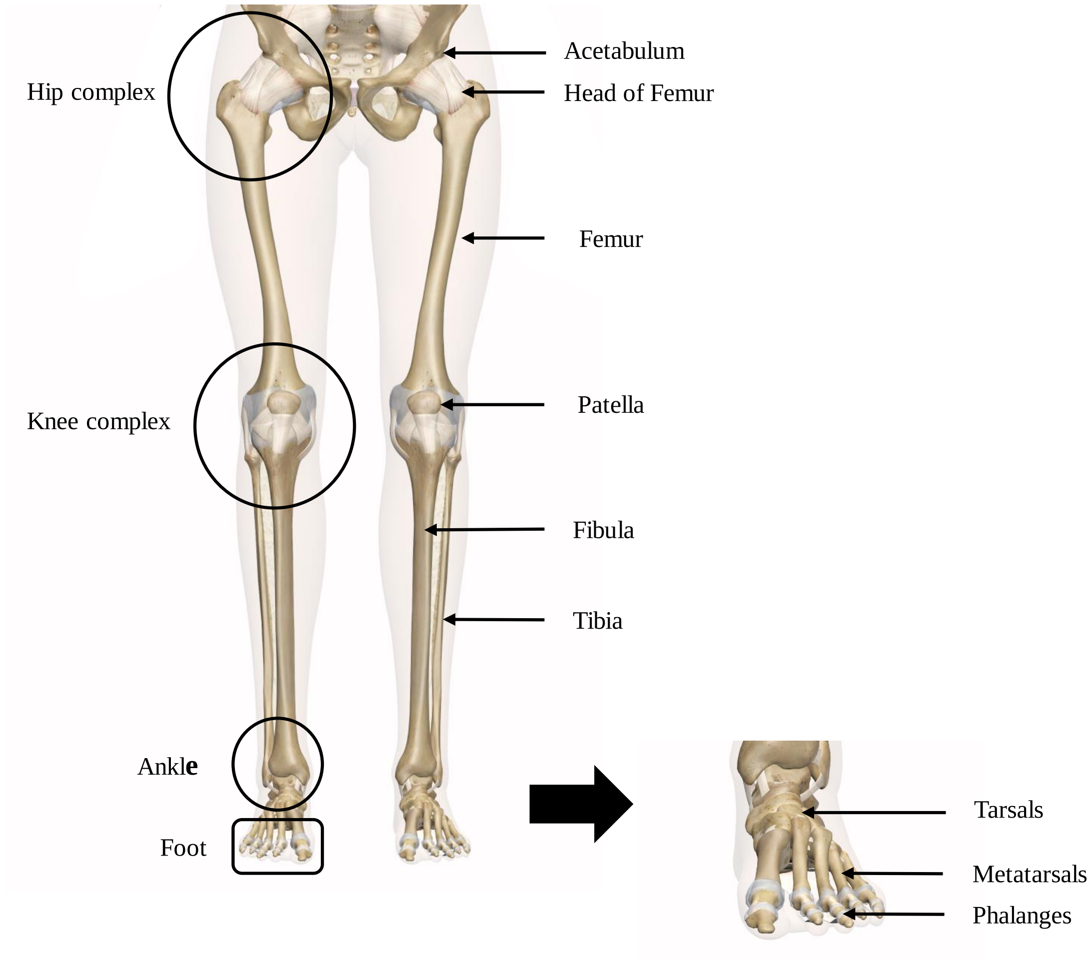

Figure B.1: The anterior view of the human lower limb.

articulating the femur's head and the pelvis's acetabulum. The other end of the femur bone is joined with two long bones, the tibia, and fibula, which build the knee complex. The patella bone in the complex serves as a knee cap in the joint. There are 26 bones in the foot complex: seven tarsals, five metatarsals, and fourteen phalanges. The ankle complex is formed by the end of the tibia and fibular bones with talus bone [12]. [see figure B.1] The hip complex has 3 degrees of freedom (DoF) motions: extension/flexion, abduction/adduction, and medial rotation and lateral rotation [see figure 2.2]. Table 2.1 shows the rage of motions (ROM) of the hip complex [13].

Figure B.2 shows the knee complex and ankle patterns of motions. The knee

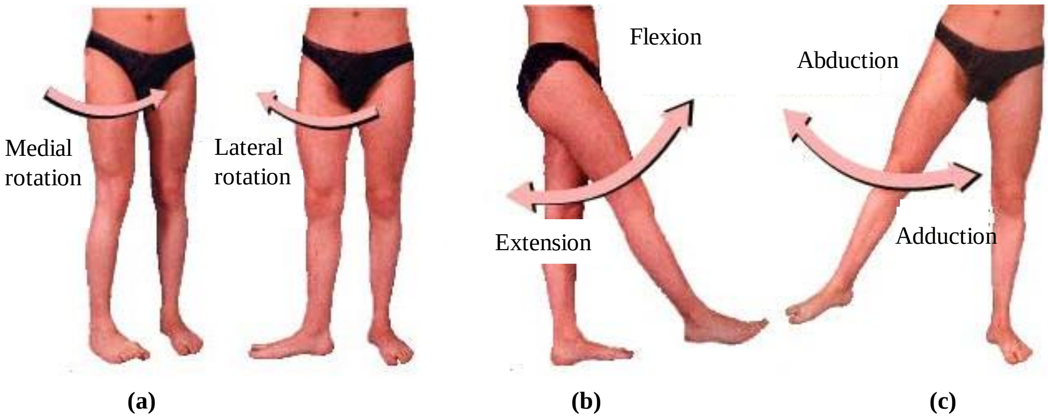

Figure B.2: Motions of the hip: (a) hip medial rotation/lateral rotation, (b) hip extension/flexion, (d) hip abdution/aduction.

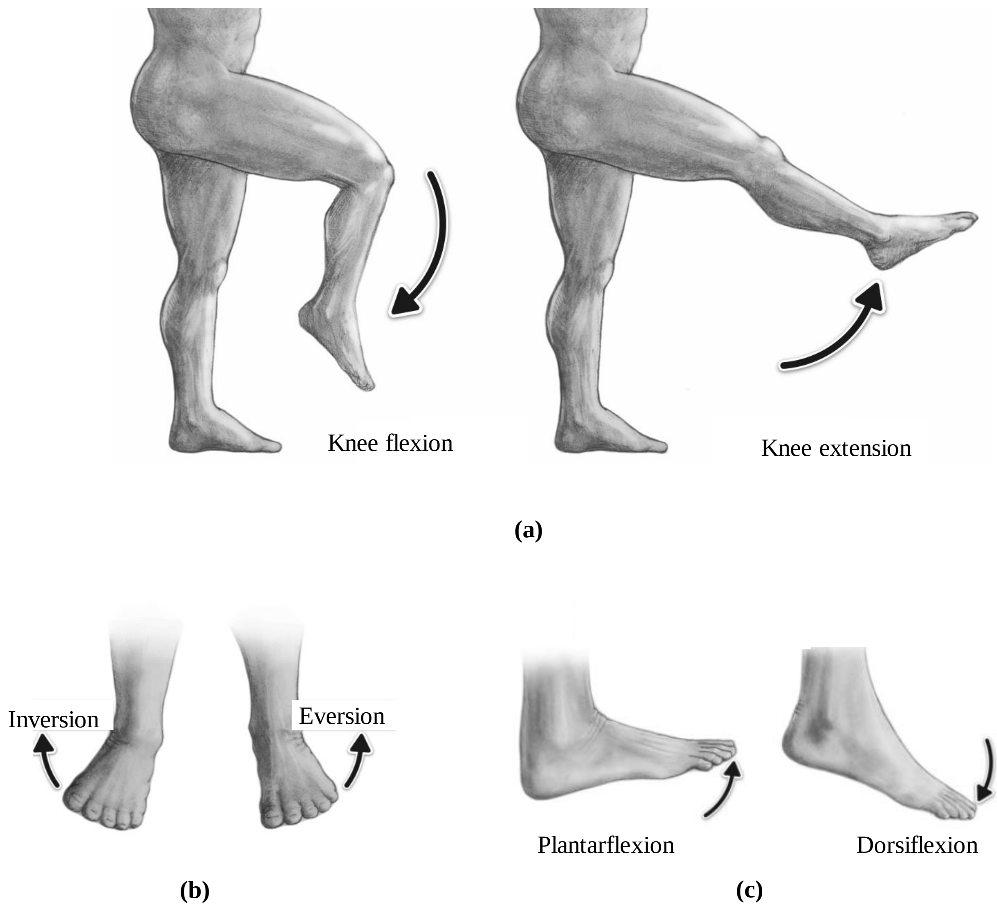

Figure B.3: Motions of the knee and ankle: (a) knee flexion/extension, (b) Inversion/eversion, (d)Plantarflexion/dorsiflexion.

Table B.1: ROM of the human hip complex [13]

Motions of Hip	**ROM**
Extension	9.5°
Flexion	120.4°
Abduction	38.4°
Adduction	30.5°
Medial Rotation	32.5°
Lateral Rotation	33.7°

complex can be considered as only 1 DoF joint. The ankle joint has two DoFs. The ROM angles of the knee complex and the ankle are summarized in table 2.2. The amplitudes of motions of the left and right joins were approximately similar [13].

The human body weight-bearing and locomotion are the primary functions of the human lower limbs. Moreover, dynamic and static pose (position + orientation) and balance of the human maintain by the lower limb muscles and hip, knee, and ankle movements. The kinematic structure of the lower limb will be explained in the next section.

Kinematics of Lower Limb

Kinematics can be identified as an analysis of movements apart from the forces that cause the movements, which is essential for analyzing the lower limb's biomechanics. As explained in the previous section, There 3 DoF motions in the hip complex, 1 DoF motion in the knee complex, and 2 DoF motions in the ankle.

Table B.2: ROM of the human knee complex and ankle [13]

Motions	**ROM**
Knee Extension	143.7°
Knee Flexion	15.3°
Dorsiflexion	39.6°
Plantarflexion	27.9°
Eversion	−1.7°
Inversion	27.8°

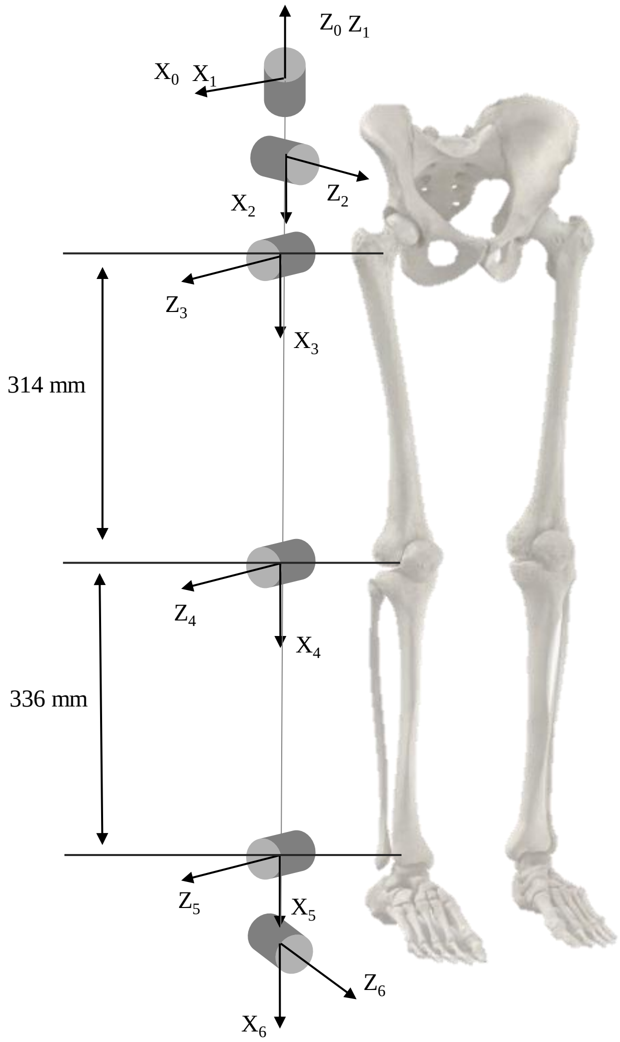

Figure B.4: Simplified human lower limb kinematic model of the lower limb

These motions can be represented as revolute joint motions [14]. In this section, the lower limb's kinematics are simplified and analyzed using DH (Denavit-Hartenberg) convention [see Figure 2.4].

The motion of the ankle (end effector) is represented concerning the base frame. Therefore, the hip represents the base of the kinematic model. The knee and the ankle coordinates frames are attached to the base frame ($[X_0, Y_0, Z_0]$). The $Z-axis$ is determined according to the right-hand rule of rotation of the$X-axis$ in the same reference coordinates system. Axes rotation of the hip medial rotation/lateral rotation, abduction/adduction, and flexion/exertion represented

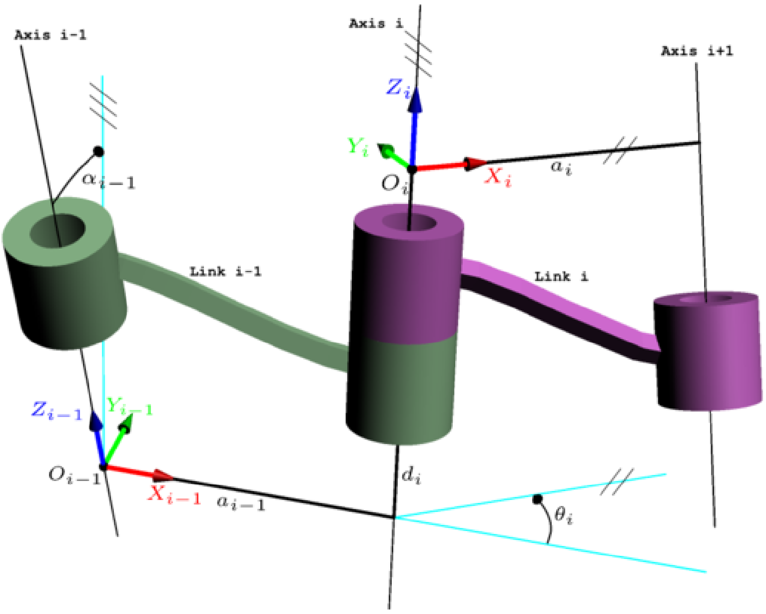

Figure B.5: Definition of D-H parameters. [1]

by Z_1, Z_2, and Z_3, respectively. The $X - axis$ is determined using the common perpendicular between the $Z - axis$ the $Z_{i+1} - axis$. The $Y - axis$ can be determined from the right-hand rule. The length of the femur and the tibia bones are extracted from [1].

There are four parameters in the D-H kinematic model: α_{i-1} (represents the angle between Z_{i-1} toZ_i measured about X_{i-1}), a_{i-1} (represents the distance from Z_{i-1} to Z_i along $X_i - 1$), d_i (represents the distance from $X_{i-1}$to X_i measured along with Z_i), and θ_i (represents the angle between X_{i-1} and X_i measured about Z_i)[refer Figure 2.5].

$$T_i^{i-1} = \begin{pmatrix} cos\theta_i & -sin\theta_i & 0 & a_{i-1} \\ sin\theta_i cos\alpha_{i-1} & cos\theta_i cos\alpha_{i-1} & -sin\alpha_{i-1} & -sin\alpha_{i-1} d_i \\ sin\theta_i sin\alpha_{i-1} & cos\theta_i sin\alpha_{i-1} & sin\alpha_{i-1} & cos\alpha_{i-1} d_i \\ 0 & 0 & 0 & 1 \end{pmatrix} \tag{B.1}$$

Table B.3: DH Parameters of human Lower Limb

Link	α_{i-1}	$a_{i-1}(mm)$	$d_i(mm)$	θ_i
1	0	0	0	θ_1
2	$-\pi/2$	0	0	θ_2
3	$\pi/2$	304	0	θ_3
4	0	314	0	θ_4
5	0	336	0	θ_5
6	$-\pi/2$	0	0	θ_6

DH matrix represents the transform from one coordinate frame to the next coordinated frame [see 2.1 equation]. There are six motion transformation matrices are given according to the simplified human lower limb model. These transformation matrices can be derived using the human lower limb model DH parameters given in table 2.3.

B.2 Lower limb Exoskeletons

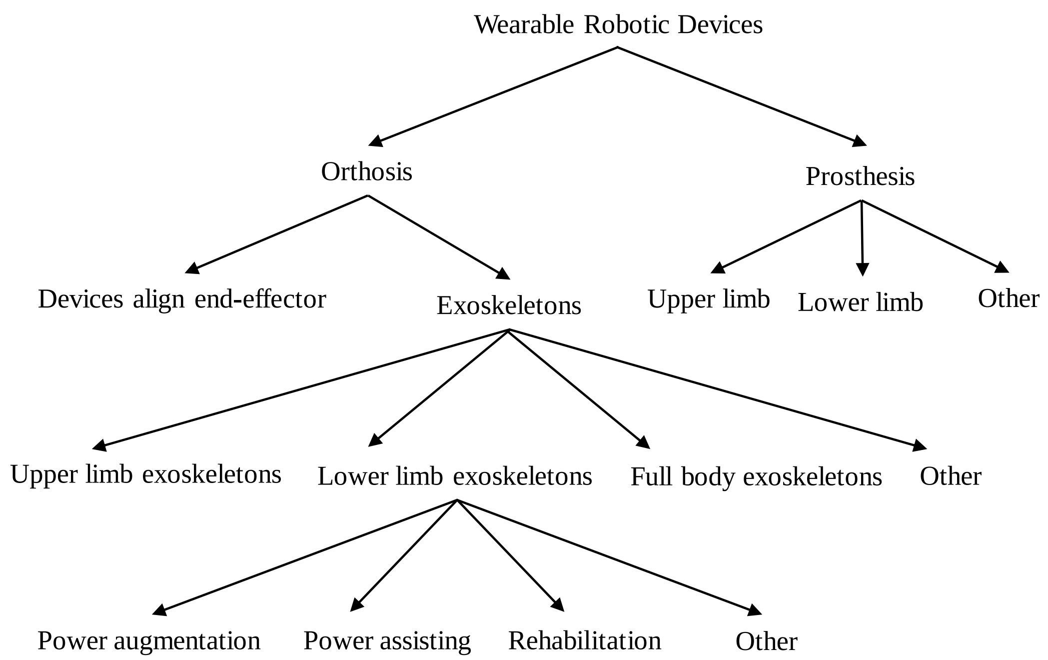

Figure B.6: Classification of lower limb exoskeletons based on the area of application.

The lower limb exoskeletons have been developed for various applications. In general, lower limb exoskeletons can be categorized into four different categories depending on their tasks: power augmentation, power assisting, rehabilitation and other purposes lower limb exoskeletons. The power augmentation lower limb exoskeletons that are made for the lift or carry heavy loads of a healthy wearer. The power assisting lower limb exoskeletons provided further assistant and capacity to wearers locomotions. The rehabilitation lower limb exoskeletons are used for rehabilitation purposes for lower limb disability people. The other purposes exoskeletons are used for various purposes like as entertainment, virtual reality(VR) and simulations [15]. [see figure 2.6].

Since lower limb exoskeletons have been developed for various locomotions, these lower limb exoskeletons can be classified further depending on the wearer's attachment locations: Trunk-Hip-Knee-Ankle-Foot(THKAF) exoskeletons, Trunk-Hip-Knee (THK) exoskeletons, Hip-Knee-Ankle-Foot exoskeletons (HKAF), Hip-Knee (HK) exoskeletons, Knee-Ankle-Foot (KAF) exoskeletons and single joint lower limb exoskeletons [See figure 2.7]. To understand the mechanical designs and HRI, recently developed lower limb exoskeletons are described in this section [16].

B.2.1 Trunk-Hip-Knee-Ankle-Foot (THKAF) exoskeletons

The THKAF exoskeletons are mainly designed to stable the trunk and hip region of the human lower limb. Moreover, these exoskeletons are used to rehabilitate paraplegic subjects and the power augmentation of healthy people to carry external loads.

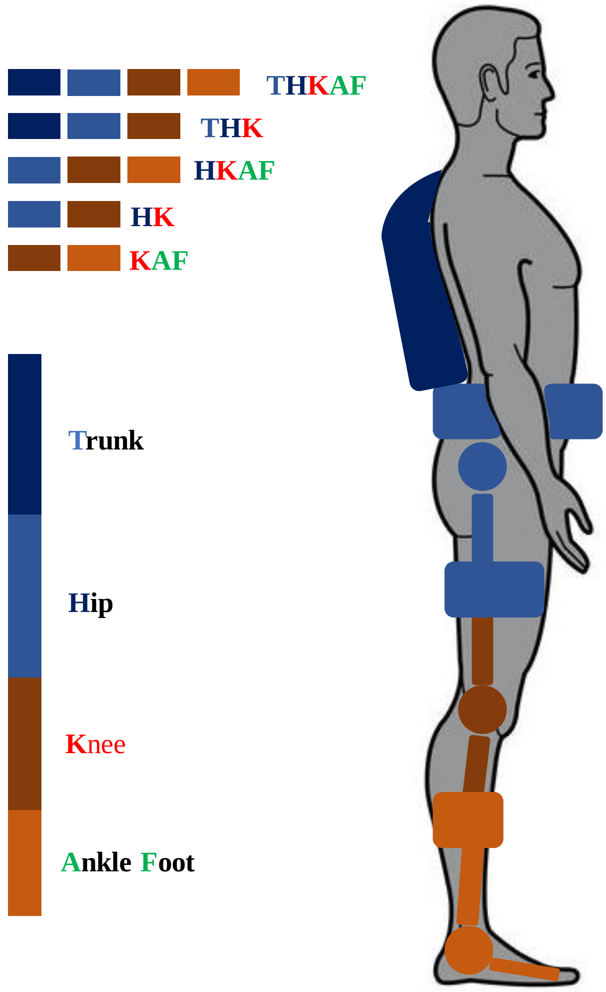

Figure B.7: Classification of lower limb exoskeletons based on wearer's attachment locations

Berkeley Lower Extremity Exoskeleton (BLEEX)

The BLEEX is the first lower limb exoskeleton capable of carrying an additional load. This device contains anthropomorphically designed two legs platforms that are driven by linear hydraulic actuators. Furthermore, It can perform seven DoFs motions per leg to augment human locomotions. The seven DoFs consist of hip flexion/extension, hip abduction/adduction, knee flexion/extension and ankle dorsiflexion/plantarflexion powered motions and other passive motions [17, 18]. [See figure 2.8 (a)]

Body Extender (BE)

The BE is a full-body exoskeleton developed by the PERCRO laboratory. This exoskeleton is designed explicitly to enhance human strength to handle heavy objects. Furthermore, the BE can perform twenty-two DoFs motions while the entire weight of the system is transferred through legs to the ground [19]. [See figure 2.8 (b)]

MIT Exoskeleton

The MIT exoskeleton is designed for reducing the metabolic cost by harnessing the metabolic payload forces. This exoskeleton consists of variable damper mechanisms for hip and knee joints and passive springs for ankle joint. Furthermore, In the evaluation experiments, it is observed that up 90% of the carrying payload can be transferred to the ground [20]. [See figure 2.8 (c)]

HUALEX

HUALEX (Human Power Augmentation Lower Exoskeleton) has been developed with ten DoFs for power augmentation purposes. Each DoFs having a revolute joint where knee and thigh joints are active with DC motors. Furthermore, These actuated joints are designed with multilink pendulums, which are parallel to the shank and thigh [21]. [See figure 2.8 (d)]

MINDWALKER

This exoskeleton has actively controlled hip abduction/adduction, which is essential for dynamic balance in the human stand and walks. In addition to powered hip abduction/adduction, hip flexion/extension and knee flexion/extension powered with series elastic actuator joints. Moreover, This exoskeleton can be used on healthy and paraplegic subjects [22, 23]. [See figure 2.8 (e)]

EksoNr

EksoNr is the first commercially available exoskeleton cleared by the United States food and drug administration (FDA) for rehabilitation purposes. In this exoskeleton, other than using powered actuators, Function Electrical Stimulation (FES) uses a method called Function Electrical Stimulation (FES) to create artificial muscle contractions in the rehabilitation patients. However, mechanical design and actuator categories are not mentioned in the literature [24]. [See figure 2.8 (f)]

BioComEx

Biomimetic compliant lower limb exoskeleton robot (BioComEx) has active hip, knee and ankle joints. The series of elastic actuators powered the knee and the hip joints the same as MINDWALKER exoskeleton and the ankle joint performs as variable stiffness actuators. Furthermore, load cells (force sensors) were attached to measure interaction forces for developing modular forced algorithms [25]. [See figure 2.8 (g)]

CHPU

CHPU stands for the compact hydraulic power unit. Unlike most of the powered lower-limb exoskeletons, this exoskeleton proposed a two-stroke internal combustion engine for the power source. Moreover, this unit has a high power-to-weight ratio, which can be easily integrated into a wearable robotic design. However, the dynamic model of this device was only validated by the prototype test [26]. [See figure 2.8 (h)]

XoR2

The hybrid drive exoskeleton robot (XoR2) is designed with pneumatic muscles and electric motors by arranging an optimal strategy to get the necessary motions. XoR2 is an improved version of XoR. Furthermore, this exoskeleton developed with fourteen joints along with six powered joints. Primarily experimental results show that XoR2 can support up to 30 kg of additional weight [27].[See figure 2.8 (i)]

Anthro-X

Anthro-X lower limb exoskeleton is developed by Bionics laboratory, University of Moratuwa. This exoskeleton supports five DoFs per limb while hip and knee joints are powered, and a novel articulated joint mechanism for the hip joint. Furthermore, a unique mechanism based on the four-bar linkage system supports the knee joint's polycentric motion [28]. [See figure 2.8 (j)]

B.2.2 Hip-Knee-Ankle-Foot (HKAF) exoskeletons

Hip-Knee-ankle-foot (HKAF) exoskeletons are the same as Knee-ankle-foot (KAF) exoskeletons except for the hip connection. These devices are designed for free or locking hip flexion/extension and abduction/adduction movement.

The hybrid assistive limb (HAL) is an HKAF exoskeleton, developed by Tsukuba University and Cyberdyne company, Japan. The flexion/extension of the hip and knee joints are powered with actuators while dorsiflexion/plantarflexion of the ankle is passive [29] [See figure 2.9 (a)]. Wearable walking helper (WWH) is another HKAF exoskeleton that supports human locomotions. This exoskeleton can compensate the gravity forces by harvesting the torque obtains from the locomotions. Furthermore, this device supports lower-limb muscles without using biological signals [30]. Another novel lower limb motion assist exoskeleton has been developed by He and Kiguchi for locomotion assistance. This device has a passive ankle joint and the hip and knee joints are passive [31].

Figure B.8: Trunk-Hip-Knee-Ankle-Foot (THKAF) exoskeletons: (a) Berkeley Lower Extremity Exoskeleton (BLEEX) [17, 18] , (b) Body Extender (BE) [19], (c) MIT Exoskeleton [20], (d) HUALEX [21], (e) MINDWALKER [22] (f) EksoNr [24], (g) Biomimetic compliant lower limb exoskeleton robot (BioComEx) [25], (h) CHPU [26], (i) Hybrid drive exoskeleton robot (XoR2) [27] and (j) Anthro-X [28]

Walking Power Assist Leg (WPAL) is another novel HKAF exoskeleton for assistive purposes. WPAL supports three DoFs for the hip joint and one DoF per the knee joint, ankle joint, and metatarsophalangeal joint [32, 33] [See figure 2.9 (b)]. In other exoskeleton research work, H2 exoskeleton was developed for stroke rehabilitation patients. This device can support 1.50 m to 1.95 m range height and up to 100 kg of body weight adults. Furthermore, this device has actuated hip, knee, and ankle joints [34, 35] [See figure 2.9 (c)].

B.2.3 Trunk-Hip-Knee (THK) exoskeletons

Trunk-Hip-Knee (THK) exoskeleton devices can support the human trunk, hip, and knee motions and orientations. Zhang and Hashimoto developed a walking support exoskeleton suit with actuated hip and knee joints in this category [36]. ReWalkTM is another THK exoskeleton developed for paraplegic users. This exoskeleton has a wrist pad controller to power the daily locomotions [37] [See figure 2.9 (d)] . ALEX-I (Asian Institute of Technology (AIT) leg exoskeleton -I consist of twelve DC motors to achieve three DoFs at the hip, one DoF at the knee, one DoF at the knee, and two DoFs at the ankle joints [38, 39].

B.2.4 Hip-Knee (HK) exoskeletons

A treadmill-based HK exoskeleton has been developed by Tagliamonte et al. for assisting human locomotions. The flexion/extension movements of the hip and knee joints are active in the exoskeleton—the exoskeleton bear's whole weight by the external treadmill system [40]. Exoskeleton for Patients and the Old by the Sogang University (EXPOS) designed with an external walking support system that can support heavy electrical components. Furthermore, the exoskeleton device hip and knee joints were powered by tendon connecting motors and pulleys [41] [See figure 2.10 (a)].

(a) (b) (c) (d)

Figure B.9: Hip-Knee-Ankle-Foot (HKAF) and Trunk-Hip-Knee (THK) exoskeletons: (a) Hybrid assistive limb (HAL) [29], (b) Walking Power Assist Leg (WPAL) [32], (c) H2 exoskeleton [34, 35], and (d) ReWalkTM [37]

In another research work, Vanderbilt et al. HK orthosis was designed to rehabilitate spinal cord injury subjects. This device supports four motion modules: standing, right forward, left forward and sitting with the hip and knee flexion/extension motions [42] [See figure 2.10 (b)]. Another powered HK exoskeleton has been developed to support sit-to-stand, walking, and stand-to-sit for spinal cord injury patients by actuating the hip and knee joints [42]. A further, ABLE powered HK exoskeleton is developed for performs three significant functions: lower limb exoskeleton assistance, maintaining balance with the wearer's crutches, and assisting the left and right moving platform movements. These functions can be achieved from moving in a standing position, standing up from a chair, and stair climbing motions from the device [42] [See figure 2.10 (c)]. Moreover, a commercially available HK exoskeleton has been developed by Beltforte et al. with a pneumatic actuation system to assist hip and knee flexion/extension movements [43] [See figure 2.10 (d)].

B.2.5 Knee-Ankle-Foot (KAF) exoskeletons

Knee- Ankle-Foot (KAF) exoskeletons support the knee joint while the rest of the lower limb maintains a proper motion for the wearer. A KAF exoskeleton device developed by Yeh et al. with pneumatic muscles actuators. This exoskeleton consists of powered the knee flexion/extension and passive ankle joint [44] [See figure 2.10 (e)]. Another KAF exoskeleton has been developed by Sawicki and Ferris [45] by modifying the KFO device of Kao et al. This device supports ankle dorsiflexion/plantarflexion and knee flexion/extension. Chen et al. developed a KAF exoskeleton device by using ball bearing attachments. This exoskeleton is designed for rehabilitation purposes [42] [See figure 2.10 (f)].

These multi-joint exoskeleton devices are grouped in table 2.4 according to three major types: power assisting exoskeletons, rehabilitation exoskeletons, and power augmentation exoskeletons. Power assisting exoskeletons are generally used to help wearers who cannot perform daily tasks due to muscle weakness, injuries, or diseases. Rehabilitation exoskeletons are developed to recover the limb motions abilities, and strength. This rehabilitation can be done by continuous limb motions with exoskeletons while gradually decreasing the power assistance. Lastly, power augmentation exoskeletons are used to increase wearer's muscle strength for carrying external loads. Apart from other exoskeletons, These exoskeletons are mainly designed for healthy subjects who need to amplify the strength and endurance such as military and industrial workers [42].

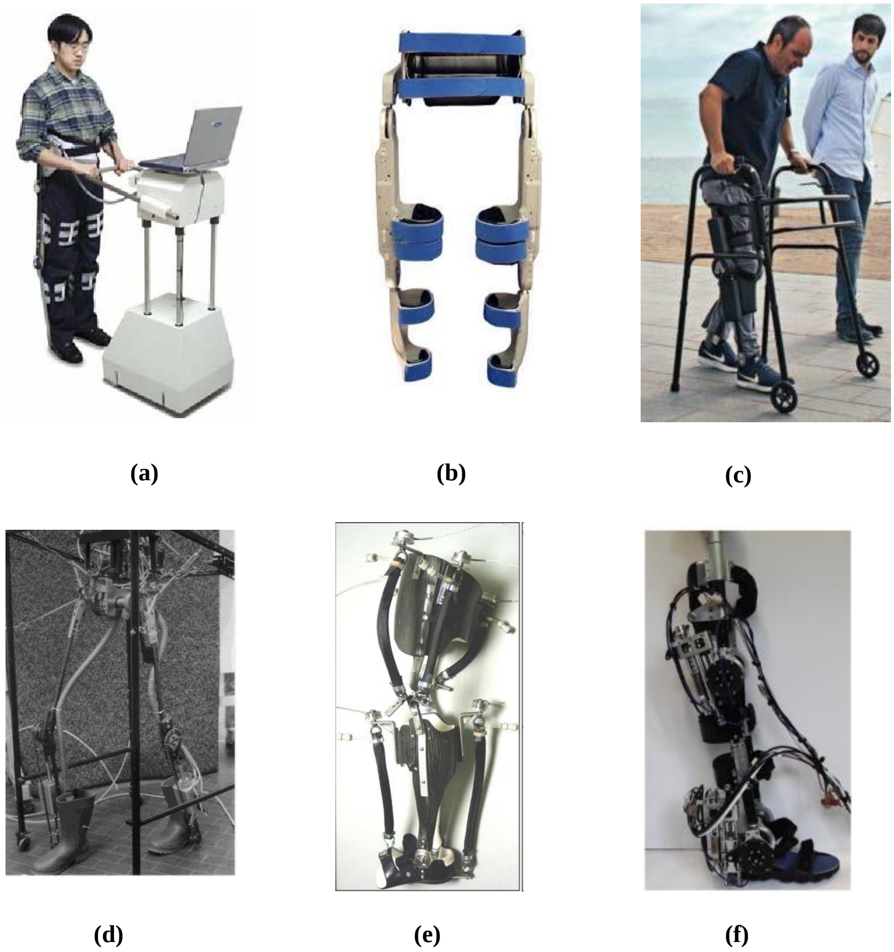

Figure B.10: Hip-Knee (HK) and Knee-Ankle-Foot (KAF) exoskeletons: (a) Exoskeleton for Patients and the Old by the Sogang University (EXPOS) [41] , (b) Vanderbilt HK orthosis [42], (c) ABLE, [42] (d) Pneumatic active gait orthosis by Belforte et al. [43] , (e) Pneumatic muscles orthosis by Yeh et al. [44], and (f) exoskeleton developed by Chen et al. [42]

Table B.4: Classification of multi-joint exoskeletons

Multi-joint Exoskeleton	**Power Assisting exoskeleton**	**Rehabilitation exoskeleton**	**Power Augmentation exoskeleton**
THKAF	MINDWALKER [22], BioComEx [25],	XoR2 [27],	BLEEX [17, 18], BE [19], HUALEX [21], CHPU [26], MIT Exoskeleton [20], EksoNr [24]
HKAF	WWH [30], WPAL [32], Lowerlimb motion assist exoskeleton by He and Kiguchi [31]	HAL [29], H2 robotic exoskeleton [34, 35]	N/A
THK	ReWalk™ [37]	ALEX-I [[46]]	N/A
HK	EXPOS [41], Vanderbilt HK orthosis, ABLE, Pneumatic active gait orthosis by Belforte et al. [43]	lower limb powered exoskeleton robot Wu et al. [42] ,	Lower-limb exoskeleton by Tagliamonte et al. [40]

B.2.6 Single joint exoskeletons

There are major single joint lower exoskeletons: hip exoskeletons, knee exoskeletons, and ankle foot exoskeletons [46]. Functions of these joints vary from each different locomotions. As an example, knee joint acts differently for each of the walking stages. When the leg is in the swing stage, knee joints act as a damping free joint, and in the stance phase, it acts as a locked joint.

Hip exoskeletons

Lower Extremity Powered Exoskeleton (LOPES) is a treadmill mounted hip exoskeleton. This exoskeleton consists of actuated hip flexion/extension and abduction/adduction motions [47] [See figure 2.11 (a)]. Active Leg Exoskeleton (ALEX II) is also a treadmill mounted hip exoskeleton with powered hip flex-

Figure B.11: Hip, knee and ankle-foot exoskeletons: (a) Lower Extremity Powered Exoskeleton (LOPES) [47], (b) Active Leg Exoskeleton (ALEX II) [48], (c) Powered Knee Orthosis (PKO) [49], (d) RoboKnee [50], (e) Stance control knee–ankle–foot orthosis (SCKAFOs) [51], (f) Knee extension assist (KNE) [52], (g) MIT robotic knee [53], (h) Stewart-platform-type AFO [54], and (i) The active ankle-foot orthosis (MIT AAFO) [55].

ion/extension motion [48] [See figure 2.11 (b)]. Olinger developed a single DOF exoskeleton hip exoskeleton for support hip joint swing phase by acquiring the hip flexors' power .

Knee exoskeletons

Powered Knee Orthosis (PKO) is designed to assist gait disorder patients to achieve regular locomotions. This device consists of the active knee joint, where the joint motion pattern developed based on the human walking data [49] [See figure 2.11 (c)]. RoboKnee has been developed with linear series elastic actuators connected with thigh and shank braces to support the knee joint [50] [See figure 2.11 (d)]. Stance control knee–ankle–foot orthosis (SCKAFOs) is another knee exoskeleton designed to assist poliomyelitis patients. When the patient's affected leg in mid-swing, the device supply flexion torque to help the locomotion [51] [See figure 2.11 (e)]. Spring et al. designed knee extension assist (KNE) exoskeleton using spring and pneumatic actuators to assist sit-to-stand motion. The wearer's weight is stored in the spring when the user tries to sit from the stand position. Afterward, the knee extension motion is powered by pneumatic muscle and loaded springs [52][See figure 2.11 (f)]. MIT robotic knee is another quasi-passive exoskeleton developed to assist running. This device consists of a passive spring to power the knee joint [53] [See figure 2.11 (g)].

Ankle Foot exoskeletons

The University of Michigan developed an ankle-foot orthosis (AFO) with two pneumatic actuator muscle for the ankle dorsiflexion/plantarflexion motion . Another AF exoskeleton has been designed with the Steward platform method with six linear actuators to support the ankle. Each actuator is attached between the leg and footplates [54][See figure 2.11 (h)]. The active ankle-foot orthosis (MIT AAFO) is designed with a series elastic actuator to assist the foot motions. Furthermore, this exoskeleton is specially developed for drop-foot patients [55] [See figure 2.11 (i)].

B.3 Human-Robot Interaction

Continuous development of exoskeletons (wearable robots) is essential to enhance the user experiences and wearable devices' performances. Therefore, human intentions and the comfort levels of wearable robots must be determined . In that context, human-robot interaction (HRI) should be studied. Cognitive human-robot (cHRI) interaction and physical human-robot interaction (pHRI) are the two main aspects of HRI [7].

B.3.1 Cognitive Human-Robot Interaction

cHRI involves the identification of complex human expression and physiological aspects. A human being's cognitive process has three major aspects: reasoning, planning, and executing a predefined goal. This information can be acquired and transmitted bidirectionally using a connection between humans and robots (human-robot cognitive interface). Therefore, new advanced smart sensors, actuators, and control strategies have been recently developed to gather and decode complex cognitive pieces of information.

Electroencephalogram (EEG), and electromyography (EMG) are the main sensing levels in cHRI. Electroencephalogram (EEG) is a method for identifying the electrical activity of the human brain [56]. These signals can be classified using both frequency and time domain parameters.

Electromyography (EMG)

Electromyography (EMG) is an electrodiagnostic technique for identifying the electrical activity produced by the muscles. EMG signals are generated by muscle cells when the cells are electrical or neurologically activated. These signals can be identified using an instrument called an electromyograph. There are two types of EMG signals: surface and intramuscular EMG signals. Surface EMG signals extract non-invasively from the surface of the muscle using surface electrodes. Intramuscular EMG signals extract by inserting needle electrodes into the muscles [57] .

In the biomechanics field, three applications dominate surface EMG signals' uses: an indicator of muscle activation initiation, identification of the force produced by a muscle, and an index of fatigue processes within a muscle. The EMG signal's causative factors are affected by the muscle's physiological, anatomical, and biochemical characteristics. Unlike the extrinsic factors, these cannot be controlled due to limited knowledge and technology [58].

B.3.2 Physical Human-Robot Interaction

pHRI involves evaluating physical quantities such as position, force, and pressure between humans and robots. The human skin consists of mechanoreceptors, which can be simulated by mechanical forces. These mechanoreceptors can identify pressure, touch, vibration, strain and tactile sensations. Pressure and tactile receptors can detect skin deformations, and these are located deeper in the skin. Mechanomyogram (MMG) and surface muscle pressure (SMP) are widely used for sensing pHRI. MMG can identify muscle activities by detecting micro-vibration on the skin [59]. The SMP can identify muscle volume and stiffness changes sensing the surface pressure [60].

pHRI is the most critical interaction between human and robots. Any physical interaction between robot and human must be soft and acceptable to the human body. Therefore, wearable robotics designs need to be considered particular design goals: safety, actuator performance, ergonomics and comfort, application of loads to humans, control strategies, and ease of use of the wearable robotic device [7].

Appendix C

DEVELOPMENT OF SURFACE MUSCLE PRESSURE MONITORING SYSTEM

As mentioned in previous sections, the lower limb exoskeleton's performances and usability depend on the effectiveness of HRI. Furthermore, inappropriate use of wearable robot interfaces will cause poor performance and musculoskeletal system pain and harm. Hence, it is crucial to study the pHRI between the wearer and robotic interface to develop wearable robotics. In the literature, SMP validated as pHRI analyzing method between robotic devices interface and wearer. Nevertheless, there are no conventional sensors for detecting SMP. This chapter describes the steps involved in developing pressure sensors for detecting SMP. Two sensor models were developed separately to achieve desirable measurements: force sensitive resisters based and pneumatic based sensor interfaces.

C.1 Force Sensitive Resistors Based Sensory System

Force sensitive resistors (FSR) are electrical sensors widely used to estimate contact pressure. These sensors detect the change in thin, flexible piezoelectric plate's electrical resistance as mechanical forces are applied. Due to versatility, thin structure, and market availability, they have been used to study muscle movement and gesture recognition tests. Hence, this subsection focused on developing an efficient method for detecting pHRI based SMP monitoring device.

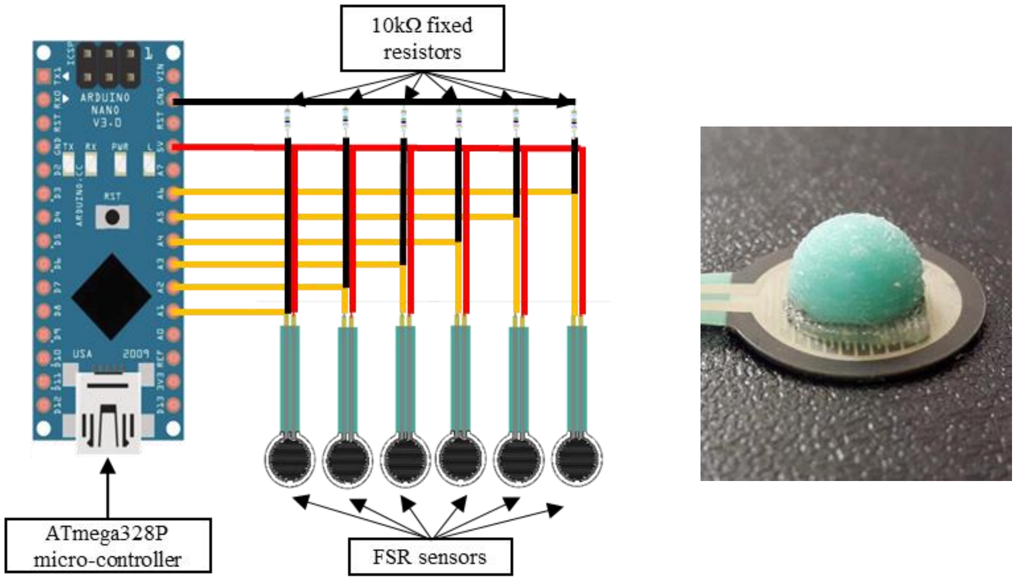

(a) (b)

Figure C.1: SMP sensory system: (a) Diagram of the sensory system , and (b) FSR sensor with a silicon button.

C.1.1 Design Concept

The FSR based SMP sensory system consists of FSR sensors and a microcontroller (ATmega328P) through a half-bridge circuit. There are six FSR sensors attached to the microcontroller with 10 $k\Omega$ fixed resistors to each sensor. In addition, each sensor consists of a measurement range of 50g – 10 kg of force [see figure 3.1. (a)]. Half-spherical silicone buttons with a diameter of 10 mm were mounted on the skin sensor interface to improve FSR sensors's sensitivity [see figure 3.1 (b)]. The selection of button geometry was based on a trial and error approach. Telemetry Viewer software has been used to process SMP results of this system.

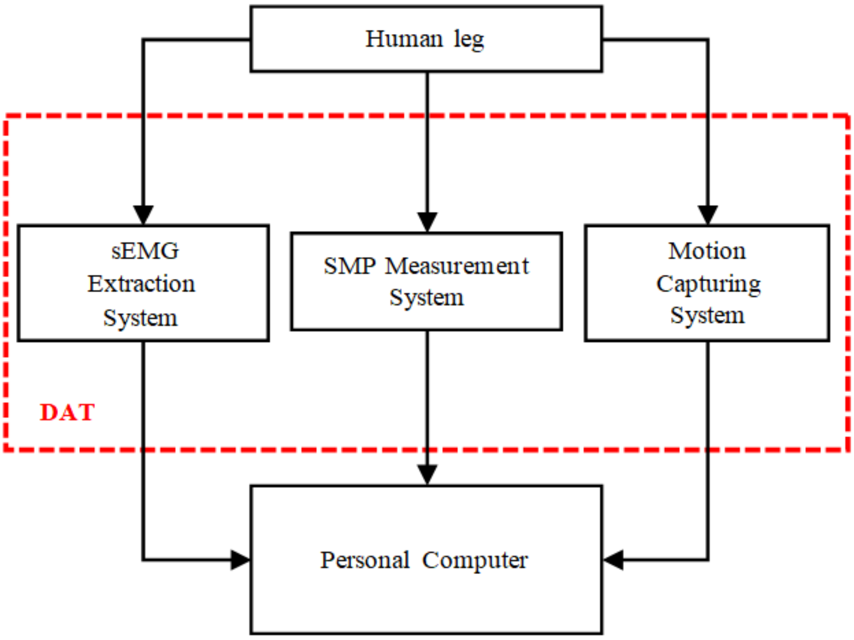

Figure C.2: Experimental setup: DELSYS Bangoli sEMG extraction system, SMP measurement system motion capturing system.

C.1.2 Experiment Setup and Protocols

In order to evaluate the SMP sensory system for pHRI acquisition, an experimental setup is proposed [see figure 3.2]. The experimental setup data acquisition tool (DAT) consists of three major parts: SMP sensory system, sEMG extraction system, and Motion capturing system. The SMP sensory system and the sEMG extraction system are used for obtaining lower limb muscle activities. The DELSYS Bangoli sEMG extraction device consists of a main amplifier with a ±5V output, an input module with 16 analog channels, and a wired sEMG electrode. The sEMG extraction system's main amplifier is connected to a personal computer via a data acquisition (DAQ) card, and DELSYS's EMGworks software is used to acquires and analyze the sEMG data [61]. The lower limb motions of the human subjects were captured using a motion camera (GOPRO Hero4). Then, KINOVEA motion analysis software is used to extract the motion analysis data.

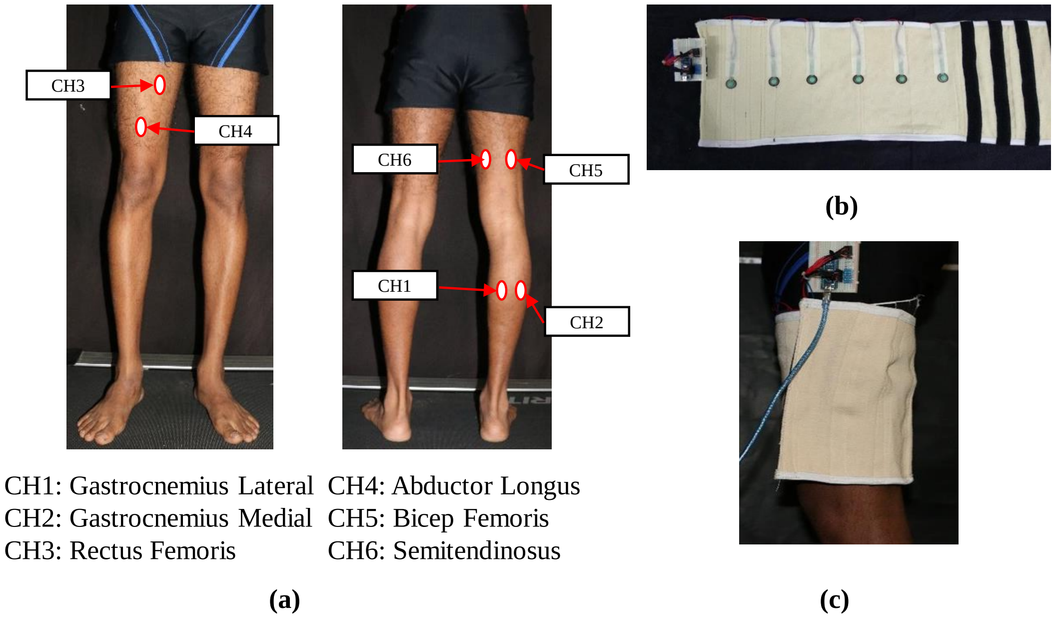

Figure C.3: SMP sensory system sEMG acquisition system attachments: (a) Attachment locations of sEMG electrodes, (b) SMP measurement system with FSR array, and (c) SMP measurement system placed on thigh.

The research was performed with 10 stable male subjects (age: 24±1 yrs, height: 168±5 cm, weight: 60±7) attached to the University of Moratuwa. All participants issued informed consent after clarification of the intent and technical details of the research. They were asked to respond to a questionnaire that included personal information and comfort experienced during the studies. Subjects with hypertension, diabetes, muscle injuries, musculoskeletal injuries, and medical problems were removed from the experiment. Subsequently, participants were directed to perform low-limb warm-up and stretching exercises to enhance the experiment results' quality.

In order to connect the sEMG electrodes to the muscle belly, The skins of the subjects were cleansed by rubbing alcohol to enhance electrical conductivity. Afterward, sEMG electrodes were connected to the lower lime muscles (CH1:Gastroscnemius Lateral, CH2: Gastroscnemius Medial, CH3: RectusFemoris, CH4: Abductor Longus, CH5: Bicep Femoris and CH6: Semitendinosus), and the reference electrodes were attached to an inactive muscle during the experiments (belly muscle) [see figure 3.3 (a)]. Then SMP sensors were attached to quadriceps muscles and hamstring muscles without interfering with the sEMG electrodes [see figure 3.3 (a), and (b)]. In the end, motion tracking markers were mounted on the expected axis of rotation of the hip, knee, and ankle joints.

After adding all the sensors and markers, the experimental procedure was started. Subjects have been advised to perform squats for 20 seconds. Every participant performed an average of seven squats for the 20-second time interval and was asked to follow the metronome in order to ensure a steady squatting pace. The experiment was repeated three times for each subject, and one minute recovery time was given.

The collected raw sEMG signals were post-processed using the root mean square (RMS) averaging technique. It is a widely used feature extraction technique for sEMG signals in the time domain[]. The RMS values of the captured SEMG signals have been computed from the EMGworks program by DELSYS. The RMS of sEMG is calculated from the sample size of 100 (3.1).

$$RMS = \sqrt{\frac{\sum_{n=1}^{N} {x_n}^2}{N}} \tag{C.1}$$

Where RMS, xn and N are channel RMS n (n=1,2..), channel n raw EMG, and sample size, respectively. The squatting moves were analyzed using KINOVEA software by detecting the motion recognition markers. The angles of the knee can be determined as (3.2).

$$ANG = \arctan(\frac{y_2 - y_1}{x_2 - x_1}) + \arctan(\frac{y_3 - y_1}{x_3 - x_1}) \tag{C.2}$$

Where ANG is the angle of the knee and (x1, y1), (x2, y2), (x3, y3) are the relative coordinates of Cartesian over the sagittal plane of the hip, knee and ankle

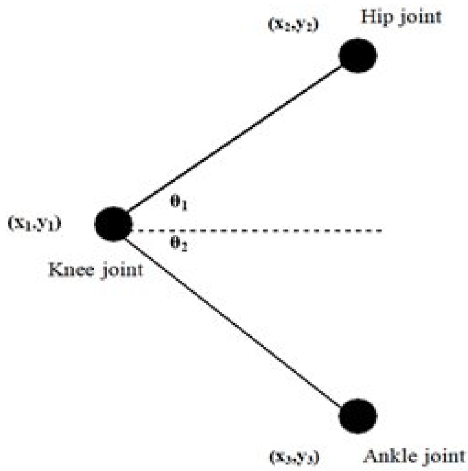

Figure C.4: Angular deflection of knee using cartesian coordinates of hip, knee and ankle joints

joints. The SMP signal was analyzed using a MATLAB program and a band-pass filter was used to process raw data [see figure 3.4].

C.1.3 Experimental Results and Discussion

In order to evaluate muscle activities, SMP , sEMG, and knee angle graphs were plotted against each other during the squatting motion. sEMG signal variations for different muscles were also plotted separately to identify the variability between test subjects. The correlation between the SEMG signal level, the SMP signal level, and the knee angle during squatting is shown in figure 4.5. Note that consistent flexion and extension magnitudes were found during squatting exercises for all subjects of hip, knee, and ankle joints.

The knee angle range of motion was measured to be between 58^0 and 180^0. During squatting, gastrocnemius lateral, gastrocnemius medial, rectus femoris, bicep femoris, abductor longus, and semitendinosus muscles were activated. sEMG peaks were recorded for each squatting period, and an average of seven squatting cycles every 20 second time frame was recorded. SMP amplitudes were measured for each squatting cycle in the same manner as the sEMG signals (sensor 1, sensor

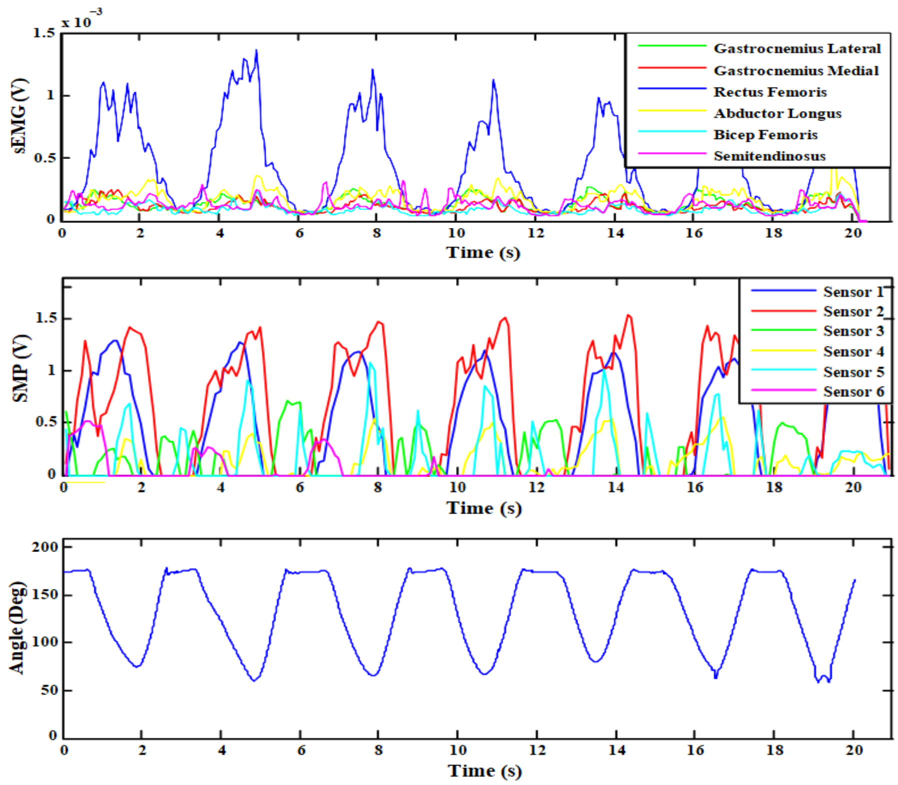

Figure C.5: sEMG, SMP and Knee Angle for seven squatting cycles

2 and sensor 3 measured quadriceps and sensor 4, sensor 5 and sensor 6 measured ham-string muscles). In addition, when the sEMG signals displayed no significant differences, the hamstring SMP amplitudes reached peak values (sensor 3, sensor 4 and sensor 5).

Figure 3.6 (a) and figure 3.6 (b) show the activation levels of the calf muscles (gastrocnemius lateral and gastrocnemius medial) in the squatting cycle. Generally, both muscles did not exhibit noticeable amplitude during the study, and there were no significant peak levels during the squatting cycle relative to the other lower limb muscles. Apart from that, these muscles remain active throughout the squatting period. Rectus femoris and abductor longus muscles exhibited significant sEMG signal amplitudes during the study [see figure 3.6 (c) and (d)].

sEMG signals in both muscles were significant for most participants during the

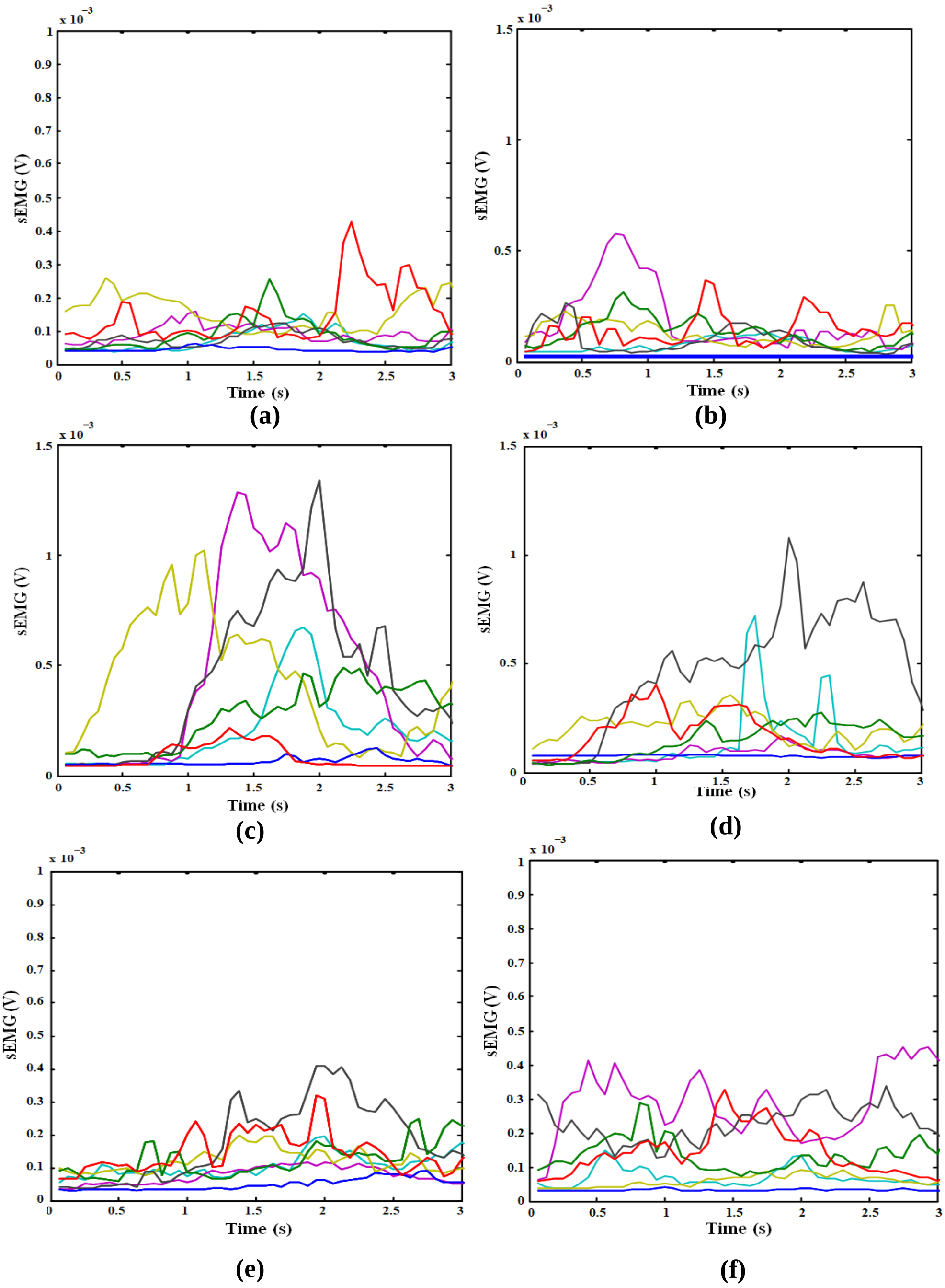

Figure C.6: (a) sEMG of grastrocnemius lateral for 10 subjects, (b) sEMG of grastrocnemius medial, (c) sEMG of rectus femoris, (d) sEMG of abductor longus, (e) sEMG of bicep femori, and (f) sEMG of semitendinosus for 10 subjects squatting cycle. Compared to the other lower limb muscle's signal amplitudes, the rectus femoris muscle displayed the highest amplitude. b Bicep femoris and semitendinosus muscles have the same behaviour as most of the lower limb muscles [see figure 3.6 (e) and (f)]. Bicep femoris muscle displayed a peak amplitude in a cycle. However, the semitendinosus muscle had no noticeable amplitude peak.

sEMG signals in both muscles were significant for most participants during the squatting cycle. Compared to the other lower limb muscle's signal amplitudes, the rectus femoris muscle displayed the highest amplitude. b Bicep femoris and semitendinosus muscles have the same behavior as most of the lower limb muscles [see figure 3.6 (e) and (f)]. Bicep femoris muscle displayed a peak amplitude in a cycle. However, the semitendinosus muscle had no noticeable amplitude peak. The subjects had different skin surface features, body fat level, muscle volume and capacity to perform squatting. Therefore, the signal amplitude of The sEMG and SMP derived from the same muscle varied for different subjects. For future studies, lower limb muscle volume and skin fat concentrations should be considered.

In this study, the lower-limb muscle functions were studied during squatting motion for ten young male participants. Instead of using a single muscle activity detection tool, a mixture of sEMG and SMP was suggested to determine muscle activity levels. In this analysis, time-domain features have been successfully derived from sEMG and SMP signals to analyze lower-limb muscle action. The relationship between lower limb muscle pHRI levels was analyzed. However, inconsistency, nonlinearity and lack of durability in the FSR results were identified in the experiment. Therefore, FSR based sensory system is not ideal for detecting pHRI between the robotic interface and the wearer.

C.2 Pneumatic Surface Muscle Pressure Sensory System

As deduced in subsection 3.1, the FSR-based sensory system can not produce consistent measurements to analyze human comfort levels. Hence, this section aimed to establish another effective method for detecting muscle function based on SMP monitoring. In the literature, pneumatic pressure measurement systems have been proposed to measure mini-scale pressure measurements, such as SMP. Unlike FSR sensors, Pneumatic pressure measurement devices have consistency, greater sensitivity and accuracy in measurements. Numerous pneumatic pressure sensors have been developed for the sensing of muscle movement. In addition, the sensor-human interface can be ergonomically built conveniently. Air pocket and air bladder versions The sensor-human interface presented in the studies. However, these sensors are only used for actuation and motion recognition purposes. Therefore, the sensor-human interface of the muscle contacting surface was reduced. Air bladder consisting of spiral-shaped air tubes was proposed in some of the studies. These sensor-human interfaces constrain the sensor's sensitivity due to spiral shape bladder. In order to overcome these facts, this section proposed a novel pneumatic sensory system for measuring SMP.

C.2.1 Design Concept

The SMP monitoring system was developed to detect the SMP of the muscles. Figure 3.7 shows the four main units of the system: a custom-made silicone pressurized air pouch (PAP), a pressure cuff (PC), a pneumatic pressure sensor (Honeywell ABPDANT005PGAA5) and a microcontroller (ATmega328P). The PAP is the sensor human interface. Its physical characteristics are approximately similar to natural human skin. This pouch has been sealed with compressed air and kept over the muscle surface's belly to monitor SMP variations. The PC is made out of a latex rubber bladder. It is attached over the silicone pouches around the limb segment to determine the overall changes of muscle form and volume.

(a) (b) (c) (d)

Figure C.7: Units of SMP monitoring system, (a) proposed pressurized air pouch (PAP), (b) pressure cuff (PC) (c) pneumatic pressure sensor, (d) microcontroller

Accordingly, the muscle movement can be identified during muscle contraction. As the muscle contracts, volume, stiffness and/or length of the muscle change based on the contraction type. These physical changes of the muscles affect the internal pressure of the PAP and PC. The pneumatic pressure sensors are placed on these units to detect and monitor SMP variations using the microcontroller.

The PC is responsible for applying consistent pressure across the limb segment, which response to variations in the limb's shape or volume during muscle contractions. As a result, PC monitors the global pressure changes. However, PAP captures changes in local pressure due to the interaction forces between the muscle belly and the PC. SMP variations for a given muscle are then determined by taking the difference between the internal PAP and PC pressures. The flexible PC allows the muscles more space to bulge as compared to a rigid cuff. In comparison, the pressure added to the human interface is homogeneously distributed; hence the device is ergonomically favourable.

A mathematical model is formulated to evaluate the behaviour of PAP silicone. Figure 3.8 displays both the schematic of the physical model and the simplified model. The silicone PAP's viscoelastic properties are expressed as a spring in the simplified model and two major assumptions considered. They are no inertia effects and no air leakage in the PAP. The absolute internal PAP pressure and

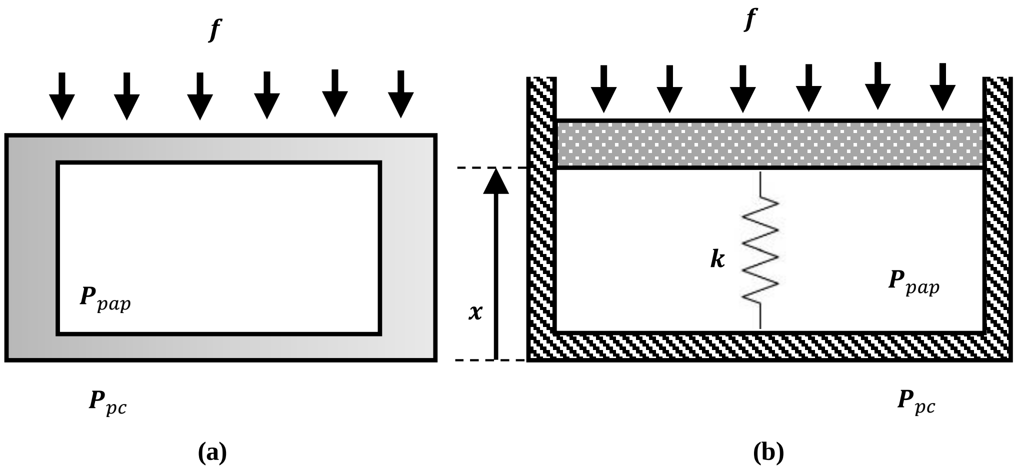

Figure C.8: Silicone pressurized air pouch (PAP), (a) physical model, (b) simplified model

the PC's PAP pressure were represented from Ppap and Ppc, respectively. The distribution of pressure over the PAP by the muscle belly is expressed as f. The forced equilibrium of the equation is expressed in (3.3).

$$P_{pap}A - P_{pc}A - k(x - x_0) - f = 0 \tag{C.3}$$

where, x_0 is initial height, x is deformed height, k is stiffness constant and A is effective area of the PAP. In, (1) P_{pc} and P_{pap} are measured by respective pressure sensors, and f is to be calculated. If the deformation is small $(x - x_0 \approx 0)$, then $k(x - x_0)$ can be neglected and determination of viscoelasticity characteristic is unnecessary. The ideal gas equation is given by (3.4).

$$P_{pap} = \frac{nRT}{Ax} \tag{C.4}$$

where parameters are described in table 3.1

Table C.1: Physical properties of air pouch

Property	Quantity
Effective cross-sectional area, A	$7.0686 \times 10^{-4}\ m^2$
Inside volume without deformed, Ax_0	$5.6549 \times 10^{-6}\ m^3$
The number of moles, n	$4.2075 \times 10^{-9}\ mol$
Universal gas constant, R	$8.3145\ m^3 PaK^{-1} mol^{-1}$
nRT at T=300K	$1.0494 \times 10^{-5}\ Pam^3$

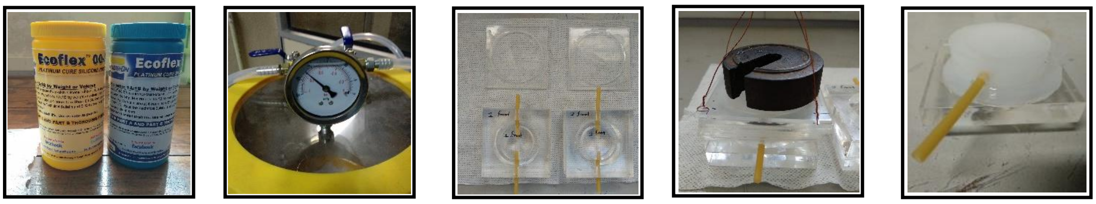

(a) **(b)** **(c)** **(d)** **(e)**

Figure C.9: Fabrication process of PAP, (a) Ecoflex-30 silicone material, (b) vacuum chamber, (c) perspex moulds, (d) PAP assembly, (e) final fabricated PAP

C.2.2 Fabrication Process

Ecoflex 30 Silicone material shown in figure 3.9 (a) has similar properties to human skin and is used to manufacture PAPs. The mixture of silicone content remained under zero atmospheric pressure for three minutes to obtain persistent, homogeneous, and air bubble-free silicone walls and diaphragms, as seen in figure 3.9 (b). As shown in figure 3.9 (c), the moulds were made of laser-cut perspex plates to ensure the PAP surface's smoothness. After extracting the air bubbles, the uncured silicone resin was poured into the moulds and left slightly cured for two hours. After then, half cured silicone PAPs and diaphragms were extracted from the moulds and glued together by adding external pressures as seen in figure 3.9 (d) for several hours. Then the 3 mm diameter flexible rubber tubes with air valves were connected to the PAPs, as shown in figure 3.8 (e). The PAPs were examined underwater to ensure airtightness. Subsequently, the pneumatic pressure sensors were mounted to the microcontroller using the Arduino-Nano module. The flexible PAP air tubes were attached to the barbed ports of the

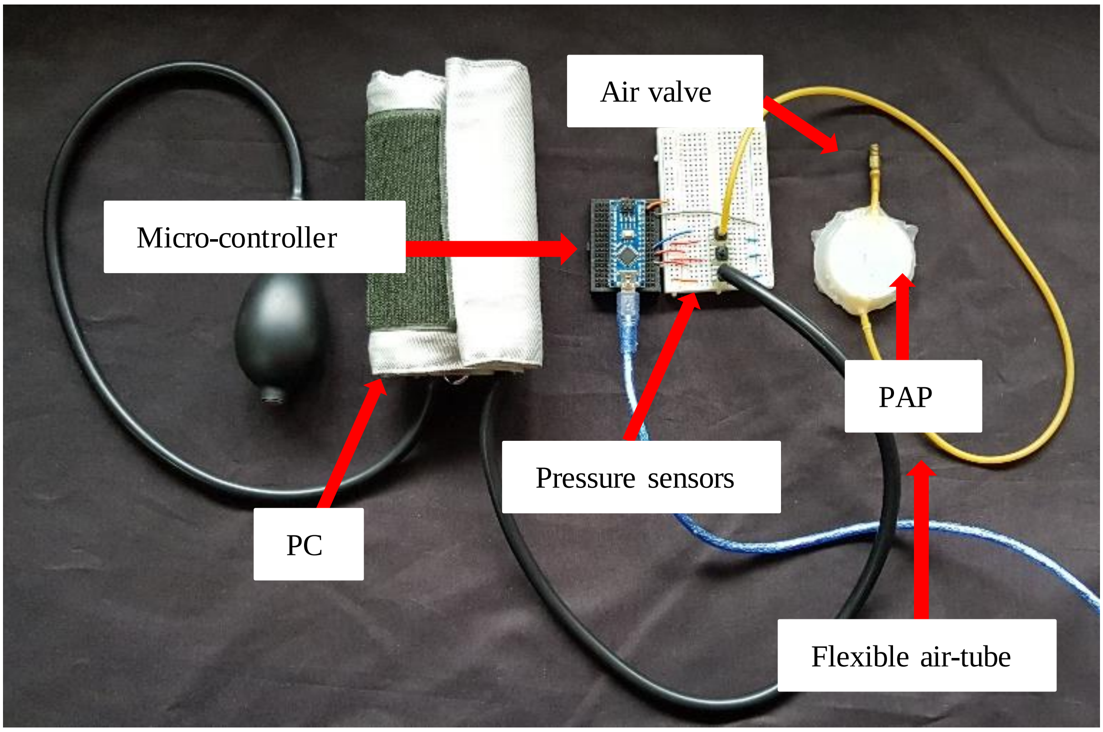

Figure C.10: Developed SMP monitoring system (PAP, PC, pneumatic pressure sensor and micro-controller

pneumatic pressure sensors. The completed SMP monitoring system is shown in figure 3.10.

C.2.3 Data Acquisition Tools and Protocols

The Data Equitation Tool (DAT) consists of two main subsystems. These are the SMP monitoring system and the sEMG extraction system, as shown in Figure 3.11. The hardware development of the device has been discussed in the previous section. The Telemetry software was used to acquire SMP data, and The DELSYS Bagnoli sEMG extraction system, was used for the extraction of sEMG. sEMG data were post-process using RMS feature extraction method. The research was performed with young, healthy male participants (age = 26y). Before the tests, the participant was instructed to conduct mild stretching exercises for the dominant arm. After stretching exercises, the skin's surface of the Bicep

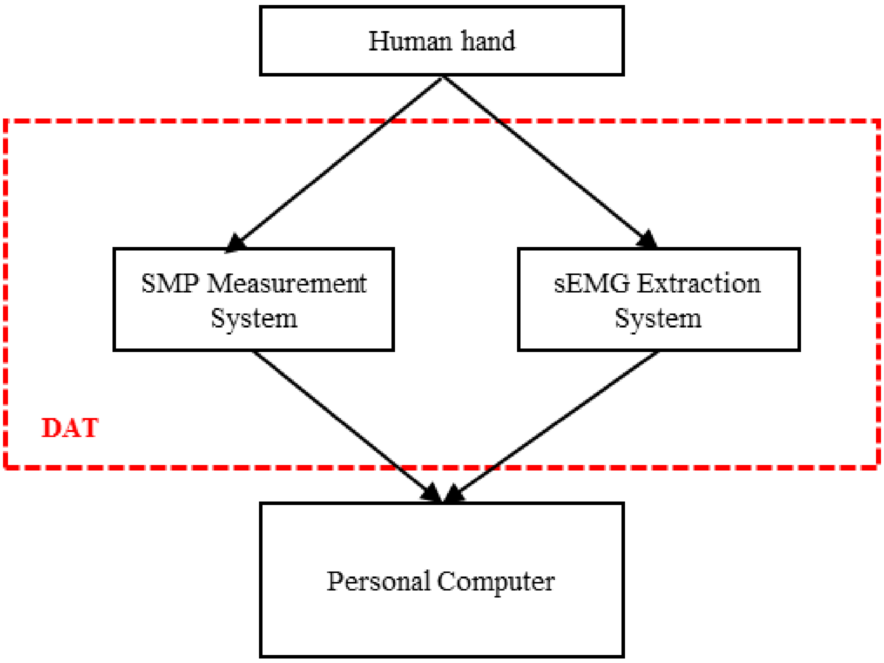

Figure C.11: Experimental setup (Developed SMP monitoring system and sEMG extraction system)

brachii and the Triceps brachii [see Figure 3.12 (a)] was wiped with a surgical spirit. PAPs and sEMG electrodes were then connected to the muscle, as shown in Figure 3.12 (b) where Sensor 01 on Biceps brachii and Sensor 02 on Triceps brachii. The reference SEMG electrode was applied to the skin's electrically inactive surface (the subject's belly). Later, the PC was mounted over the upper arm as shown in figure 3.12 (c). PAPs and PCs were pressurized to 20 mmHg. The subject was advised to synchronize with a 30 BPM monotrode to perform flexion/extension of the elbow joint for 10 cycles. The range of motion was limited to between 0^0 and 120^0. The tests were repeated three times without weight and with a 4 kg dumbbell in hand. Between each trial, one minute of recovery time was provided to prevent the symptoms of muscle fatigue

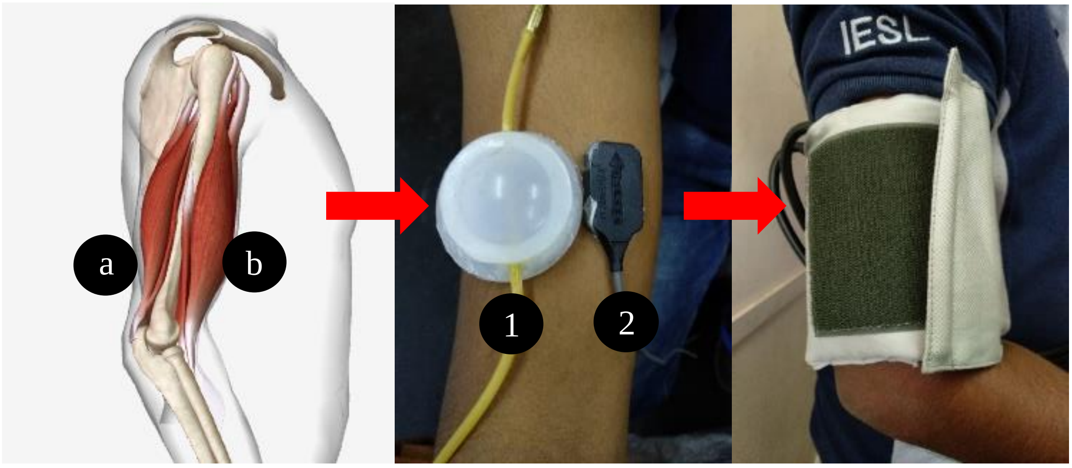

(a) **(b)** **(c)**

Figure C.12: Assembly of SMP monitoring system, (a) Triceps brachii - T and Biceps brachii - B, (b) PAP and sEMG electrode on Biceps brachii, (c) PC over the upper arm)

C.2.4 Experimental Results and Evaluation

Figure 3.13 shows the deformation of PAP silicone at different internal pressures (Ppap). It was measured using a Vernier caliper. The plotted cubic fit line can be represented using the (3.4).

$$y = A + Bx + Cx^2 + Dx^3 \tag{C.5}$$

The parameters are listed in table 3.2. The polynomial curve fits of the adjusted R-square values are closer to 1 (0.99987, 0.99713). As a result, it can be concluded that the curve fit was successful. In addition, the PAP silicon deformation is found to be linear with an internal pressure range of 10 to 30 mmHg

The fabricated SMP monitoring system was experimented with different forces for different internal pressures to determine the results of the variation (Ppap). As

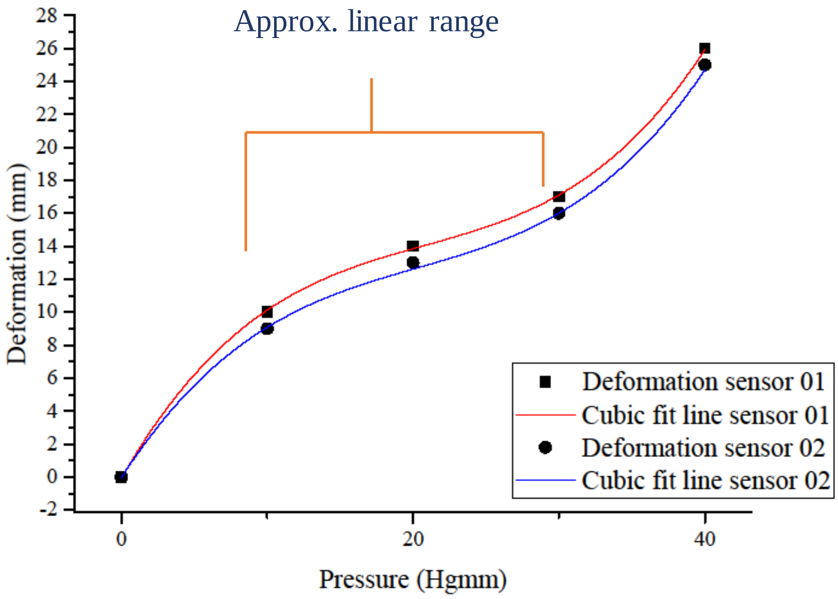

Figure C.13: Deformation of PAP for different internal pressures

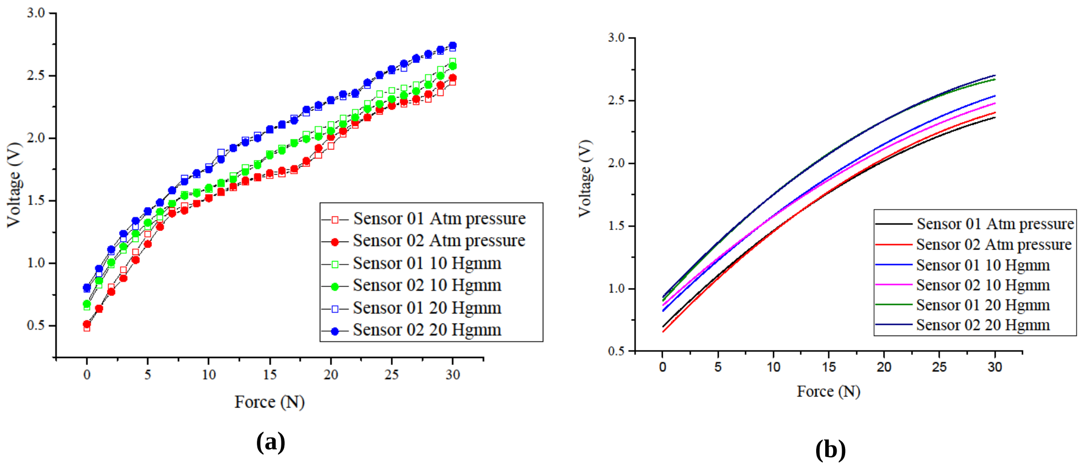

Figure C.14: Deformation of PAP for different internal pressures a result of nonlinear deformation, PAP was unable to measure more than 20mmHg of internal pressure. Thus, the applied force scale was 0 30N, and the internal pressure range was ambient pressure: 20mmHg. The findings were plotted in scattering chart [see Figure 3.14 (a)]. The output range is 0.48V 2.74V. Figure 4.14 (b) displays the polynomial plots for output results referring to the scattering graph. Sensor 01 and sensor 02 produce equivalent outputs. In fact, linear nature decreases with increasing pressure. Considering the findings of sensor 01 and sensor 02, the adjusted R-square values for 20 mmHg internal pressure are closer to 1 (0.99378, 0.99215). Therefore, the most reasonable internal pressure for the proposed PAP is 20 mmHg.

In order to evaluate the SMP monitoring system, SMP and sEMG variants were analyzed for the two separate test cases. In addition, the standard derivation of results is included in table 3.2. In the case without any weight in hand, the SMP and SEMG results for Biceps brachii during elbow flexion/extension are compared in figure 3.15 (a). Similarly, the results of Triceps bracii are shown in 3.15 (b) in the same evaluation condition. The peaks and valleys of the two graphs reflect the motion phases of the arm.. Sensor 01, attached to the Bicep brachii, indicated a higher amplitude than sensor 02, attached to the Triceps brachii. Similarly, the Bicep brachii sEMG signal amplitudes are more significant than the Triceps brachii sEMG signals. Therefore, SMP and sEMG signal amplitudes are well synchronized.

Figure 3.15 (c) and figure 3.15 (d) displays SMP and sEMG signals for test situations with a weight of 4 kg in hand. Variations in SMP and SEMG signals

Table C.2: Statistical Data of Deformation Curve Fits

Parameters	**Value (S1 and S2)**	**Standard error (S1 and S2)**
A	-7.92E-2, -4.24E-2	3.89E-1, 4.88E-1
B	1.54, 1.37	7.79E-2, 1.24E-1
C	-6.24E-2, -5.51E-2	4.53E-3, 7.88E-3
D	1.00E-3, 9.07E-4	7.33E-5, 1.29E-4
Adjusted R-square	9.99E-1, 9.97E-1	

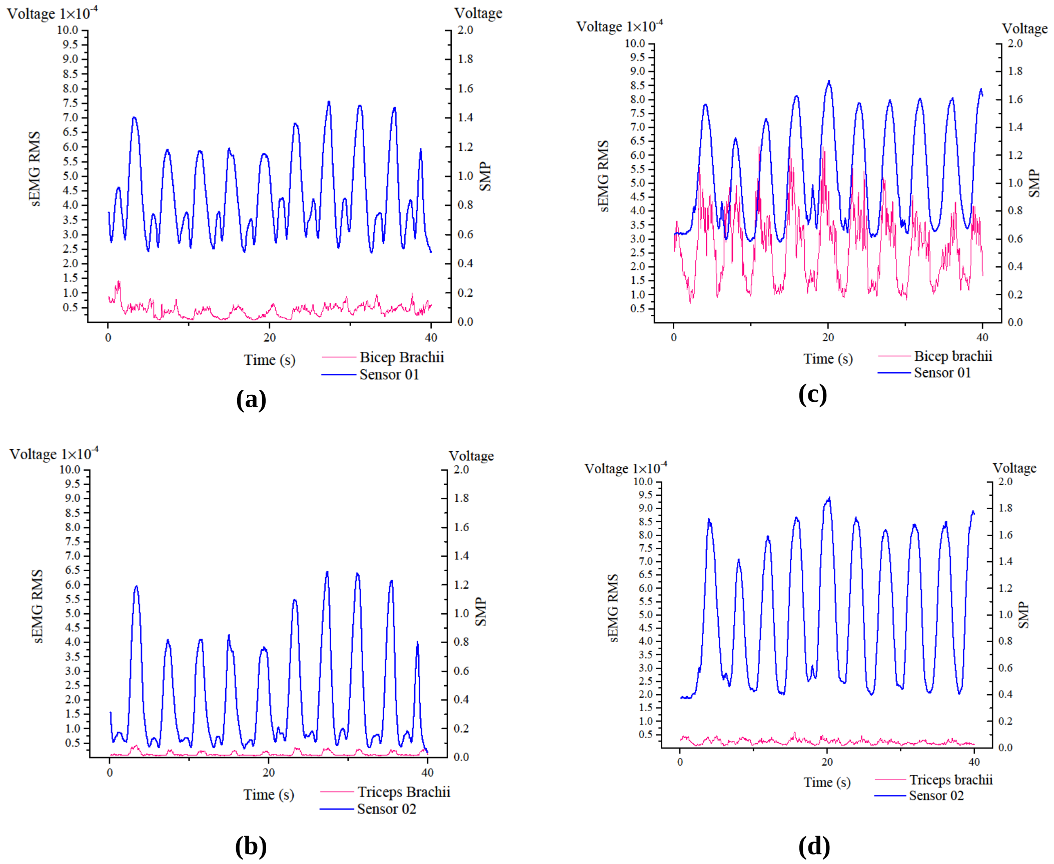

Figure C.15: SMP and sEMG variation graphs, (a) Biceps without weight, (c) Triceps without weight, (c) Biceps with 4kg dumbbell, and Triceps with 4kg dumbbell.

are similar to previous performance. Furthermore, there is a significant increment in muscle activation levels. However, minor SMP signal peaks were not noticeable for the increased weight in hand checks. Since skin surface state, skin fat level and mental disorders affect the signals of SEMG, muscle activity for various subjects is not comparable. In addition, SEMG signals are responsive to muscle fatigue. Alternatively, as in the experiments, the SMP signals are reliable and reproducible. This confirms the ability to be used to monitor wearable robots with a higher degree of fidelity.

pHRI methods for the detection of muscle movement have been studied in this research. The proposed two SMP sensory devices were calibrated and evaluated.

SMP and sEMG Time Domain functionality has been extracted to test the validity of the SMP sensory systems. Hence, the pneumatic SMP sensory system was proposed to detect the interaction between robotic interface and the wearer.

Appendix D

EXPERIMENTS AND RESULTS

This chapter describes the steps involved in experiments and results to determine the effect HRI with the lower limb exoskeletons. Since many lower limb exoskeleton categories were described in the literature, a dummy exoskeleton prototype was designed and manufactured for the HRI experients. Furthermore, a human model designed in Anybody software to evaluate the kinematics and dynamics of experimental subjects. In order to obtain the HRI results, an experiment setup and a protocol were proposed. Finally, the obtained experimental results were analyzed and discussed.

D.1 Development of Dummy Exoskeleton

As mentioned in chapter 2, the lower limb exoskeletons can be classified depending on the wearer's attachment locations: Trunk-Hip-Knee-Ankle-Foot(THKAF) exoskeletons, Trunk-Hip-Knee (THK) exoskeletons, Hip-Knee-Ankle-Foot exoskeletons (HKAF), Hip-Knee (HK) exoskeletons, Knee-Ankle-Foot (KAF) exoskeletons, and single-joint lower limb exoskeletons. The aforementioned exoskeleton's functionality and movements should be considered to determine the effect of HRI with lower limb exoskeletons. Hence, an inactive dummy exoskeleton has been developed considering each exoskeleton wearable device's mechanical aspects and biomechanics of the wearer. Furthermore, the human-robot attachment interface of the exoskeleton was developed with lightweight user comfortable materials.

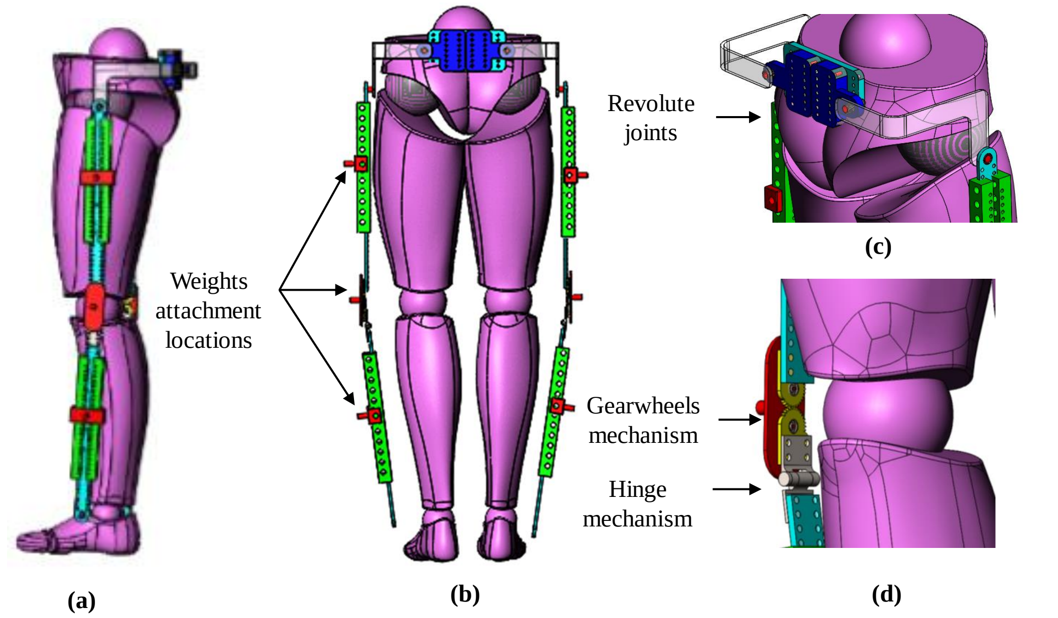

Figure D.1: Dummy exoskeleton, (a) lateral view of the exoskeleton, (b) frontal view of the exoskeleton, (c) hip mechanism, and (d) knee mechanism.

D.1.1 Mechanical Design

The proposed lower limb exoskeleton is designed with 5th to 95th percentile anthropometry for adult subjects. Therefore the lengths of each limb segment of the exoskeleton can be changed 300mm - 600mm range [see figure 4.1 (a) and (b)]. The design consists of ergonomically comfortable eight joints [see figure 4.1 (c)] to generate human-like locomotion variations. Four of them are revolute joints in the hip section to assist hip extension/flexion and abduction/adduction movements. The knee joint is designed with two gear wheels to mimic the poly-centric knee motion. Furthermore, to adopt the human knee joint formation, a hinge mechanism was introduced. Moreover, it facilitates six weight attachment locations to change the weight distribution. Four of these attachment locations can be change up to 200mm in length, while others are fixed in the knee joint [see figure 4.1 (b)].

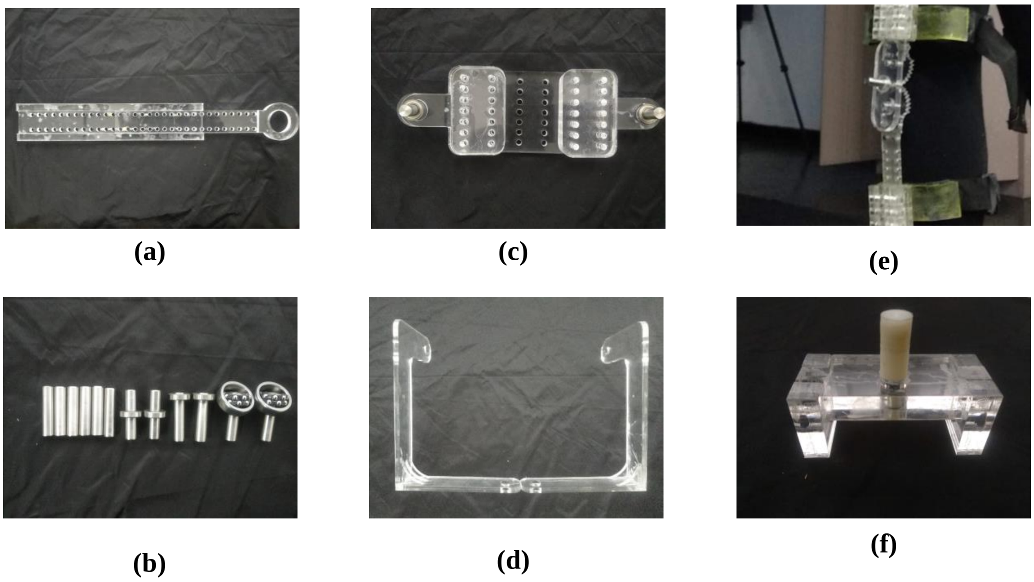

Figure D.2: The dummy exoskeleton segments, (a) variable limb segment, (b) stainless steel rods, hinges, and ball bearings, (c) and (d) hip mechanism segments, (e) knee mechanism, and (d) variable weight attachment locations.

D.1.2 Fabrication Process

The dummy exoskeleton body was manufactured with acrylic material to minimize weight. Each acrylic limb segment was punctured with 5mm diameter holes to reduce the weight further [see figure 4.2 (a) and (c)], and the acrylic material was laser cut and glued together to achieve desirable segment shapes. For the purpose of the ability to adapt human anthropometries, the acrylic limb segment length can change sliding the middle part. Figure 4.2 (b) shows the stainless steel rods, hinges and ball bearings used to mount the revolute and gear joints [see figure 4.2 (b)]. The hip consists of four passive revolute joints connected with 12 mm diameter ball bearings [see figure 4.2 (c) and (d)]. Figure 4.2 (e) shows the knee joint fabricated with two acrylic gear wheels, ball bearings and a hinge mechanism to mimic the human knee motions. Moreover, special sliding weight attachments were fabricated [see figure 4.2 (f)] to attached weights and all the joints of the exoskeleton were passively enabled to achieve ergonomic locomotions.

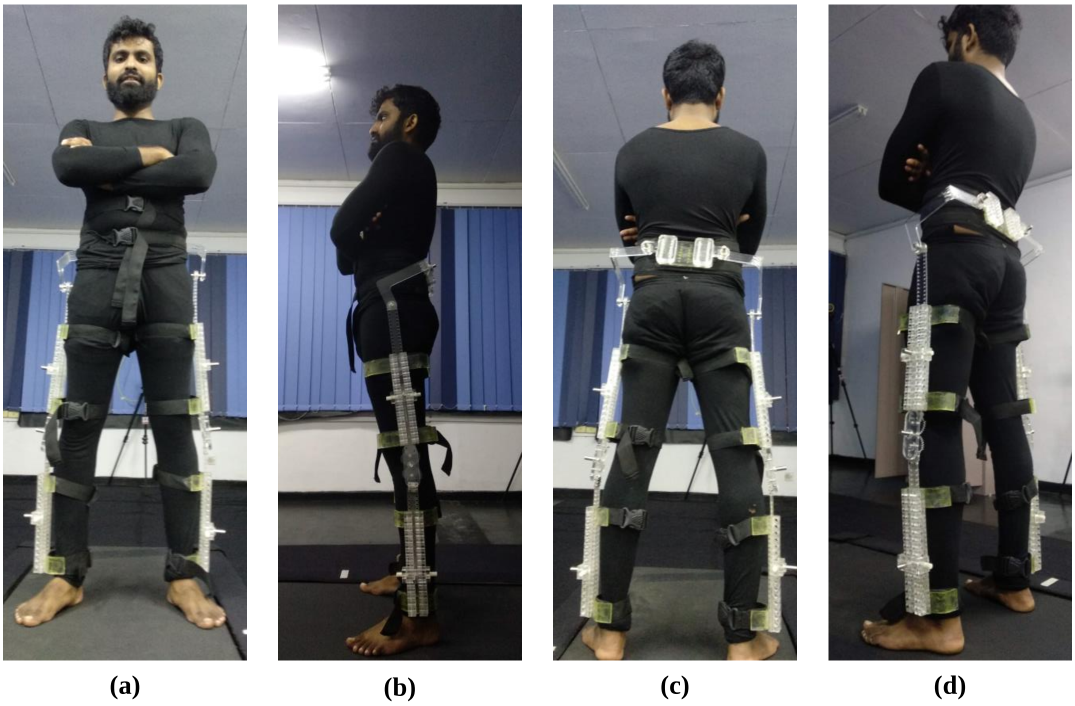

Figure D.3: The test subject wearing the dummy exoskeleton, (a) anterior view, (b) lateral view, (c) posterior view, and (c) posterior three-quarter view.

D.2 Simulation Model

Human dynamics is a significant factor in determining desirable HRI for motions. Therefore, a state of art modeling and simulation software (AnyBody software) is used to develop a simulation human model to determine the kinematics and kinetics of the experimental subjects. The AnyBody software consists of AnyBody managed model repository customized human model and can be used on specific motion applications. Hence, a customized human body model was developed to simulate actual kinematics data. Furthermore, a ground force reaction prediction model was improved to perform inverse dynamics analysis [62].

D.2.1 Lower Limb Motion Analysis Model

The Anybody lower limb motion analysis model is developed with the Twente lower extremity model version 2 (TLEM2) combined with motion analysis markers [see figure 4.4 (a) and (b)]. The TLEM2 model is based on actual anatomical data produced in the University of Twente project and contains six DoFs and 169 muscles. Moreover, the body segment mass and the fat percentage estimated using literature [63]. The body limb segment lengths were changed using the experimental subject's anthropometry and additional weights were attached to the lower limb model locations respective to the dummy exoskeleton attachments, to change the weight distribution . The motion analysis markers were used to simulate the lower limb model motions and determine the kinematics.

D.2.2 Ground Reaction Force Prediction

In order to compute the inverse dynamics of the human model, motion capture data and ground reaction force must be captured with the force plates. However, this facility is not available in the experimental setup. Therefore, a ground reaction force prediction model with force plates was added to the human model to predict the force measurements based on motion analysis data. The ground reaction force prediction model depends on the foot conditional contact points. Hence, twenty-five contact points were added to each foot to generate the necessary normal and frictional forces. The force plate ground velocity can be changed according to the experimental setup treadmill speed, and the ground frictional coefficient value is fixed to 0.5. Figure 4.5 shows the overall architecture of the human model.

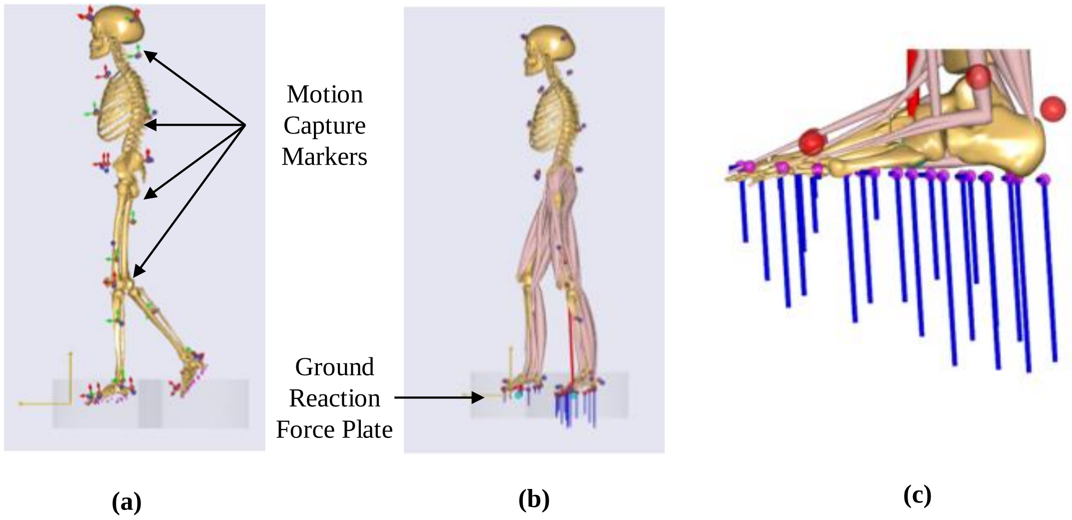

Figure D.4: AnyBody human model (a) skeletal model, (b) lower limb musculoskeletal model, and (c) ground contact force model

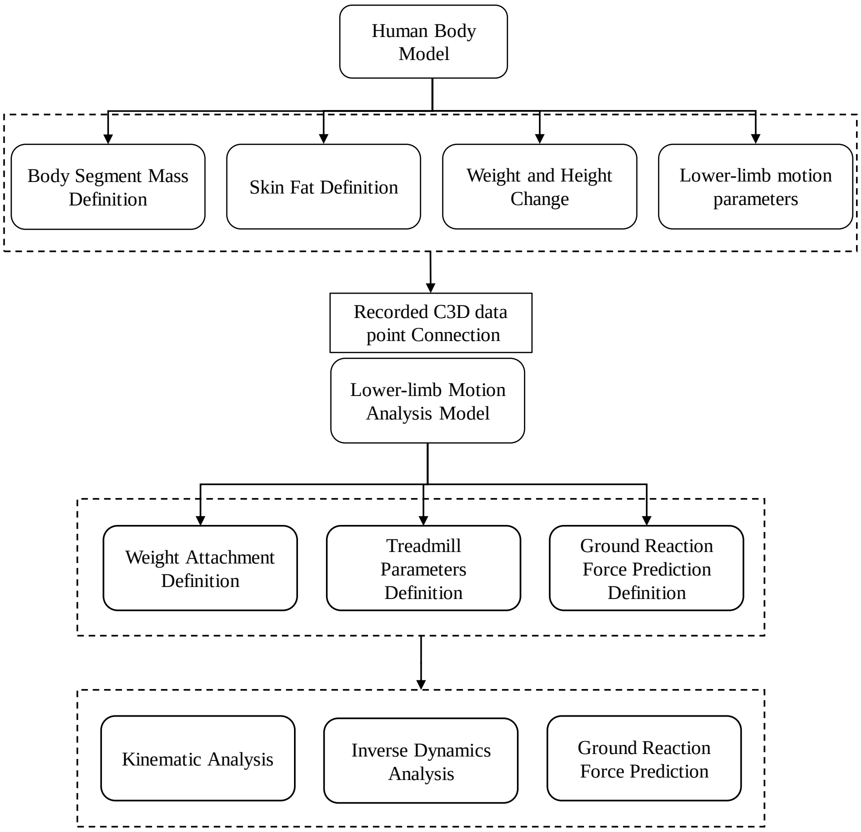

Figure D.5: AnyBody human model simulation architecture

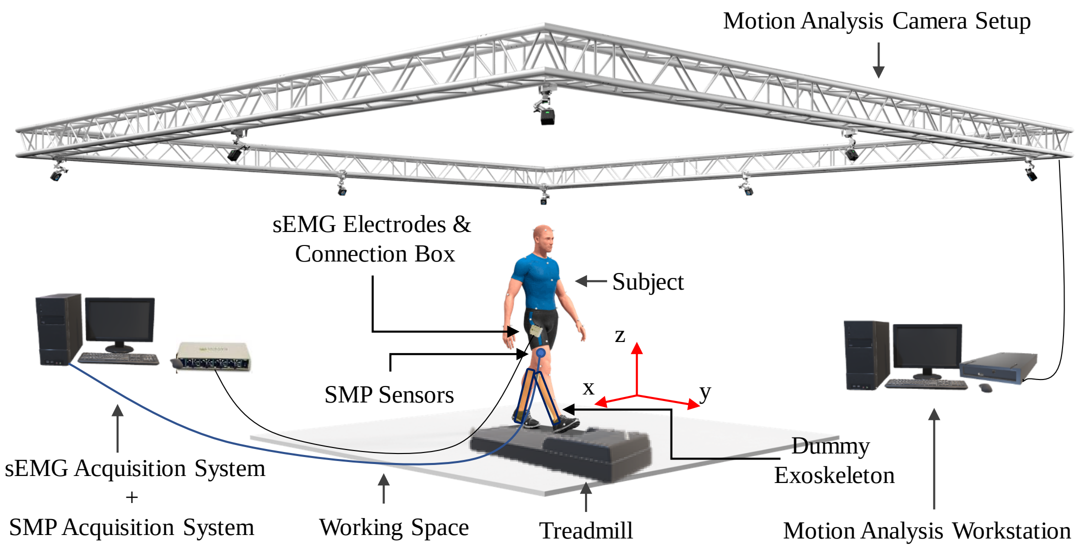

Figure D.6: The experimental setup

D.3 Experiment Setup

The experiment setup consisted of the sEMG acquisition system (DELSYS Bagnoli 16 channel, sEMG electrodes, and the EMGWorks software), SMP sensory system (Developed in chapter 3), motion analysis system (SIMI motion analysis system), and XT 185 treadmill [see figure 4.6]. The SIMI motion analysis system cameras (8 cameras, 120 frames per second) were calibrated and mounted to determine the working space and origin. In order to capture the subject's full-body view, the treadmill handles and display board were removed. Furthermore, the treadmill was placed on the origin of the workspace. The SMP and the sEMG acquisition systems were connected with the same computer, while the SIMI motion system was connected to a workstation.

The experiments were conducted with five male and one female subjects (Age 27.5±2.5 Height 170±13cm weight 70±22kg).A sample size analysis (paired t-test) was conducted using STATA software [figure 4.7] to determine the statistical significance of the subjects and a sample experiment sEMG data were used to calculate the analysis [64]. The paired t-test results were given in table 4.1.

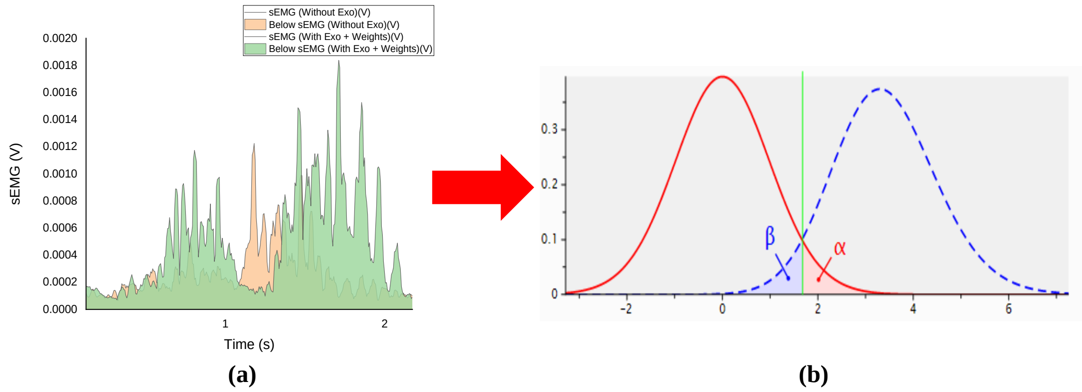

Figure D.7: Sample size analysis data

Table D.1: Sample size analysis data

Significant level	**Power**	**Pearson's Correlation**	**Sample Size**
0.005	0.8	0.0314	4

D.4 Experimental Protocol

Before starting the experiments, the subjects were advised to perform light warm-up lower limb exercises. Then, sEMG electrodes were attached to Rectus femoris, Biceps femoris, and Gastrocnemius medialis muscles of the dominant leg [see figure 4.8 (a)]. The reference electrode of the sEMG acquisition system is attached to an electrically inactive muscle during the locomotions (belly muscle). After that, the subjects were guided to wear special black cloth and the dummy lower limb exoskeleton. Later, SMP sensory system was attached between the dominant lower limb and the exoskeleton interface [see figure 4.8 (b)]. Finally, retro-reflective markers were attached to the subject to capture the motion analysis data [see figure 4.10 (b)].

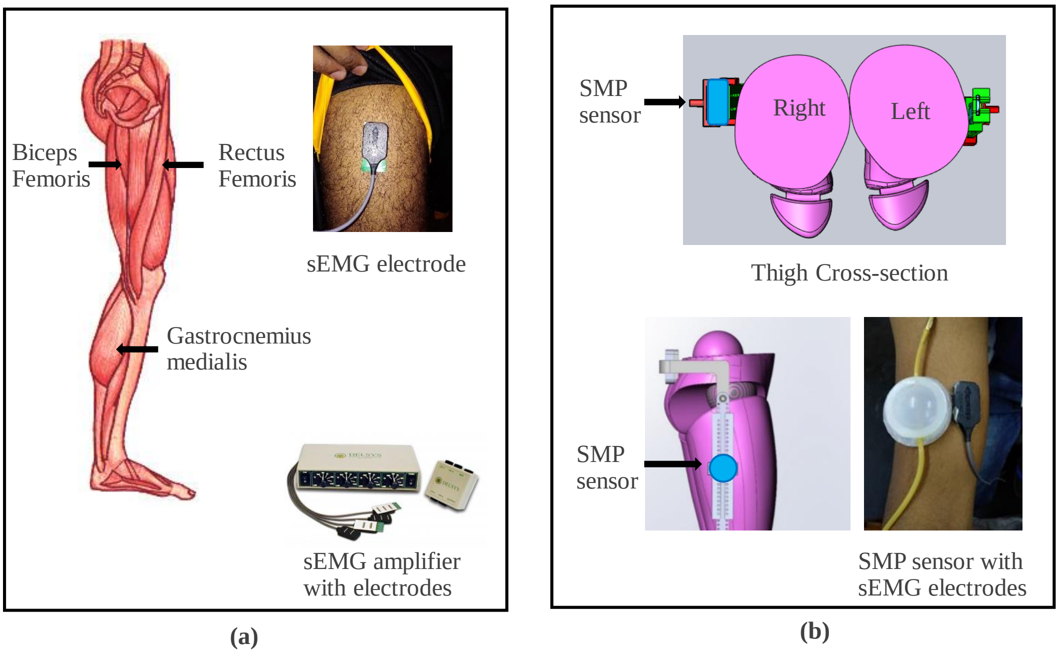

Figure D.8: sEMG and SMP sensory acquisition systems attachments (a) sEMG electrode attachments, and (b) SMP sensor attachements

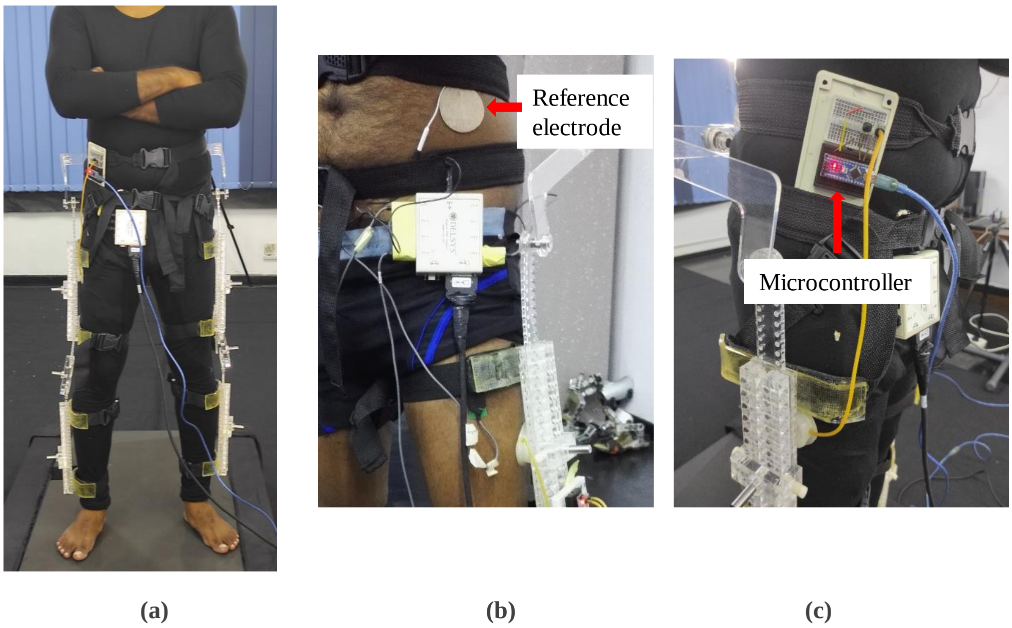

Figure D.9: The test subject wearing dummy exoskeleton with sEMG and SMP acquisition systems (a) Frontal view, (b) sEMG reference electrode, and (b) SMP sensor microcontroller.

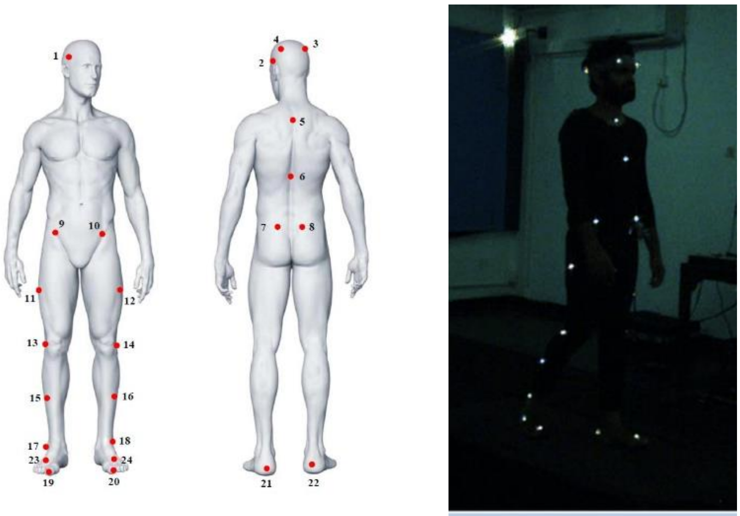

(a) (b)

Figure D.10: Motion capture reflective markers locations (a) marker location diagram, and (b) test subject wearing the markers

After attaching reflective markers, sEMG electrodes, and SMP sensors, the experimental procedure was started. The experiment was performed under two treadmill speeds 1 m/s (average human walking speed) and 0.5 m/s (half of the average human walking speed). Then, the subjects were instructed to perform 30 seconds walking cycle before capturing the data to adopt the experiment setup. Then, sEMG, SMP, and motion analysis data were capture simultaneously for one minute walking cycle. Each experiment was performed without the exoskeleton, with the exoskeleton, and with exoskeleton plus weights conditions. Furthermore, weights and weight attachment locations were changed accordingly in both legs [see table 4.2 and figure 4.11] . Simultaneously, a qualitative analysis was carried out using a comparative comfortable level chart based on 0 to 10 Borg's scale [65](0- very comfortable and 10- very uncomfortable).

The recorded raw SMP and sEMG data from the walking cycle were filtered and average using Matlab software. In the post processing, it was filtered using

Table D.2: Weight attachments

Speed	Without Exo	With Exo	With Exo 1.25kg	With Exo 2.5kg	With Exo 3.75kg
$1ms^{-1}$	$\surd$	$\surd$	$\surd$	$\times$	$\times$
$0.5ms^{-1}$	$\surd$	$\surd$	$\surd$	$\surd$	$\surd$

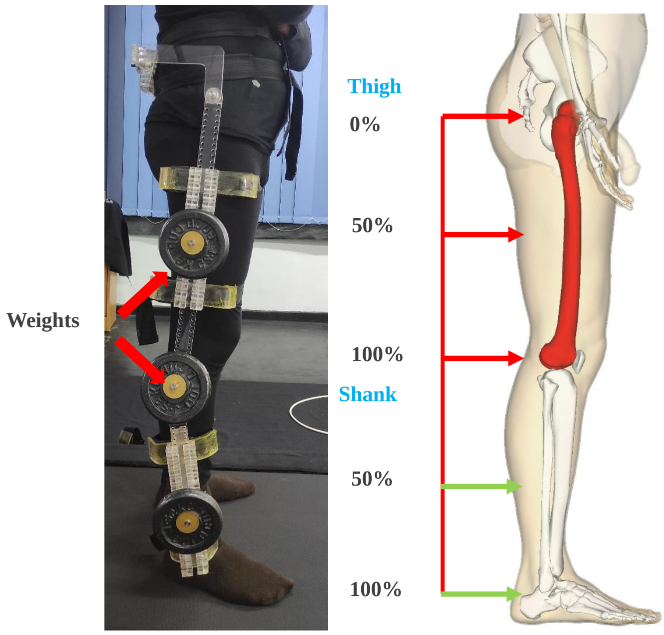

Figure D.11: The weight attachment locations of the dummy exoskeleton

the FFT analysis method to remove the treadmill electromagnetic noise from the sEMG data. Afterwards, sEMG results were feature extracted using RMS method. Furthermore, inverse dynamics and qualitative data were also normalized and averaged using Matlab software

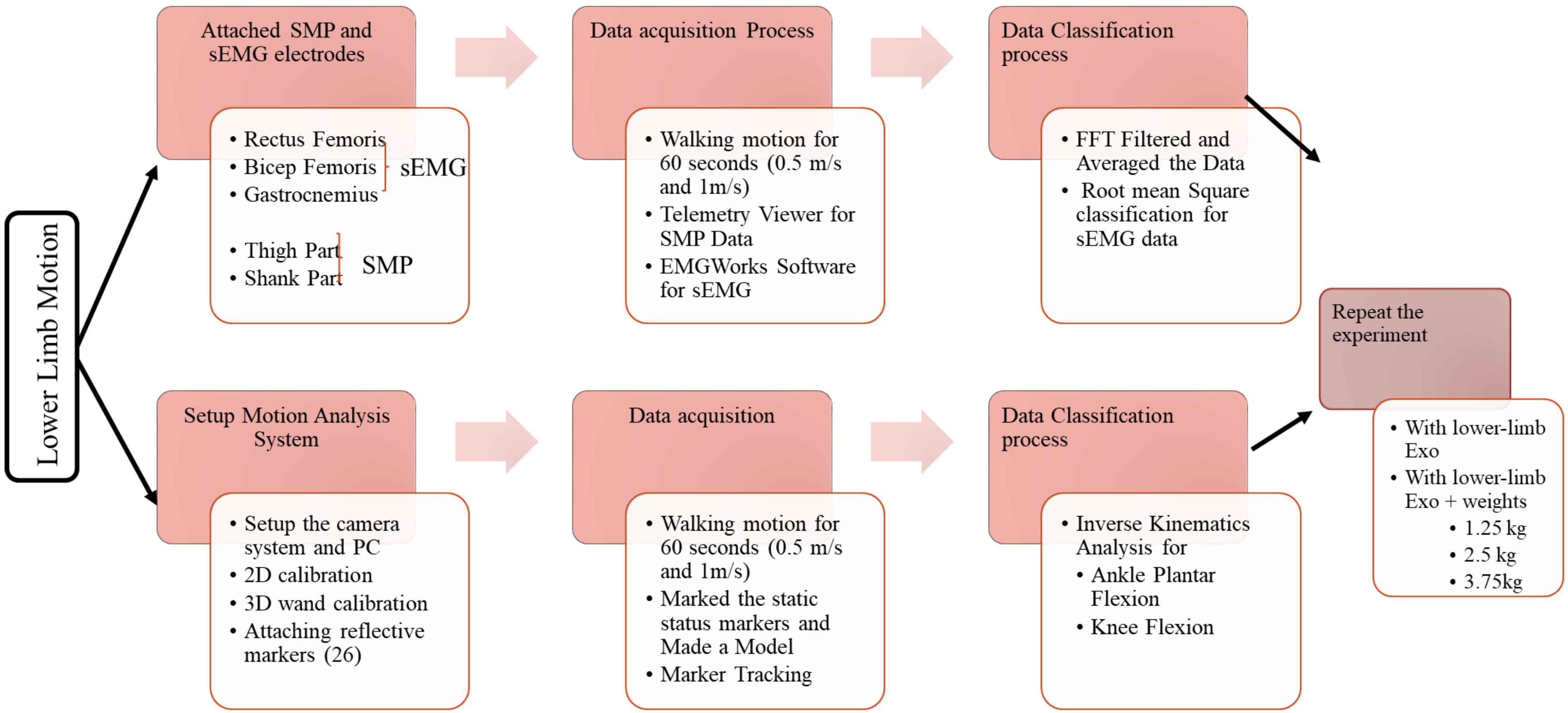

Figure D.12: Summary of the experiment process

D.5 Results

To determine the effect of HRI, exceptional and complex conditions were deducted using four major assumptions: The environmental conditions were consistent and did not affect the user comfort during all the experiments, the average walking speed was the same for the experimental subjects, there is no relative motion between lower limb and the exoskeleton attachments, and psychological and physiological factors of the experimental subjects were restful before starting the experiments. Some of these assumptions were confirmed in the qualitative analysis. Afterward, the qualitative and quantitative results were averaged and analyzed.

The sEMG variations for the different conditions (weight attachment variations) in 0.5 m/s speed were plotted in Figures 4.13. The peak values of the graphs represent the averaged walking gait cycle with respect to maximum voluntary contraction. The maximum peak sEMG values of Rectus femoris, Biceps femoris, and Gastrocnemius medialis were obtained in exoskeleton plus 3.75kg condition and the mimum values obtained for without exoskeleton condition. There is no significant sEMG signal increment with in without exoskeleton and with exoskeleton conditions.

Figure 4.14 shows The sEMG variations for the different conditions (weight attachment variations) in 1 m/s walking speed. the maximum sEMG peak values were obtained for the with exoskeleton + 2.25kg attachment condition and the minimum values were obtained for without exoskeleton conditions. Considering Rectus Femoris muscle, There is huge sEMG (0.002v) increment in knee 1.25 kg condition and other conditions. Furthermore, the average 1 m/s speed experiment sEMG peak values greater than the values of the 0.5 m/s speed experiment.

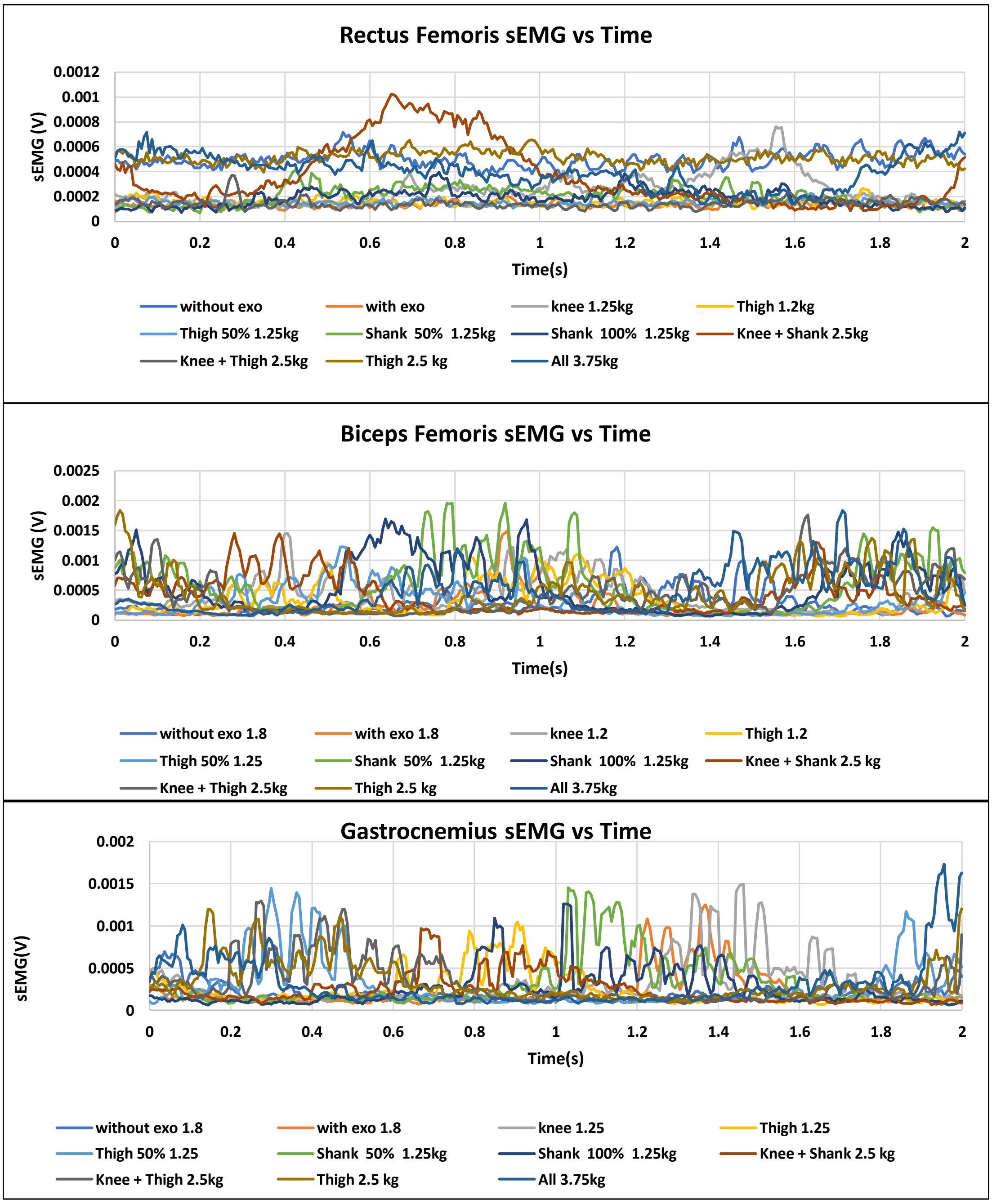

Figure D.13: sEMG results for 0.5 m/s speed

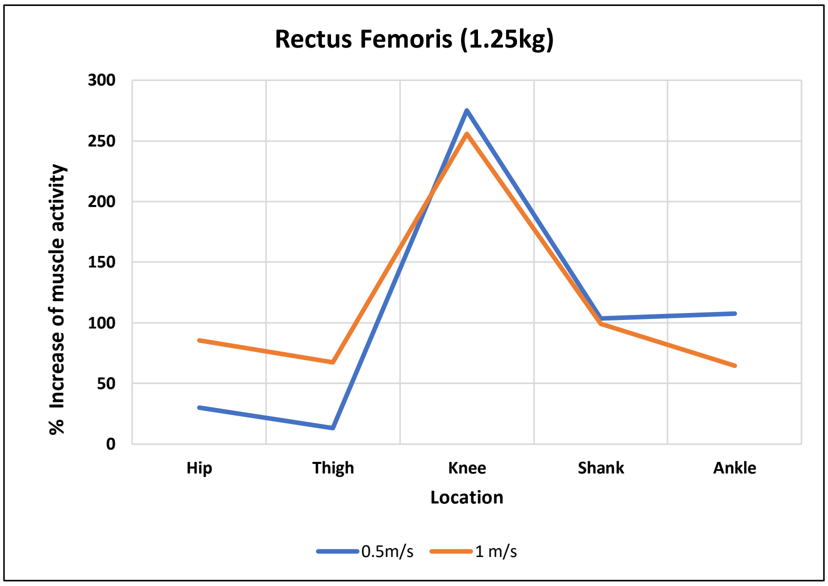

(a)

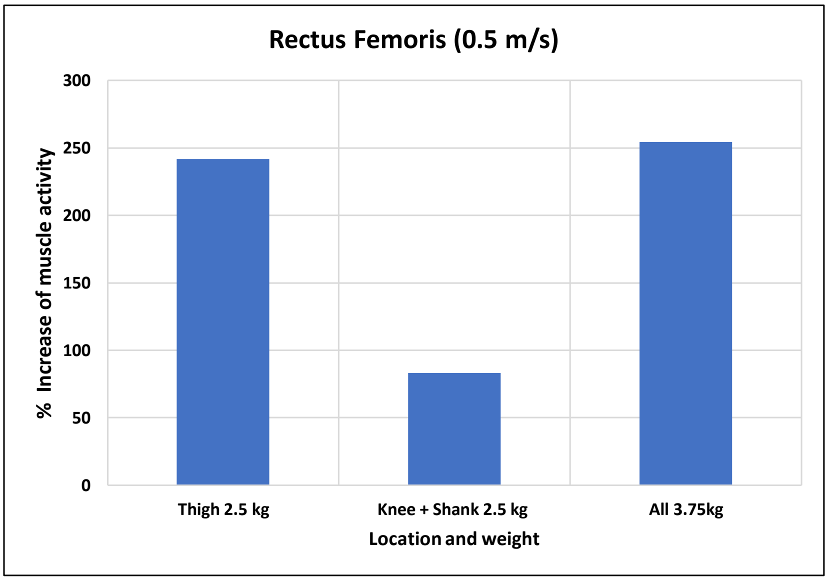

(b)

Figure D.14: sEMG results for 1 m/s speed

Figure 4.15 (a) shows the increment of Rectus Femoris muscle activity with respect to with exoskeleton condition for 1.25kg attachment. 255% and 275% muscle activity increments obtained in knee attachment for 0.5 m/s and 1 m/s speed respectively. Furthermore, thigh region attachment obtained minimum muscle activity. The significant amount of sEMG decrement observed in Knee + Shank 2.5kg attachment [see Figure 4.15 (b)]. Considering Biceps Femoris muscle activity increment, the knee location attachment obtained the maximum muscle activity to 0.5 m/s speed and the shank location obtained the 1 m/s speed maximum [see Figure 4.16(a)]. A Similar peaks can be observed in Grastrocnemius muscle for the knee and shank locations [see Figure 4.17(a)].

In order to validate the dummy exoskeleton motions, knee flexion/extension and ankle plantarflexion/dorsiflexion angles were plotted in the figure 4.18. However,there is no significant angle rage between without and with lower limb attachments results. Figure 4.19 shows the SMP and ground force reaction predictions. The peaks values of both graphs represent the average gait cycle. When increasing the attachments weights, significant of pressure and force increment can be noted. Maximum surface muscle pressure obtained for 3.75 kg attachment.

Qualitative analysis results of both walking speeds were represented in Figure 4.20. Compared to the 0.5 m/s speed data, the 1 m/s speed data shows higher discomfort values. Furthermore, gradual discomfort increment can be observed without exoskeleton to with exoskeleton + hip weight attachment conditions. However, Hip location to knee location had no noticeable discomfort increments. Alternatively, as in the experiments, the Borg's scale is reliable as qualitative measurement. This confirms the ability to be used to monitor discomfort levels with a higher degree of fidelity.

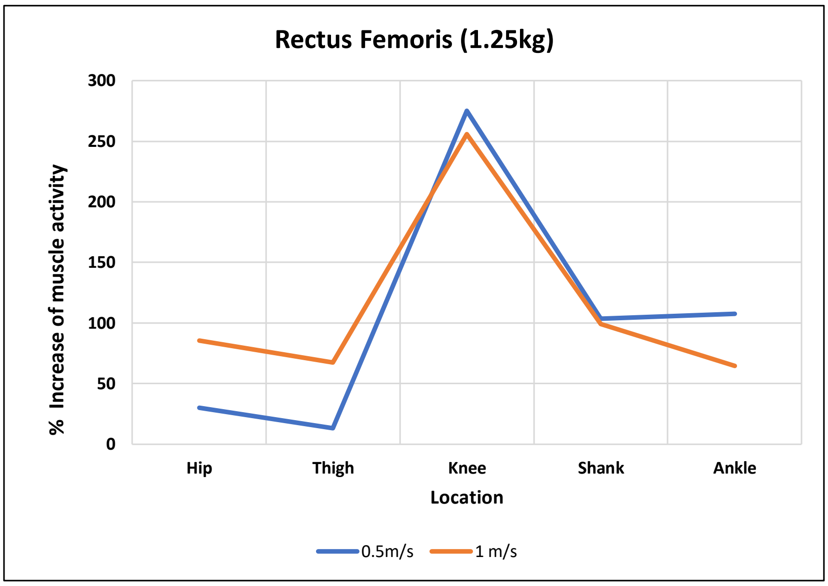

(a)

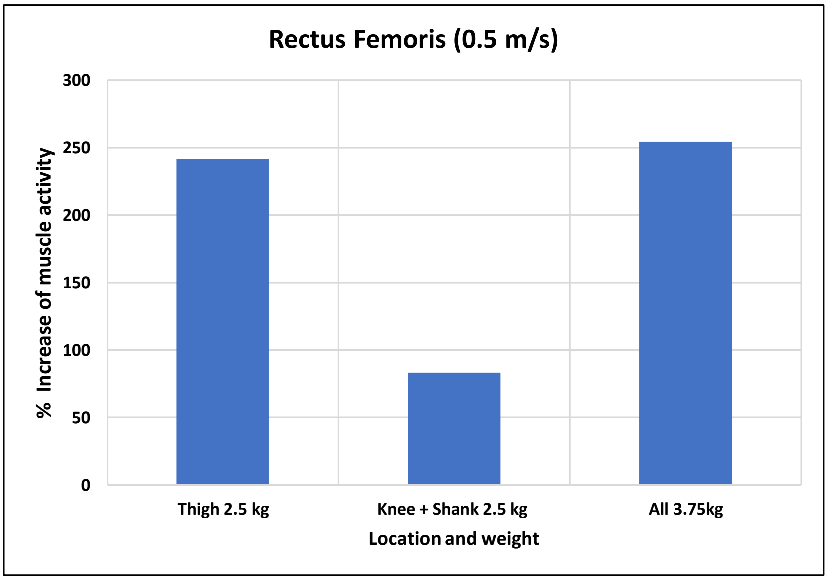

(b)

Figure D.15: sEMG peaks values increments of Rectus Femoris with respect to with Exoskeleton value (a) sEMG peaks values increments for 1.25 kg attachment, (b) sEMG peaks values increments for 0.5 m/s speed

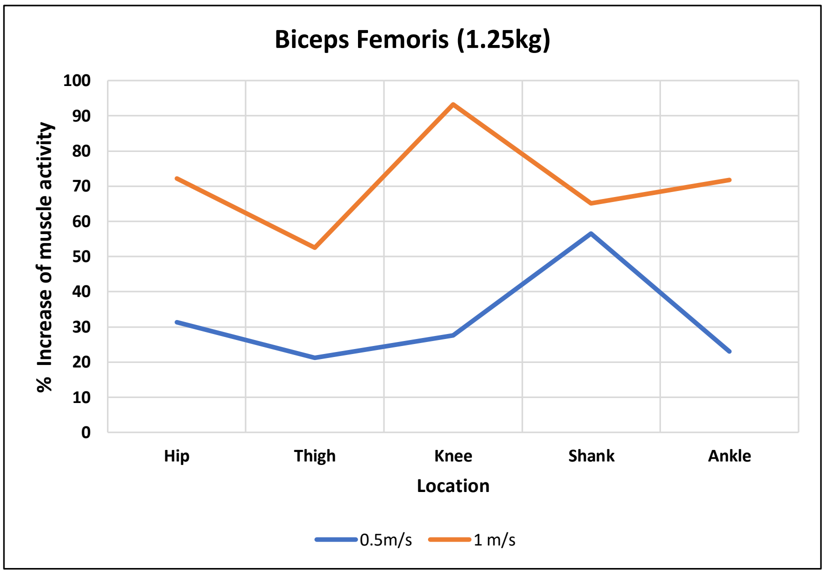

(a)

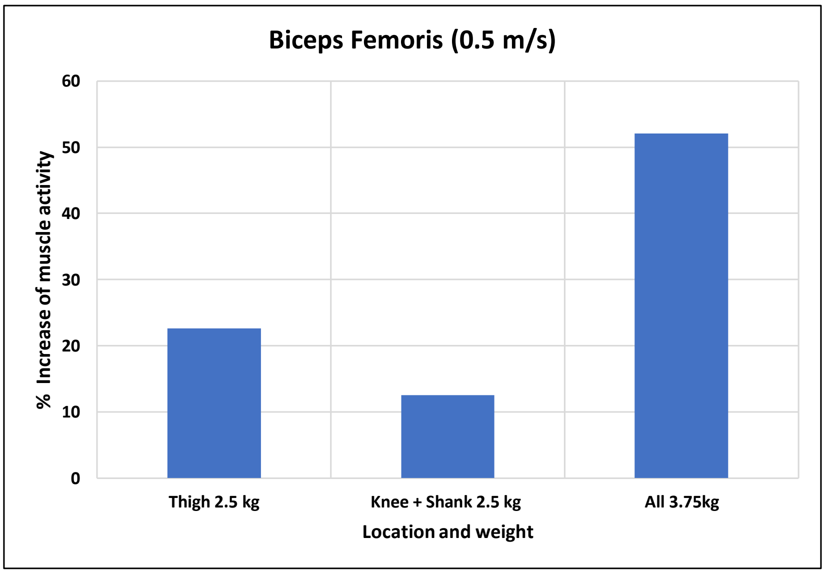

(b)

Figure D.16: sEMG peaks values increments of Biceps Femoris with respect to with Exoskeleton value (a) sEMG peaks values increments for 1.25 kg attachment, (b) sEMG peaks values increments for 0.5 m/s speed

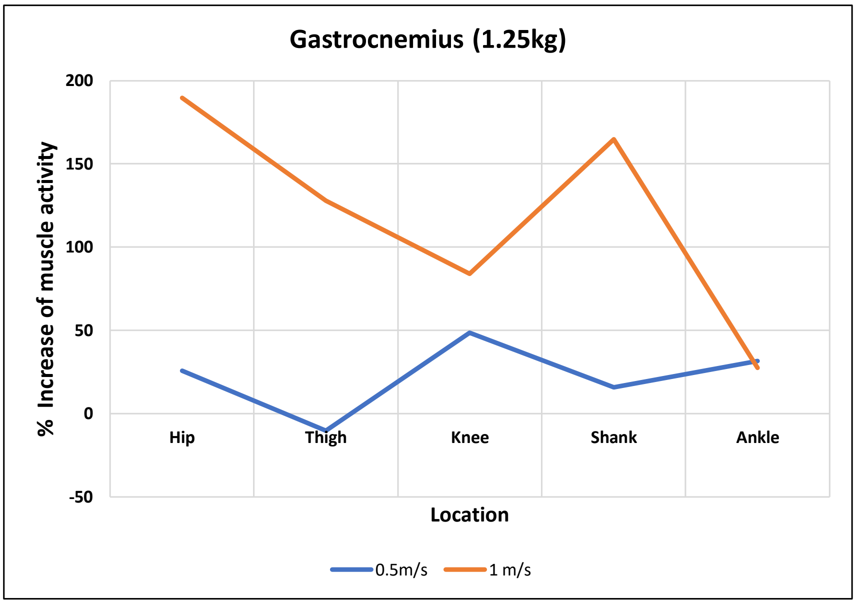

(a)

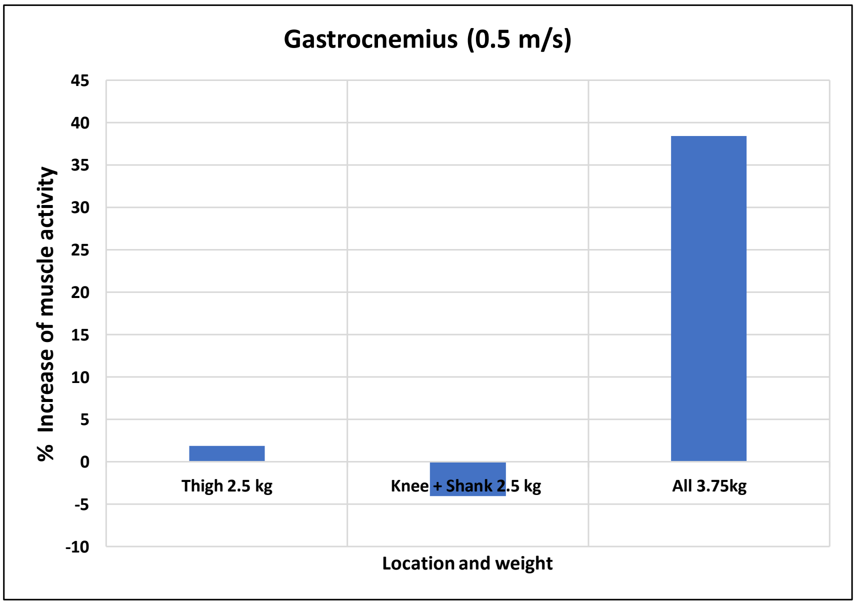

(b)

Figure D.17: sEMG peaks values increments of Gastrocnemius with respect to with Exoskeleton value (a) sEMG peaks values increments for 1.25 kg attachment, (b) sEMG peaks values increments for 0.5 m/s speed

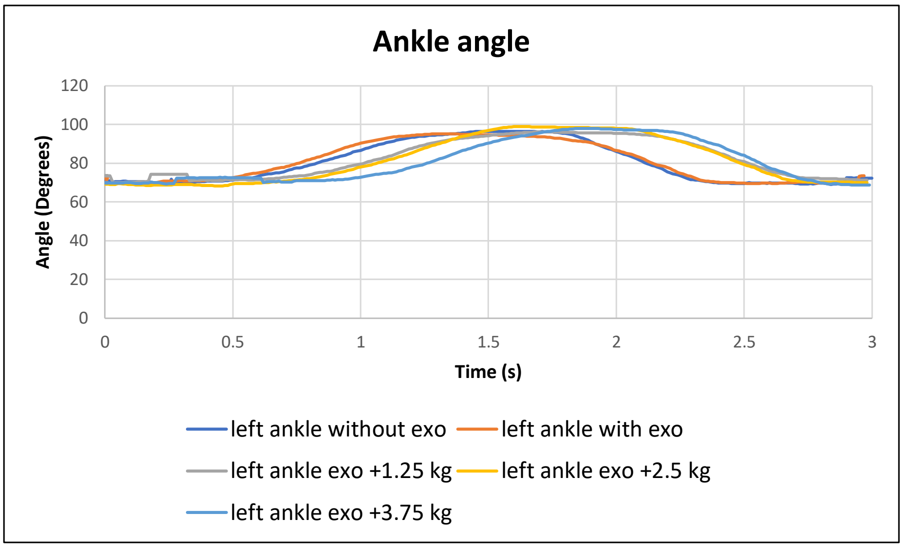

(a)

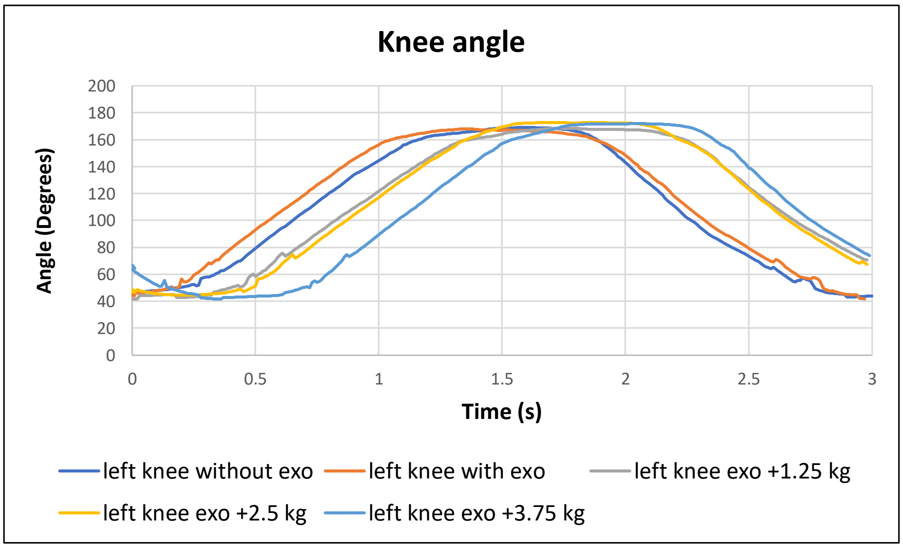

(b)

Figure D.18: Kinematic data (a) Ankle angle, (b) Knee angle

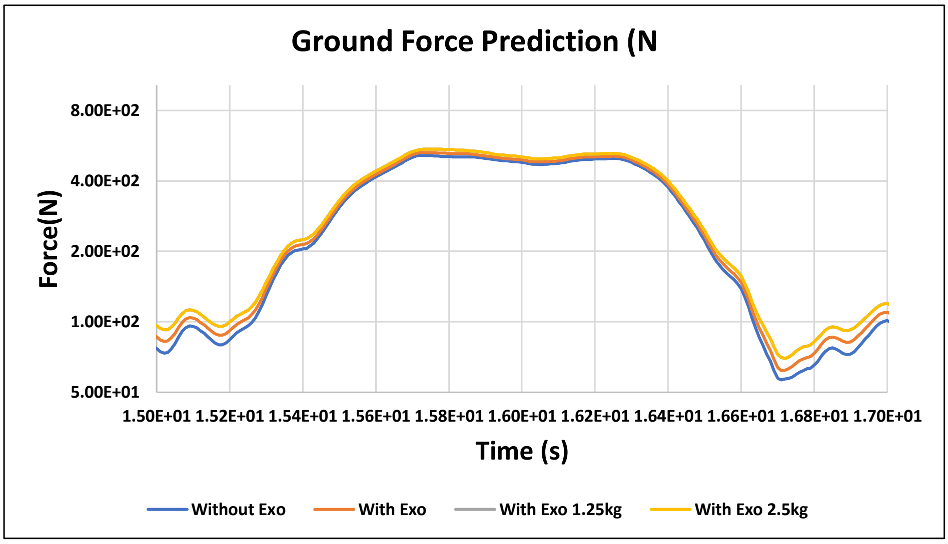

(a)

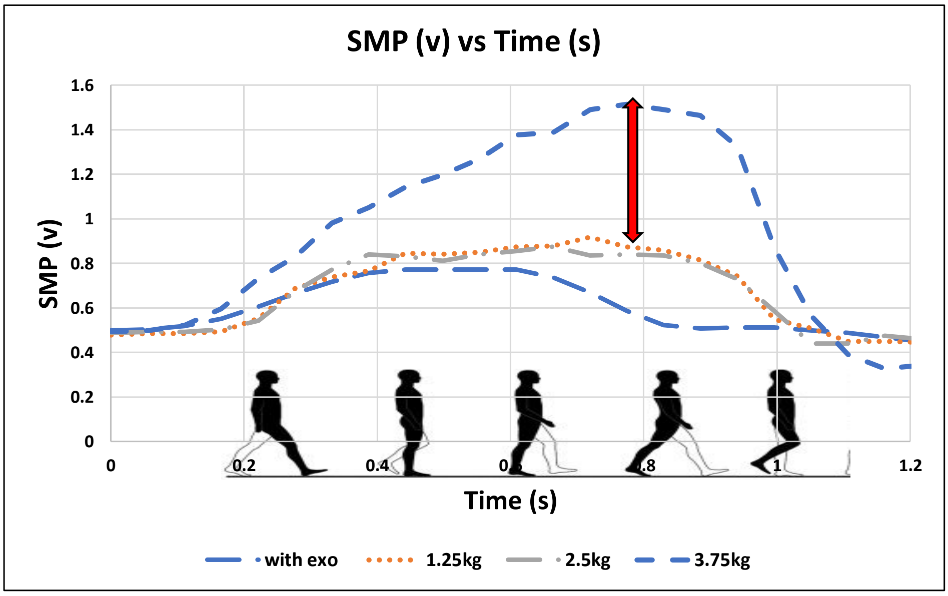

(b)

Figure D.19: Force and SMP data for 0.5 m/s speed (a) Ground force prediction (b) Surface muscle pressure

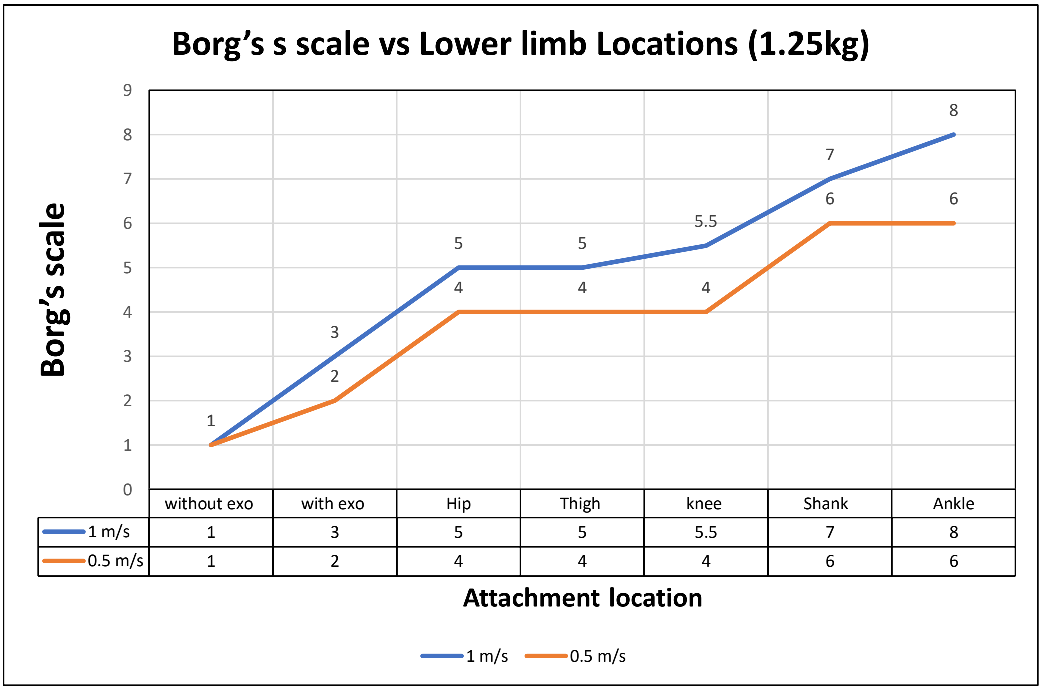

(a)

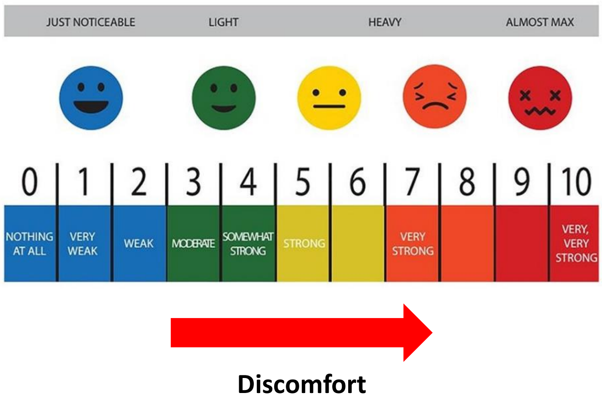

(b)

Figure D.20: Qualitative analysis for lower limb attachment locations and weights (a) Borg's scale result for 1.25kg attachment, (b) Reference Borg's scale for discomfort levels

D.5.1 Guideline for design of lower limb exoskeletons

In this thesis, the HRI of lower limb exoskeletons was analyzed to evaluate the user endurance and comfort level. Therefore, to increase the lower limb werable device's ergonomics and efficiency, a guideline was developed based on the experimental data and the literature.

- Human anthropometric data – the lower limb wearable device should be designed to compatible with the wearer's dimensions and shapes. Therefore, human anthropometric data should be considered to device's shape and dimension. Moreover, if the wearable device is designing for a specific population, the 5th to 95th percentile anthropometric data of the population should be considered.
- Range of Motion – The human lower limb consists of 30 DoFs. Nevertheless, seven crucial DoFs can be identified for customary motions. Therefore, at least ankle: dorsiflexion/plantarflexion, inversion/eversion, abduction/adduction, knee: extension/flexion, and hip: extension/flexion, abduction/adduction, and medial rotation, lateral rotation range of motion should be designed in the devices.
- Joint Centers – The device's joint centers should be aligned with the wearer's joints for better ergonomic movements.
- Weight and attachment locations – In this research, human comfort level behavior with and without weight attachments was observed. Furthermore, the optimal weights and locations were determined from the observations [see table 4.3]. Therefore, these data can be used for designing ergonomically comfortable Trunk-Hip-Knee-Ankle-Foot(THKAF) exoskeletons, Trunk-Hip-Knee (THK) exoskeletons, Hip-Knee-Ankle-Foot exoskeletons (HKAF), Hip-Knee (HK) exoskeletons, Knee-Ankle-Foot (KAF) exoskeletons and single joint lower limb exoskeletons.

Table D.3: Comfort level matrix

Weight Location	**1.25kg**	**2.5kg**	**3.75kg**
Hip	High	High	High
Mid thigh	High	High	Moderate
Knee	High	Moderate	Low
Mid shank	Moderate	Low	N/A
Ankle	Moderate	Low	N/A

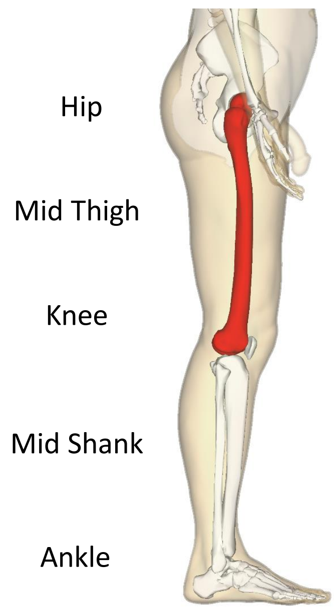

Figure D.21: Lower limb weight attachment locations

Appendix E

CONCLUSION AND FUTURE DIRECTIONS

In this thesis, the effect of human-robot interaction (HRI) with lower limb exoskeletons was investigated using an experimental setup. The relationship between weight distribution and weight locations of lower limb wearable devices was observed with locomotions. Moreover, A guideline has been derived for lower limb exoskeleton designs to improve user comfort and ergonomics. Moreover, the future direction towards improving the efficiency and ergonomics of the wearable devices has been presented.

- A pneumatic SMP sensory system has been validated and used to determine pHRI between the wearable interface and the wearer. Moreover, SMP sensory system can detect more accurate and consistent data rather than commonly available FSR sensors. Therefore, this sensory system can be used to identify user intentions to control wearable robotic devices. Moreover, due to high accuracy, this device can be used to determine intramuscular pressure to detect musculoskeletal diseases.

- The developed dummy exoskeleton has been validated for ergonomically comfortable locomotions using healthy subjects. Therefore, the mechanical design of the exoskeleton attachment can be used for future endurance and comfortable analysis. However, due to the devices' inactive joints, HRI can not be evaluated by varying the joint torque. Therefore, variable joint actuation is proposed to the dummy exoskeleton for future experiments.

- In order to determine the inverse dynamics, a lower limb human simulation model combined with ground reaction force prediction was developed in this study. This model was validated from the literature, and it can predict the data of the inverse dynamics without using the force plate data. Furthermore, joint torques and power can be calculated from the model. Therefore, from this model, wearable design can be evaluated from the simulation.

- In this research, pHRI and cHRI based endurance and comfortable analysis experimental setup was proposed. The experimental results were evaluated from qualitative analysis based on comfort levels. Furthermore, this setup can be improved using VO2 max acquisition setup.

- This study proposed a guideline to design ergonomically efficient and comfortable lower limb wearable devices. The optimal weights and the weight attachment locations can be identified for lower limb wearable devices. Moreover, the guideline was derived based exclusively on weight attachment locations and weight variations. In order to design better ergonomically, efficient wearable devices, joint torques should be considered. Therefore, variable joint torque analysis was proposed for future studies.

LIST OF PUBLICATIONS

---

1. **Chandrasiri, M.D.S.D**, R.K.P.S. Ranaweera, and R.A.R.C. Gopura, "Development of a surface muscle pressure monitoring system for wearable robotic devices. ," in *Moratuwa Engineering Research Conference (MERCon)*, Colombo, Sri Lanka, (pp. 544-549). IEEE. 2019.

2. **Chandrasiri, M.D.S.D**, R.K.P.S. Ranaweera, and R.A.R.C. Gopura, Kazuo Kiguchi, "Development of a sensory system to detect surface muscle pressure," in *2018 6th international Conference on Sri Lanka - Japan Collaborative Research* , Kandy, Sri lanka, 2018.

3. **Chandrasiri, M.D.S.D**, R.K.P.S. Ranaweera, and R.A.R.C. Gopura, "Electromyography and surface muscle-pressure as measures of lower-limb muscle activities during squatting," in *2018 4th International Conference on Control, Automation and Robotics (ICCAR)* ,New Zealand,(pp. 257-261). IEEE. 2018.

REFERENCES

[1] J. J. Craig, *Introduction to robotics: mechanics and control, 3/E.* Pearson Education India, 2009.

[2] M. Hillman, "2 rehabilitation robotics from past to present–a historical perspective," in *Advances in Rehabilitation Robotics.* Springer, 2004, pp. 25–44.

[3] K. Capek, *RUR (Rossum's universal robots).* Penguin, 2004.

[4] E. Stephens and T. Heffernan, "We have always been robots: The history of robots and art," in *Robots and Art.* Springer, 2016, pp. 29–45.

[5] N. G. Hockstein, C. Gourin, R. Faust, and D. J. Terris, "A history of robots: from science fiction to surgical robotics," *Journal of robotic surgery*, vol. 1, no. 2, pp. 113–118, 2007.

[6] A. M. Dollar and H. Herr, "Lower extremity exoskeletons and active orthoses: Challenges and state-of-the-art," *IEEE Transactions on robotics*, vol. 24, no. 1, pp. 144–158, 2008.

[7] J. L. Pons, *Wearable robots: biomechatronic exoskeletons.* John Wiley & Sons, 2008.

[8] P. Dario, M. C. Carrozza, E. Guglielmelli, C. Laschi, A. Menciassi, S. Micera, and F. Vecchi, "Robotics as a future and emerging technology: biomimetics, cybernetics, and neuro-robotics in european projects," *IEEE Robotics & Automation Magazine*, vol. 12, no. 2, pp. 29–45, 2005.

[9] H. Kazerooni, B. Waibel, and S. Kim, "On the stability of robot compliant motion control: Theory and experiments," 1990.

[10] R. Bogue, “Exoskeletons and robotic prosthetics: a review of recent developments,” *Industrial Robot: an international journal*, 2009.

[11] O. Khatib, K. Yokoi, O. Brock, K. Chang, and A. Casal, “Robots in human environments: Basic autonomous capabilities,” *The International Journal of Robotics Research*, vol. 18, no. 7, pp. 684–696, 1999.

[12] F. Martini *et al.*, *Anatomy and Physiology'2007 Ed.* Rex Bookstore, Inc., 2006.

[13] A. Roaas and G. B. Andersson, “Normal range of motion of the hip, knee and ankle joints in male subjects, 30–40 years of age,” *Acta Orthopaedica Scandinavica*, vol. 53, no. 2, pp. 205–208, 1982.

[14] N. Li, L. Yan, H. Qian, J. Wu, S. Men, and Y. Li, “Design and simulation analysis of an improved lower limb exoskeleton,” *Journal of vibroengineering*, vol. 16, no. 7, pp. 3655–3664, 2014.

[15] M. Cenciarini and A. M. Dollar, “Biomechanical considerations in the design of lower limb exoskeletons,” in *2011 IEEE International conference on rehabilitation robotics.* IEEE, 2011, pp. 1–6.

[16] B. Kalita, J. Narayan, and S. K. Dwivedy, “Development of active lower limb robotic-based orthosis and exoskeleton devices: A systematic review,” *International Journal of Social Robotics*, pp. 1–19, 2020.

[17] A. Zoss, H. Kazerooni, and A. Chu, “On the mechanical design of the berkeley lower extremity exoskeleton (bleex),” in *2005 IEEE/RSJ international conference on intelligent robots and systems.* IEEE, 2005, pp. 3465–3472.

[18] A. B. Zoss, H. Kazerooni, and A. Chu, “Biomechanical design of the berkeley lower extremity exoskeleton (bleex),” *IEEE/ASME Transactions on mechatronics*, vol. 11, no. 2, pp. 128–138, 2006.

[19] S. Marcheschi, F. Salsedo, M. Fontana, and M. Bergamasco, “Body extender: Whole body exoskeleton for human power augmentation,” in *2011 IEEE*

international conference on robotics and automation. IEEE, 2011, pp. 611–616.

[20] Y. W. Hong, Y. King, W. Yeo, C. Ting, Y. Chuah, J. Lee, and E.-T. Chok, "Lower extremity exoskeleton: review and challenges surrounding the technology and its role in rehabilitation of lower limbs," *Australian Journal of Basic and Applied Sciences*, vol. 7, no. 7, pp. 520–524, 2013.

[21] R. Huang, H. Cheng, H. Guo, Q. Chen, and X. Lin, "Hierarchical interactive learning for a human-powered augmentation lower exoskeleton," in *2016 IEEE international conference on robotics and automation (ICRA).* IEEE, 2016, pp. 257–263.

[22] S. Wang, L. Wang, C. Meijneke, E. Van Asseldonk, T. Hoellinger, G. Cheron, Y. Ivanenko, V. La Scaleia, F. Sylos-Labini, M. Molinari *et al.*, "Design and control of the mindwalker exoskeleton," *IEEE transactions on neural systems and rehabilitation engineering*, vol. 23, no. 2, pp. 277–286, 2014.

[23] J. Gancet, M. Ilzkovitz, E. Motard, Y. Nevatia, P. Letier, D. De Weerdt, G. Cheron, T. Hoellinger, K. Seetharaman, M. Petieau *et al.*, "Mindwalker: Going one step further with assistive lower limbs exoskeleton for sci condition subjects," in *2012 4th IEEE RAS & EMBS International Conference on Biomedical Robotics and Biomechatronics (BioRob).* IEEE, 2012, pp. 1794–1800.

[24] E. Watson, "Posts tagged spinal cord injury."

[25] O. Baser, H. Kizilhan, and E. Kilic, "Biomimetic compliant lower limb exoskeleton (biocomex) and its experimental evaluation," *Journal of the Brazilian Society of Mechanical Sciences and Engineering*, vol. 41, no. 5, p. 226, 2019.

[26] X. Ouyang, S. Ding, B. Fan, P. Y. Li, and H. Yang, "Development of a novel compact hydraulic power unit for the exoskeleton robot," *Mechatronics*, vol. 38, pp. 68–75, 2016.

[27] S.-H. Hyon, T. Hayashi, A. Yagi, T. Noda, and J. Morimoto, "Design of hybrid drive exoskeleton robot xor2," in *2013 IEEE/RSJ International Conference on Intelligent Robots and Systems*. IEEE, 2013, pp. 4642–4648.

[28] R. Ranaweera, W. Jayasiri, W. Tharaka, J. Gunasiri, R. Gopura, T. Jayawardena, and G. Mann, "Anthro-x: Anthropomorphic lower extremity exoskeleton robot for power assistance," in *2018 4th International Conference on Control, Automation and Robotics (ICCAR)*. IEEE, 2018, pp. 82–87.

[29] Y. Sankai, "Hal: Hybrid assistive limb based on cybernics," in *Robotics research*. Springer, 2010, pp. 25–34.

[30] T. Nakamura, K. Saito, Z. Wang, and K. Kosuge, "Realizing model-based wearable antigravity muscles support with dynamics terms," in *2005 IEEE/RSJ International Conference on Intelligent Robots and Systems*. IEEE, 2005, pp. 2694–2699.

[31] H. He and K. Kiguchi, "A study on emg-based control of exoskeleton robots for human lower-limb motion assist," in *2007 6th International Special Topic Conference on Information Technology Applications in Biomedicine*. IEEE, 2007, pp. 292–295.

[32] F. Chen, Y. Yu, Y. Ge, J. Sun, and X. Deng, "Wpal for enhancing human strength and endurance during walking," in *2007 International Conference on Information Acquisition*. IEEE, 2007, pp. 487–491.

[33] F. Chen, Y. Yu, Y. Ge, and Y. Fang, "Wpal for human power assist during walking using dynamic equation," in *2009 International Conference on Mechatronics and Automation*. IEEE, 2009, pp. 1039–1043.

[34] M. Bortole, A. Venkatakrishnan, F. Zhu, J. C. Moreno, G. E. Francisco, J. L. Pons, and J. L. Contreras-Vidal, "The h2 robotic exoskeleton for gait rehabilitation after stroke: early findings from a clinical study," *Journal of neuroengineering and rehabilitation*, vol. 12, no. 1, p. 54, 2015.

[35] J. Vaughan-Graham, D. Brooks, L. Rose, G. Nejat, J. Pons, and K. Patterson, "Exoskeleton use in post-stroke gait rehabilitation: a qualitative study of the perspectives of persons post-stroke and physiotherapists," *Journal of neuroengineering and rehabilitation*, vol. 17, no. 1, pp. 1–15, 2020.

[36] X. Zhang and M. Hashimoto, "Sbc for motion assist using neural oscillator," in *2009 IEEE International Conference on Robotics and Automation*. IEEE, 2009, pp. 659–664.

[37] A. Esquenazi, M. Talaty, A. Packel, and M. Saulino, "The rewalk powered exoskeleton to restore ambulatory function to individuals with thoracic-level motor-complete spinal cord injury," *American journal of physical medicine & rehabilitation*, vol. 91, no. 11, pp. 911–921, 2012.

[38] N. Aphiratsakun and M. Parnichkun, "Balancing control of ait leg exoskeleton using zmp based flc," *International Journal of Advanced Robotic Systems*, vol. 6, no. 4, p. 34, 2009.

[39] N. Aphiratsakun, K. Chirungsarpsook, and M. Parnichkun, "Design and balancing control of ait leg exoskeleton-i (alex-i)." in *ICINCO-RA (1)*, 2008, pp. 151–158.

[40] I. Pecoraro, N. Tagliamonte, C. Tamantini, F. Cordella, F. Bentivoglio, I. Pisotta, A. Bigioni, F. Tamburella, M. Lorusso, P. Argentieri *et al.*, "Psychophysiological assessment of exoskeleton-assisted treadmill walking," in *International Conference on NeuroRehabilitation*. Springer, 2020, pp. 201–205.

[41] K. Kong and D. Jeon, "Design and control of an exoskeleton for the elderly and patients," *IEEE/ASME Transactions on mechatronics*, vol. 11, no. 4, pp. 428–432, 2006.

[42] T. Yan, M. Cempini, C. M. Oddo, and N. Vitiello, "Review of assistive strategies in powered lower-limb orthoses and exoskeletons," *Robotics and Autonomous Systems*, vol. 64, pp. 120–136, 2015.

[43] G. Belforte, G. Eula, S. Appendino, and S. Sirolli, “Pneumatic interactive gait rehabilitation orthosis: design and preliminary testing,” *Proceedings of the Institution of Mechanical Engineers, Part H: Journal of Engineering in Medicine*, vol. 225, no. 2, pp. 158–169, 2011.

[44] T.-J. Yeh, M.-J. Wu, T.-J. Lu, F.-K. Wu, and C.-R. Huang, “Control of mckibben pneumatic muscles for a power-assist, lower-limb orthosis,” *Mechatronics*, vol. 20, no. 6, pp. 686–697, 2010.

[45] G. S. Sawicki and D. P. Ferris, “Powered ankle exoskeletons reveal the metabolic cost of plantar flexor mechanical work during walking with longer steps at constant step frequency,” *Journal of Experimental Biology*, vol. 212, no. 1, pp. 21–31, 2009.

[46] D. Shi, W. Zhang, W. Zhang, and X. Ding, “A review on lower limb rehabilitation exoskeleton robots,” *Chinese Journal of Mechanical Engineering*, vol. 32, no. 1, pp. 1–11, 2019.

[47] R. Ekkelenkamp, J. Veneman, and H. Van Der Kooij, “Lopes: a lower extremity powered exoskeleton,” in *Proceedings 2007 IEEE International Conference on Robotics and Automation.* IEEE, 2007, pp. 3132–3133.

[48] K. N. Winfree, P. Stegall, and S. K. Agrawal, “Design of a minimally constraining, passively supported gait training exoskeleton: Alex ii,” in *2011 IEEE International Conference on Rehabilitation Robotics.* IEEE, 2011, pp. 1–6.

[49] W.-Y. Lai, H. Ma, W.-H. Liao, D. T.-P. Fong, and K.-M. Chan, “Hip-knee control for gait assistance with powered knee orthosis,” in *2013 IEEE international conference on robotics and biomimetics (ROBIO).* IEEE, 2013, pp. 762–767.

[50] J. E. Pratt, C. J. Morse, and S. H. Collins, “2004,” the roboknee: An exoskeleton for enhancing strength and endurance during walking,” in *Pro-*

ceedings of the IEEE Int. Conference on Robotics and Automation (ICRA. Citeseer.

[51] P. Moreira, P. Ramôa, L. F. Silva, and P. Flores, "On the biomechanical design of stance control knee ankle foot orthosis (sckafo)," 2011.

[52] A. N. Spring, J. Kofman, and E. D. Lemaire, "Design and evaluation of an orthotic knee-extension assist," *IEEE Transactions on Neural Systems and Rehabilitation Engineering*, vol. 20, no. 5, pp. 678–687, 2012.

[53] K. Low, "Robot-assisted gait rehabilitation: From exoskeletons to gait systems," in *2011 Defense Science Research Conference and Expo (DSR)*. IEEE, 2011, pp. 1–10.

[54] S. M. Cain, K. E. Gordon, and D. P. Ferris, "Locomotor adaptation to a powered ankle-foot orthosis depends on control method," *Journal of neuroengineering and rehabilitation*, vol. 4, no. 1, pp. 1–13, 2007.

[55] M. G. Alvarez-Perez, M. A. Garcia-Murillo, and J. J. Cervantes-Sánchez, "Robot-assisted ankle rehabilitation: a review," *Disability and Rehabilitation: Assistive Technology*, vol. 15, no. 4, pp. 394–408, 2020.

[56] R. Paranjape, J. Mahovsky, L. Benedicenti, and Z. Koles, "The electroencephalogram as a biometric," in *Canadian Conference on Electrical and Computer Engineering 2001. Conference Proceedings (Cat. No. 01TH8555)*, vol. 2. IEEE, 2001, pp. 1363–1366.

[57] E. Criswell, *Cram's introduction to surface electromyography*. Jones & Bartlett Publishers, 2010.

[58] M. Cifrek, V. Medved, S. Tonković, and S. Ostojić, "Surface emg based muscle fatigue evaluation in biomechanics," *Clinical biomechanics*, vol. 24, no. 4, pp. 327–340, 2009.

[59] M. A. Islam, K. Sundaraj, R. B. Ahmad, and N. U. Ahamed, "Mechanomyogram for muscle function assessment: a review," *PloS one*, vol. 8, no. 3, p. e58902, 2013.

[60] D. A. Yungher, M. T. Wininger, J. Barr, W. Craelius, and A. J. Threlkeld, "Surface muscle pressure as a measure of active and passive behavior of muscles during gait," *Medical engineering & physics*, vol. 33, no. 4, pp. 464–471, 2011.

[61] G. De Luca, "Fundamental concepts in emg signal acquisition," 2003.

[62] R. Fluit, M. S. Andersen, S. Kolk, N. Verdonschot, and H. F. Koopman, "Prediction of ground reaction forces and moments during various activities of daily living," *Journal of biomechanics*, vol. 47, no. 10, pp. 2321–2329, 2014.

[63] D. A. Winter, *Biomechanics and motor control of human movement.* John Wiley & Sons, 2009.

[64] B. D. Mowery, "The paired t-test," *Pediatric nursing*, vol. 37, no. 6, pp. 320–322, 2011.

[65] G. Borg, *Borg's perceived exertion and pain scales.* Human kinetics, 1998.

Appendix A

ANYBODY MUSCULOSKELETAL MODEL

A.1 Body Mass Scaling Factors

```
lumbar = 0.139*Body_Mass;
thorax = 0.1894*Body_Mass;
pelvis = 0.142*Body_Mass;
clavicle_r = 0.0133*Body_Mass;
upper_arm_r = 0.028*Body_Mass;
lower_arm_r = 0.016*Body_Mass;
hand_r = 0.006*Body_Mass;
clavicle_l = 0.0133*Body_Mass;
upper_arm_l = 0.028*Body_Mass;
lower_arm_l = 0.016*Body_Mass;
hand_l = 0.006*Body_Mass;
head = 0.081*Body_Mass; // head and cervical
thigh_r = 0.1*Body_Mass;
lower_leg_r = 0.0465*Body_Mass;
foot_r = 0.0145*Body_Mass;
ball_r = 0.000;
thigh_l = 0.1*Body_Mass;
lower_leg_l = 0.0465*Body_Mass;
foot_l = 0.0145*Body_Mass
```

A.2 Fat Percentage

```
FatPercent = (−0.09 + 0.0149*BMI − 0.00009*BMI^2)*100;
```

A.3 Ground Reaction Force Prediction Foot Plate Conditions

```
FootPlateConditionalContact GRF_Prediction_Right(

    NORMAL_DIRECTION = "Y",
    NUMBER_OF_NODES = 25,
    NODES_FOLDER = FootNodes,
    PLATE_BASE_FRAME = Main.EnvironmentModel.GlobalRef

) = {
    CreateFootContactNodes25 FootNodes(
        foot_ref=Main.HumanModel.BodyModel.Right.Leg.Seg.Foot
    ) = {};
};
```

```
FootPlateConditionalContact <Object_name>(
     NORMAL_DIRECTION        = "<X|Y|*Z>",
     NUMBER_OF_NODES         = [*1..200],
     NODES_BASE_FOLDER       = <AnyFolder> ,
     PLATE_BASE_FRAME        = <AnyRefFrame>,
     SHOW_TRIGGER_VOLUME = [*0|1] ) =
```

```
{
  Settings =
  {
    [ LimitDistLow = -0.10;                  ]
    [ LimitDistHigh = 0.04;                  ]
    [ LimitVelHigh = 0.8;                    ]
    [ GroundVelocity = {0.0, -1.0, 0.0};     ]
    [ Strength = 200;                        ]
    [ FrictionCoefficient = 0.5;             ]
    [ ScaleFactor = 1;                       ]
    [ ForceVectorDrawScaleFactor = 0.0005;]
  };
```

Appendix B

SEMG SIGNAL FEATURE EXTRACTION

B.1 Main Program

```
rawSig = withoutexo1_8;
windowlength = 100;
overlap = 75;
delta = windowlength - overlap;

for i = (1: 4)
     if i == 1
          withExo36_filtered = rawSig(:,i);
          withExo36_rms = rawSig(1:delta:length(rawSig),i);
else
if i == 2
withExo36_filtered(:, i) = rawSig(:,i);
withExo36_rms(:, i) = rms_output(rawSig(:,i), windowlength, overlap,
else
signal = rawSig(:,i);
signalf = peakRemove(signal, 50, 1);
signalff = peakRemove(signalf, 100, 0);
withExo36_filtered(:, i) = signalff;
withExo36_rms(:, i) = rms_output(signalff, windowlength, overlap, 1);
          end
```

```
    end
end



save('withExo36_rms.mat', 'withExo36_rms');
csvwrite('withExo36_rms.csv', withExo36_rms);

save('withExo36_filtered.mat', 'withExo36_filtered');
csvwrite('withExo36_filtered.csv', withExo36_filtered);
```

B.2 Signal Noise Reduction

```
function signalf = peakRemove(signal, peekDis, bandpass)
[f, p] = fft_transform(4000, signal);
p1 = p(1:fix(end/2));
f1 = f(1:fix(end/2));
[pks, locs] = findpeaks(p1,f1,'minPeakDistance',peekDis);
peekDis = 100

spikes = locs;
for i = (1:length(spikes))
    if spikes(i)>= 600
        spikes(i:end) = [];
        break;
    end
end
peaks = pks(1:length(spikes));
len = length(peaks);
count = 0;
```

```
for j = (1:len)
    if peaks(j-count)<= 0.5 % to preserve the muscle signal
        peaks(j-count) = [];
        spikes(j-count) = [];
        count = count + 1;
    end
end
notch_val = spikes;
signalf = signal;
for i = notch_val
   n = Notch(i);
   signalf = filter(n, signalf);
end
if bandpass == 1
    bandpass = Butterworth_emg_Sanka(20, 450, 32);
    signalf = filter(bandpass, signalf);
end
end
```

B.3 FFT Transformation

```
function [f, P1] = fft_transform(Fs, X)

f = linspace(0, Fs, length(X));
P1 = abs(fft(X));

end
```

B.4 Butterworth Bandpass Filter

```
function Hdb = Butterworth_emg_Sanka(F1, F2, Ord)

Fs = 4000;  % Sampling Frequency

N   = Ord;    % Order
Fc1 = F1;    % First Cutoff Frequency
Fc2 = F2;  % Second Cutoff Frequency

h  = fdesign.bandpass('N,F3dB1,F3dB2', N, Fc1, Fc2, Fs);
Hdb = design(h, 'butter');
```

B.5 Notch Filter

```
function n = Notch(notch_val)

.
Fs = 4000;  % Sampling Frequency


Fnotch = notch_val;  % Notch Frequency
BW     = 2;     % Bandwidth
Apass  = 1;     % Bandwidth Attenuation


[b, a] = iirnotch(Fnotch/(Fs/2), BW/(Fs/2), Apass);
n      = dfilt.df2(b, a);
```

B.6 Noise Peak Filteration

```
function signalf = peakRemove(signal, peekDis, bandpass)
[f, p] = fft_transform(4000, signal);
p1 = p(1:fix(end/2));
f1 = f(1:fix(end/2));
[pks, locs] = findpeaks(p1,f1,'minPeakDistance',peekDis);
peekDis = 100

spikes = locs;
for i = (1:length(spikes))
     if spikes(i)>= 600
          spikes(i:end) = [];
          break;
     end
end
peaks = pks(1:length(spikes));
len = length(peaks);
count = 0;
for j = (1:len)
     if peaks(j-count)<= 0.5 % to preserve the muscle signal
          peaks(j-count) = [];
          spikes(j-count) = [];
          count = count + 1;
     end
end
notch_val = spikes;
signalf = signal;
for i = notch_val
   n = Notch(i);
```

```
    signalf = filter(n, signalf);
end
if bandpass == 1
     bandpass = Butterworth_emg_Sanka(20, 450, 32);
     signalf = filter(bandpass, signalf);
end
end
```

Appendix C

ENGINEERING DRAWINGS OF DUMMY LOWER-LIMB EXOSKELETON

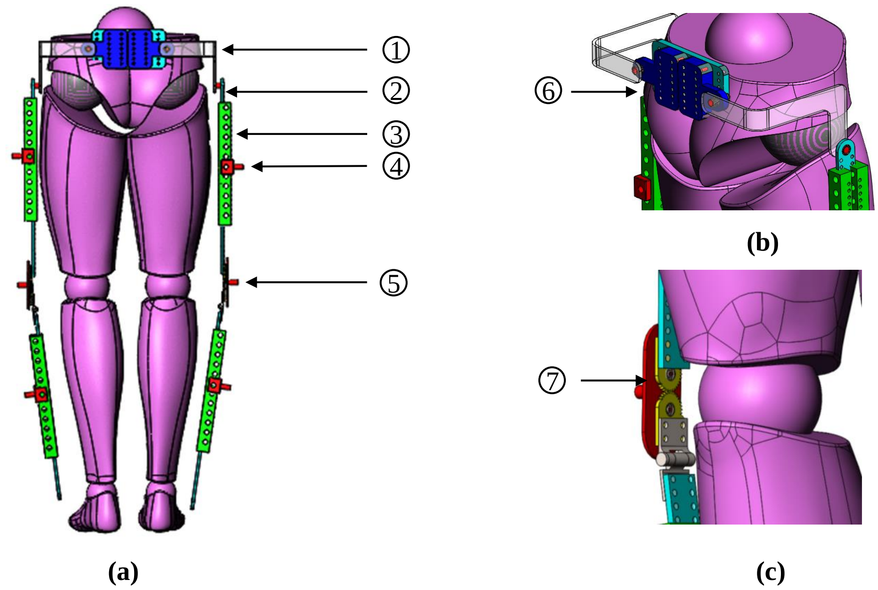

Figure C.1: Dummy exoskeleton, (a) lateral view of the exoskeleton, (b) hip mechanism, and (c) knee mechanism.

Table C.1 shows the components labeled in the Figure c.1. Engineering drawings of these components are available under this section.

Table C.1: Description of the components of the dummy exoskeleton

Item No.	Component
1	Hip curve plate
2	Limb extension plate
3	Limb extension plate holder
4	Weight attachment holder
5	Knee weight attachment holder
6	Hip back plate
7	Knee mechanism gear wheel

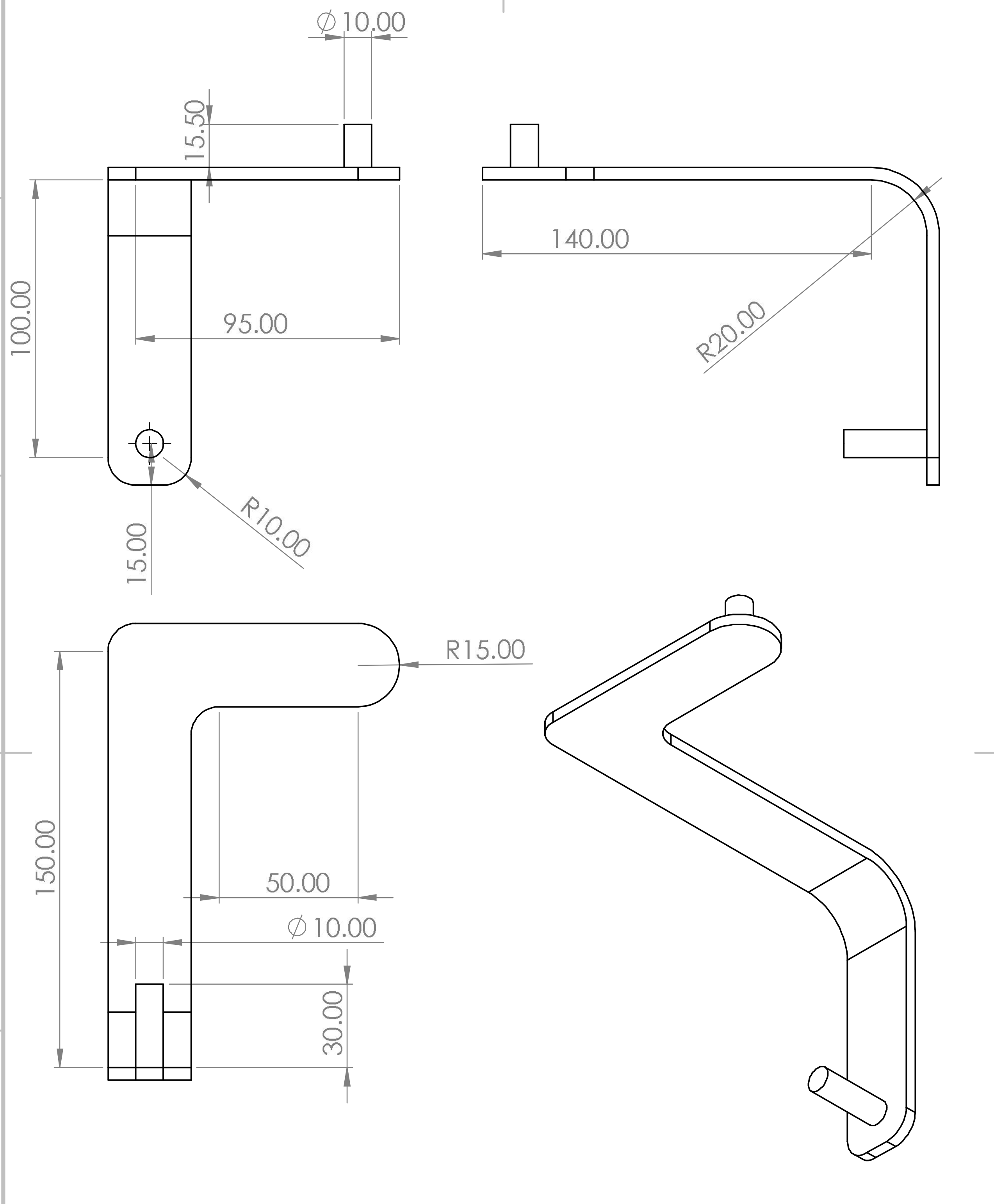

UNLESS OTHERWISE SPECIFIED: DIMENSIONS ARE IN MILLIMETERS SURFACE FINISH: TOLERANCES: LINEAR: ANGULAR:	PROPRIETARY AND CONFIDENTIAL The information contained inthis drawing is a sole property of University of Moratuwa. Any reproduction in part or as a whole without a written permission of University of Moratuwa is prohibited.	DEBURR AND BREAK SHARP EDGES	DO NOT SCALE DRAWING — REVISION

	NAME	SIGNATURE	DATE
DRAWN	MDSD Chandrasiri		
CHK'D			
APPV'D			
MFG			
Q.A			

TITLE: Hip curve plate

MATERIAL: Acrylic

DWG NO. 01

A4

WEIGHT:

SCALE:1:2

SHEET 1 OF 1

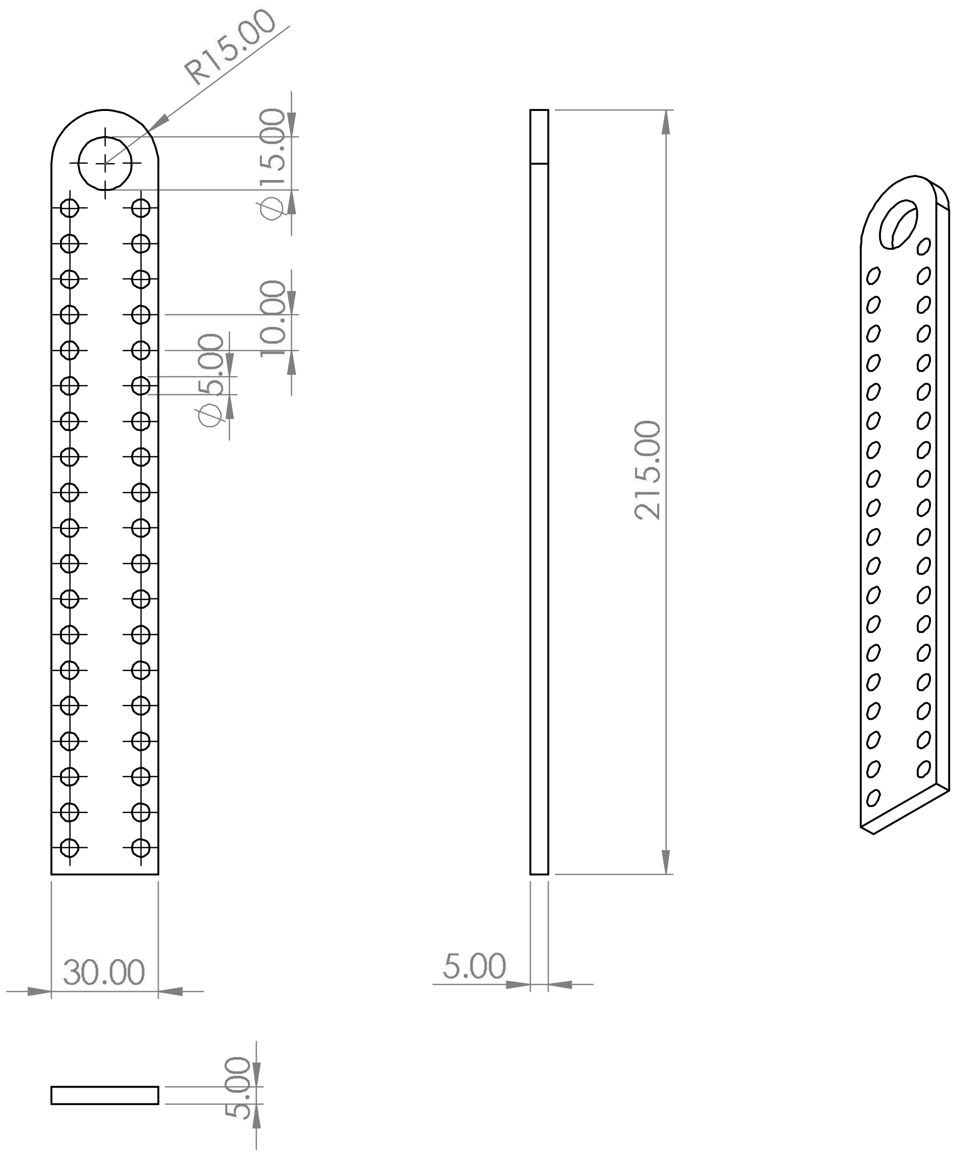

UNLESS OTHERWISE SPECIFIED:
DIMENSIONS ARE IN MILLIMETERS
SURFACE FINISH:
TOLERANCES:
LINEAR:
ANGULAR:

PROPRIETARY AND CONFIDENTIAL
The information contained inthis drawing is a sole property of University of Moratuwa. Any reproduction in part or as a whole without a written permission of University of Moratuwa is prohibited.

DEBURR AND BREAK SHARP EDGES

DO NOT SCALE DRAWING

REVISION

	NAME	SIGNATURE	DATE
DRAWN	MDSD Chandrasiri		
CHK'D			
APPV'D			
MFG			
Q.A			

TITLE:
Limb extension plate

MATERIAL:
Acrylic

DWG NO.
02

A4

WEIGHT:

SCALE:1:1

SHEET 1 OF 1

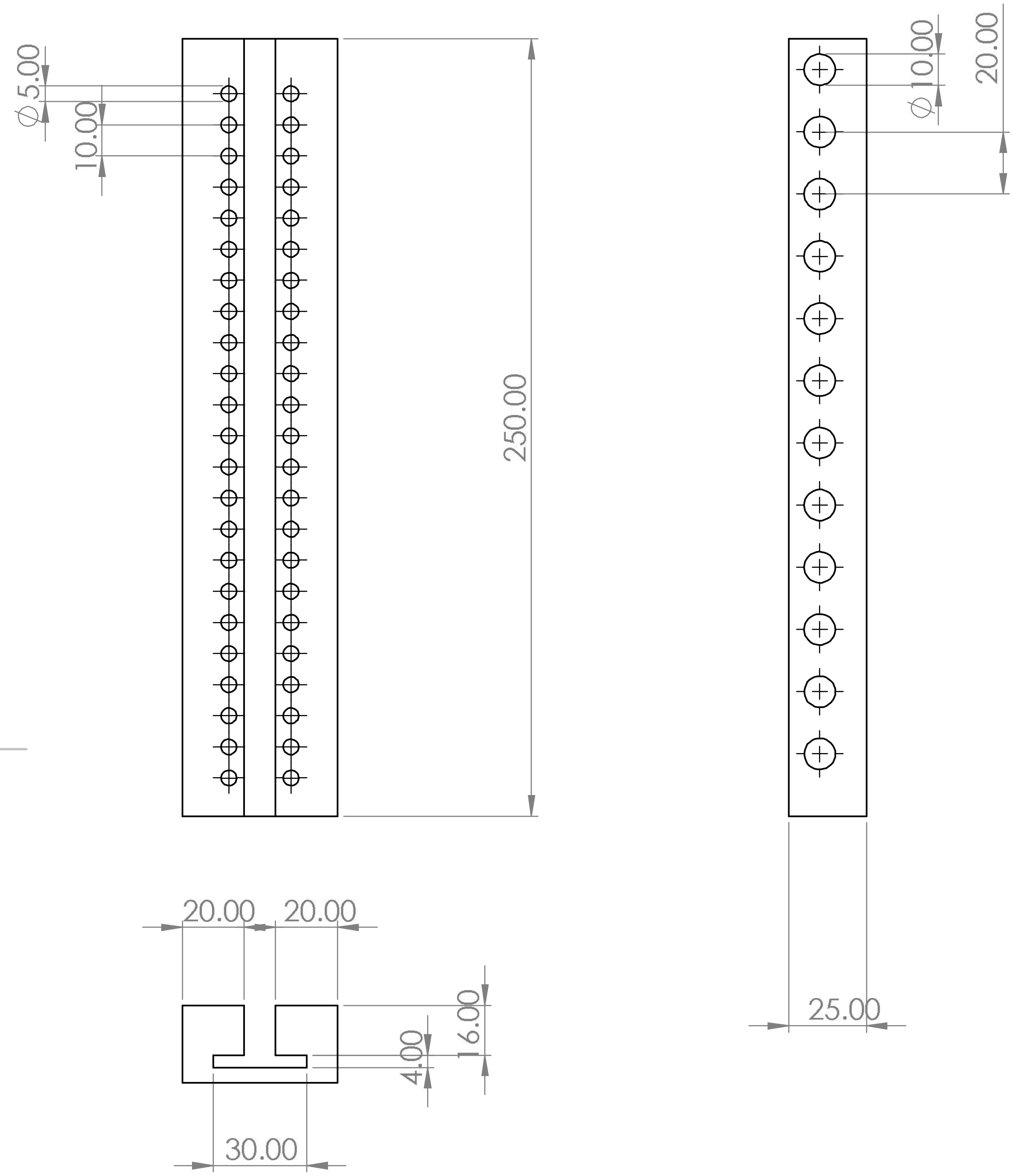

UNLESS OTHERWISE SPECIFIED:
DIMENSIONS ARE IN MILLIMETERS
SURFACE FINISH:
TOLERANCES:
LINEAR:
ANGULAR:

PROPRIETARY AND CONFIDENTIAL
The information contained inthis drawing is a sole property of University of Moratuwa. Any reproduction in part or as a whole without a written permission of University of Moratuwa is prohibited.

DEBURR AND BREAK SHARP EDGES

DO NOT SCALE DRAWING

REVISION

	NAME	SIGNATURE	DATE
DRAWN	MDSD Chandrasiri		
CHK'D			
APPV'D			
MFG			
Q.A			

TITLE:
Limb extension plate holder

MATERIAL: Acrylic

DWG NO. 03

A4

WEIGHT:

SCALE:1:2

SHEET 1 OF 1

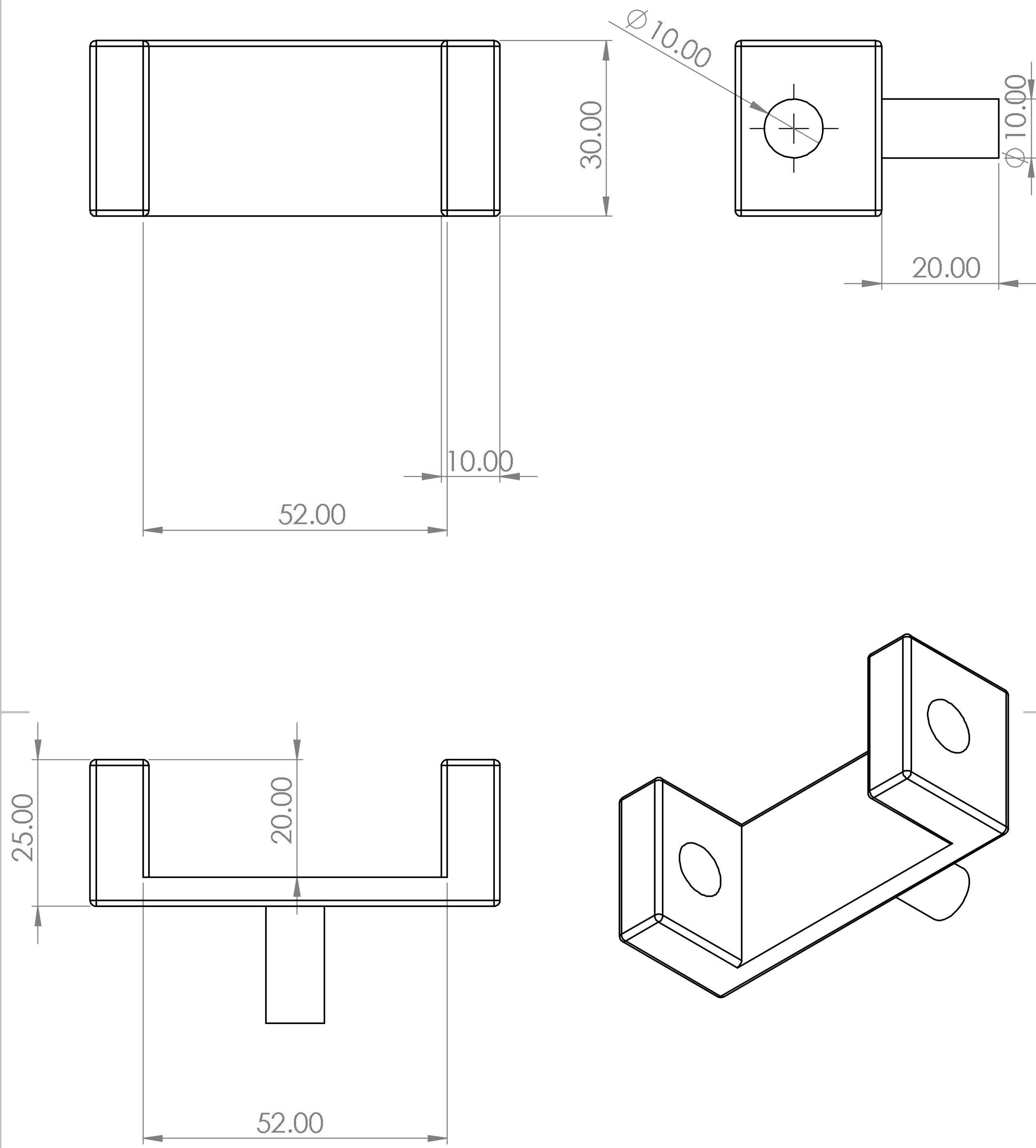

UNLESS OTHERWISE SPECIFIED:
DIMENSIONS ARE IN MILLIMETERS
SURFACE FINISH:
TOLERANCES:
LINEAR:
ANGULAR:

PROPRIETARY AND CONFIDENTIAL
The information contained inthis drawing is a sole property of University of Moratuwa. Any reproduction in part or as a whole without a written permission of University of Moratuwa is prohibited.

DEBURR AND BREAK SHARP EDGES

DO NOT SCALE DRAWING

REVISION

	NAME	SIGNATURE	DATE
DRAWN	MDSD Chandrasiri		
CHK'D			
APPV'D			
MFG			
Q.A			

TITLE: Weight attachment holder

MATERIAL: Acrylic

DWG NO. 04

A4

WEIGHT:

SCALE:1:2

SHEET 1 OF 1

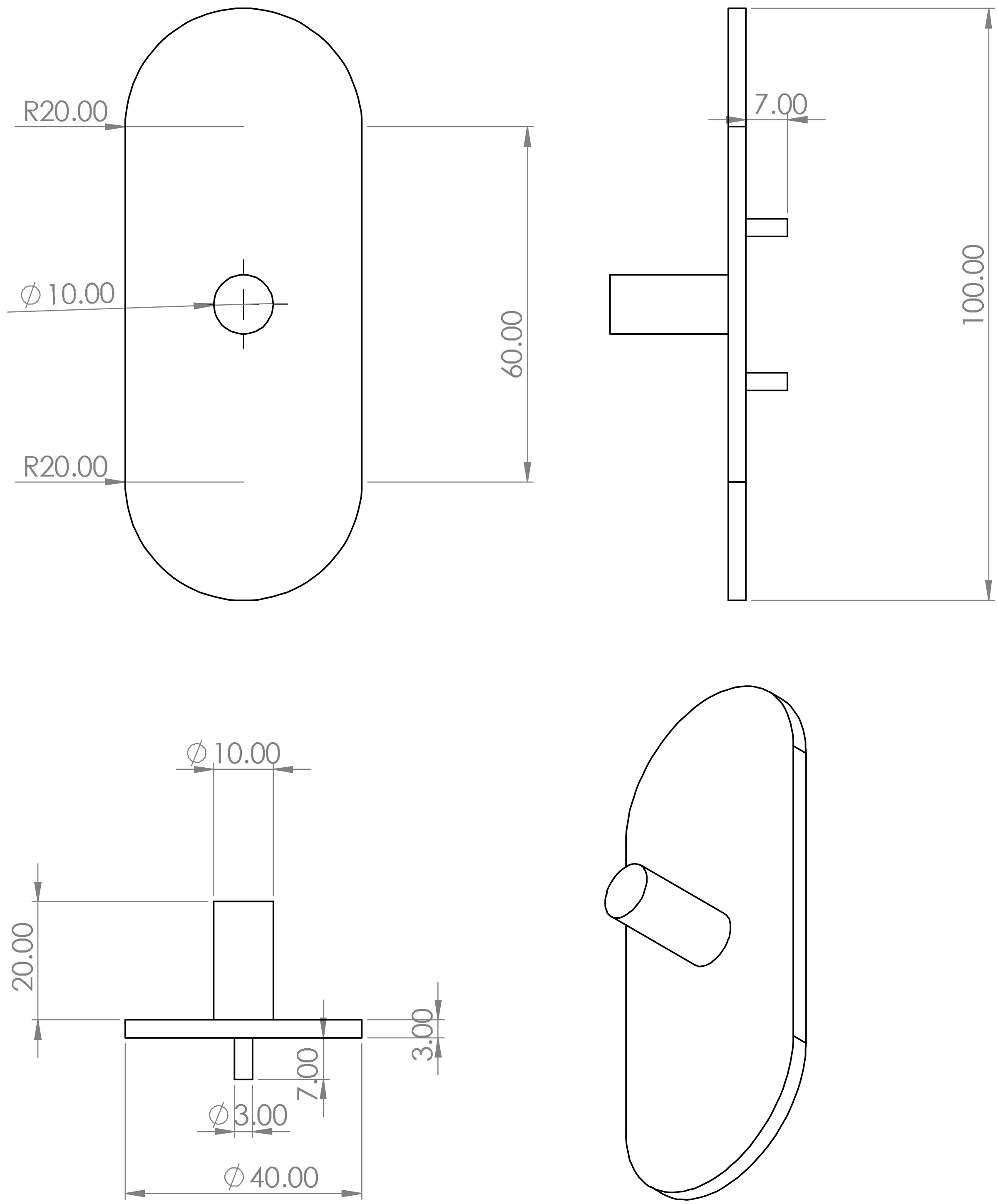

UNLESS OTHERWISE SPECIFIED:
DIMENSIONS ARE IN MILLIMETERS
SURFACE FINISH:
TOLERANCES:
LINEAR:
ANGULAR:

PROPRIETARY AND CONFIDENTIAL
The information contained inthis drawing is a sole property of University of Moratuwa. Any reproduction in part or as a whole without a written permission of University of Moratuwa is prohibited.

DEBURR AND BREAK SHARP EDGES

DO NOT SCALE DRAWING

REVISION

	NAME	SIGNATURE	DATE
DRAWN	MDSD Chandrasiri		
CHK'D			
APPV'D			
MFG			
Q.A			

TITLE: Knee weight attachment holder

MATERIAL: Acrylic

DWG NO. 05

A4

WEIGHT:

SCALE:1:1

SHEET 1 OF 1

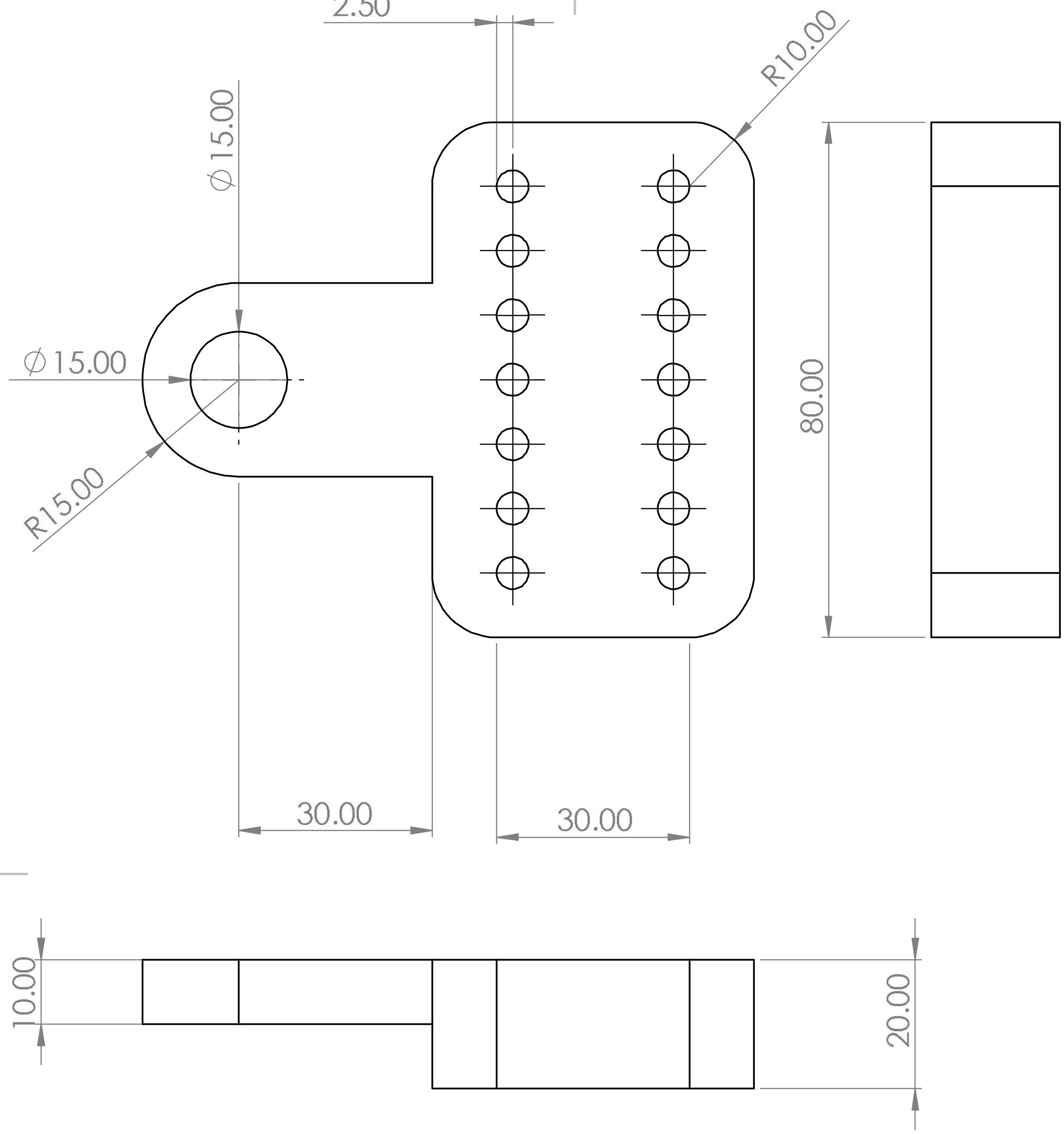

UNLESS OTHERWISE SPECIFIED:
DIMENSIONS ARE IN MILLIMETERS
SURFACE FINISH:
TOLERANCES:
LINEAR:
ANGULAR:

DEBURR AND BREAK SHARP EDGES

DO NOT SCALE DRAWING

REVISION

	NAME	SIGNATURE	DATE
DRAWN	MDSD Chandrasiri		
CHK'D			
APPV'D			
MFG			
Q.A			

TITLE: Hip back plate

MATERIAL: Acrylic

DWG NO. 06

A4

WEIGHT:

SCALE:1:1

SHEET 1 OF 1

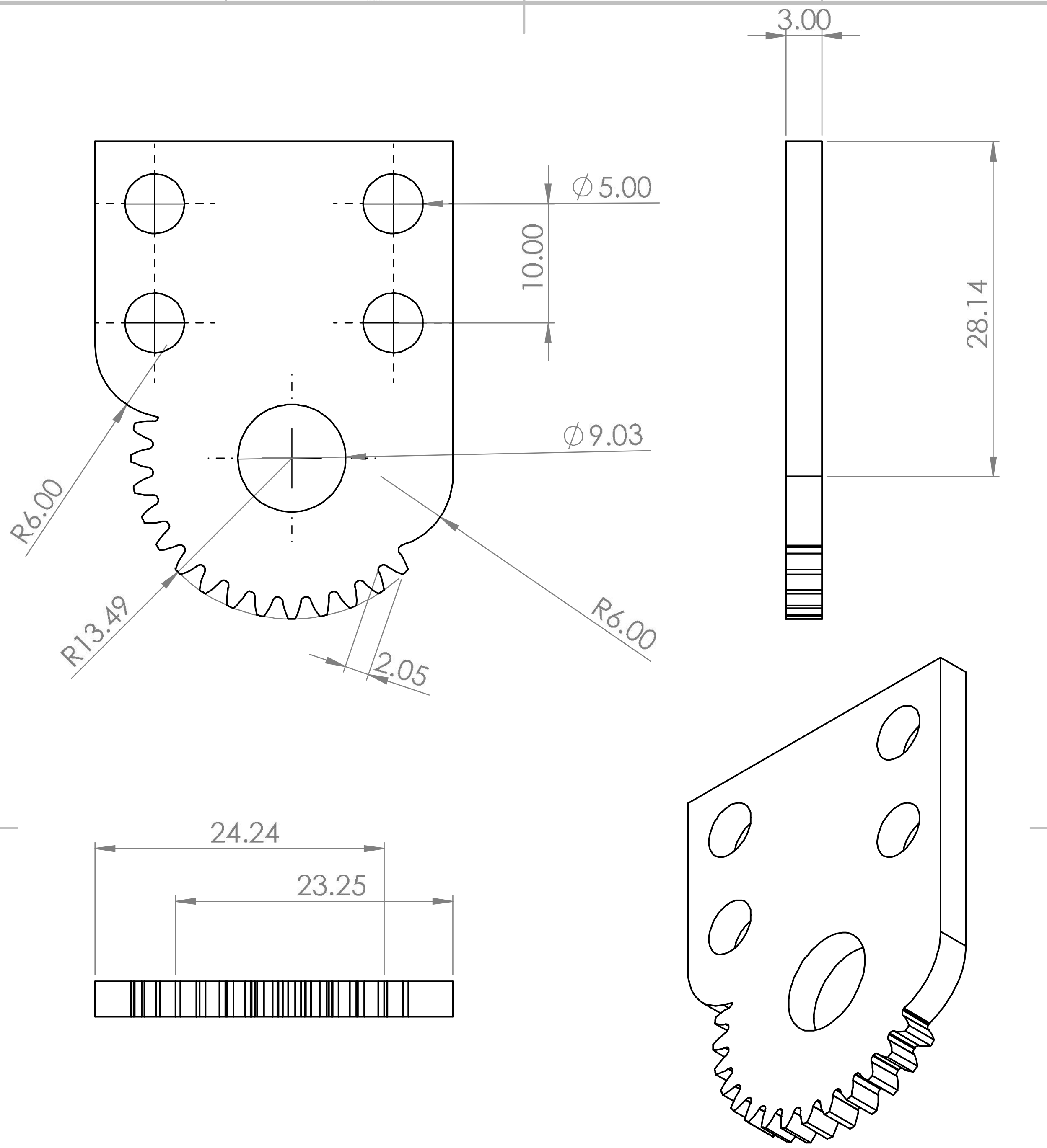

UNLESS OTHERWISE SPECIFIED: DIMENSIONS ARE IN MILLIMETERS SURFACE FINISH: TOLERANCES: LINEAR: ANGULAR:	PROPRIETARY AND CONFIDENTIAL The information contained inthis drawing is a sole property of University of Moratuwa. Any reproduction in part or as a whole without a written permission of University of Moratuwa is prohibited.	DEBURR AND BREAK SHARP EDGES	DO NOT SCALE DRAWING	REVISION	

	NAME	SIGNATURE	DATE
DRAWN	MDSD Chandrasiri		
CHK'D			
APPV'D			
MFG			
Q.A			

TITLE:

Gear wheel of the knee mechanism

MATERIAL: Acrylic

DWG NO. 07

A4

WEIGHT:

SCALE:1:1

SHEET 1 OF 1